THREE PROBLEMS IN NONLINEAR DYNAMICS

WITH 2:1 PARAMETRIC EXCITATION

A Dissertation

Presented to the Faculty of the Graduate School

of Cornell University

in Partial Fulfillment of the Requirements for the Degree of

Doctor of Philosophy

by

Tina Marie Morrison

May 2006

THREE PROBLEMS IN NONLINEAR DYNAMICS

WITH 2:1 PARAMETRIC EXCITATION

Tina Marie Morrison, Ph.D.

Cornell University 2006

Parametric excitation is epitomized by the Mathieu equation, $\ddot{x} + (\delta + \varepsilon \cos t)x = 0$, which involves the characteristic feature of 2:1 resonance. This thesis investigates three generalizations of the Mathieu equation:

1) the effect of combining 2:1 and 1:1 parametric drivers:

$$\ddot{x} + (\delta + \varepsilon \cos t + \varepsilon \cos \omega t)x = 0$$

2) the effect of combining parametric excitation near a Hopf bifurcation:

$$\ddot{x} + (\delta + \varepsilon \cos t)x + \varepsilon A\dot{x} + \varepsilon(\beta_1 x^3 + \beta_2 x^2 \dot{x} + \beta_3 x\dot{x}^2 + \beta_4 \dot{x}^3) = 0$$

3) the effect of combining delay with cubic nonlinearity:

$$\ddot{x} + (\delta + \varepsilon \cos t)x + \varepsilon\gamma x^3 = \varepsilon\beta x(t - T)$$

Chapter 3 examines the first of these systems in the neighborhood of 2:1:1 resonance. The method of multiple time scales is used including terms of $O(\varepsilon^2)$ with three time scales. By comparing our results with those of a previous work on 2:2:1 resonance, we are able to approximate scaling factors which determine the size of the instability regions as we move from one resonance to another in the δ-ω plane.

Chapter 4 treats the second system which involves the parametric excitation of a Hopf bifurcation. The slow flow obtained from a perturbation method is investigated analytically and numerically. A wide variety of bifurcations are observed,

including pitchforks, saddle-nodes, Hopfs, limit cycle folds, symmetry-breaking, homoclinic and heteroclinic bifurcations. Approximate analytic expressions for bifurcation curves are obtained using a variety of methods, including normal forms. We show that for large positive damping, the origin is stable, whereas for large negative damping, a quasiperiodic behavior occurs. These two steady states are connected by a complicated series of bifurcations which occur as the damping is varied.

Chapter 5 examines the third system listed. Three different types of phenomenon are combined in this system: 2:1 parametric excitation, cubic nonlinearity, and delay. The method of averaging is used to obtain a slow flow which is analyzed for stability and bifurcations. We show that certain combinations of the delay parameters β and T cause the 2:1 instability region in the δ-ε plane to become significantly smaller, and in some cases to disappear. We also show that the delay term behaves like effective damping, adding dissipation to a conservative system.

BIOGRAPHICAL SKETCH

"I am what I am at this moment, not what I was and certainly not all that I shall be."

– C. S. Wyatt

Tina Marie Morrison was born in 1978 to a loving mother in New Britain, CT. She grew up with her two younger siblings, Dwight Jr. and Nicole. Tina graduated from E.C. Goodwin Vocational High School in New Britain and received a degree in Mechanical Drafting. Her shop instructor, Fred Norton encouraged her to attend college and pursue a career in Mechanical Engineering.

In 1996, Tina entered the Mechanical Engineering program at the University of Connecticut, Storrs. She received her bachelor's degree along with a minor degree in Applied Mathematics. Upon graduation, the Mechanical Engineering department invited her to participate in their Accelerated One Year Master's program. She completed her master's with a concentration in Nonlinear Vibrations under the advising of Dr. Kevin Murphy.

In the spring of 2002, Tina was accepted into the doctoral program in the Theoretical and Applied Mechanics department at Cornell University. The following year, she began her research training in Nonlinear Dynamics under the guidance of Dr. Richard Rand. She received her doctorate in 2006, with a minor concentration in Applied Mathematics. Tina is the first in her family to graduate college and receive a Ph.D.

To my mother, Diane

For your love, encouragement and sacrifice

ACKNOWLEDGEMENTS

"Reflect upon your present blessings, of which every man has plenty,
not on your past misfortunes, of which all men have some."

– Charles Dickens

During my years as a doctoral candidate in Theoretical and Applied Mechanics, I received tremendous support and assistance from a number of individuals.

Foremost, I express my sincere appreciation to Richard Rand for being an excellent thesis advisor and teaching mentor. He worked closely with me to ensure my progress and success in the program. Even when I moved to Boston for a year, his support and guidance did not waiver. During my time at Cornell, Richard encouraged excellence in my research and affirmed my abilities as a teacher. For this, I am truly grateful.

Upon completing my first semester at Cornell, Steve Strogatz recognized my enthusiasm and commitment to the IGERT program and offered me an IGERT fellowship for my second year. I am appreciative of his support and encouragement during my candidacy years. In addition, I thank Alan Zehnder for carefully reading and commenting on my thesis.

Moreover, I am grateful to four very special women for being extremely helpful and supportive: Cindy Twardokus, Polly Marion, Dolores Pendell and Sreemati Mukherjee. In addition, I am thankful to Tim Healey for providing career advise and for assuring me of my place in the T&AM family.

Likewise, I am pleased to have shared my graduate experience with Geoff Recktenwald. During the course of our studies, he and I discussed research, philosophy, and world issues. We enjoyed many moments of fun and laughter. In addition,

TABLE OF CONTENTS

LIST OF FIGURES

Chapter 1

Introduction

"The goal of modeling is to find the simplest model which illustrates the phenomenon you are interested in."

– Richard Rand

Parametric excitation is the act of forcing a system by modulating a physical parameter (like stiffness or moment of inertia). The mathematical result is a time-varying coefficient (usually periodic) in the governing differential equation. In contrast with external excitation, which results in a nonhomogeneous term in the governing differential equation, small parametric excitation can produce a large response when the frequency of excitation is away from the primary resonance. In this thesis, we model this phenomenon in linear and nonlinear systems where the frequency of parametric excitation is twice that of the natural frequency of the linear unforced system.

1.1 Motivation

Parametric excitation occurs in a wide variety of engineering applications. Here are a few recent applications: Aubin et al [2] and Zalalutdinov et al [68] discovered MEMS/NEMS devices are parametrically excited when illuminated within an interference field of a continuous wave laser; Stépán et al [55] and Kalmár-Nagy [25] investigated parametric excitation in high-speed milling applications; Ramani et al [50] utilized parametric excitation to model a towed mass underwater for application to submarine dynamics; Wirkus et al [64] observed parametric excitation in the pumping of a swing; Yu [66] realized parametric excitation in a nanowire system using an oscillating electric field; Zhang et al [70] noticed parametric excitation in mass-loaded string systems such as elevators, cranes and cable-stayed bridges.

Parametric excitation dates back to Faraday in 1831 [15] when he noticed that surface waves in a fluid-filled cylinder under vertical excitation exhibited twice the period of the excitation itself. Lord Rayleigh in 1883 [27] attached a tuning fork to the end of a stretched string and observed that when the fork vibrated with frequency $2f$, the lateral vibrations of the string responded with frequency f. Stephenson in 1908 [56] predicted the possibility of converting the unstable equilibrium of an inverted pendulum by applying a vertical periodic force at the pin. Mathieu in 1868 [30] was investigating the vibrations of an elliptical membrane by separation of variables when he presented the simplest differential equation that governs the response of many systems to sinusoidal parametric excitation:

$$\ddot{x} + (\delta + \varepsilon \cos t)x = 0$$

where δ and ε are constants. This equation is known as the Mathieu equation, and has been studied extensively by many scientists. Here are a few: Bender and

Orzag [7], Minorsky [31], Nayfeh [35], Rand [42] and van der Pol [59].

In this thesis, we examine the phenomenon of parametric excitation in three different problems:

    ▷   the effect of combining 2:1 and 1:1 parametric drivers

    ▷   the effect of combining parametric excitation near a Hopf bifurcation

    ▷   the effect of delay on stabilizing a system with parametric excitation

Each of the three problems are treated separately in the following chapters of this thesis. Each chapter is self-contained with an abstract, introduction, detailed analysis of the problem, and conclusions. The references, however, follow the last chapter and are listed in the order in which they appear. The main results of each chapter are presented in the following section.

1.2   Thesis Organization

Chapter 2 is an introduction to parametric excitation demonstrated by a mass-spring system and the paradigm, the vertically driven pendulum. The motion of the mass is governed by the Mathieu equation [35]. The transition curves and stability charts are presented here.

Chapter 3 is an examination of combining 2:1 and 1:1 two parametric drivers, which is governed by the quasiperiodic Mathieu equation,

$$\ddot{x} + \left(\delta + \varepsilon \cos t + \varepsilon \cos \omega t\right) x = 0$$

which we analyze in the neighborhood of the point $\delta = 0.25$ and $\omega = 0.5$. The stability chart is self-similar at the resonance regions. We utilize the method of

multiple times scales including $O(\varepsilon^2)$ terms with three times scales for the small parameter ε. By comparing our results with those of a previous work on 2:2:1 resonance [72], we are able to approximate scaling factors which determine the size of the instability regions as we move from one resonance to another in the δ-ω plane. This leads to the conjecture that the scaling of the instability tongue's thickness goes like ε and the curvature goes like ω.

Chapter 4 is an analysis of the effect of 2:1 parametric excitation on the stability of a system that exhibits a Hopf bifurcation as linear damping is varied. The system we analyze consists of a simple harmonic oscillator with small nonlinearity, small damping and small parametric excitation in the neighborhod of 2:1 resonance:

$$\ddot{z} + \varepsilon A \dot{z} + (1 + \varepsilon k_1 + \varepsilon B \cos 2t)z + \varepsilon(\beta_1 z^3 + \beta_2 z^2 \dot{z} + \beta_3 z \dot{z}^2 + \beta_4 \dot{z}^3) = 0$$

where A is linear damping, k_1 is detuning off the 2:1 resonance, B is the amplitude of parametric forcing, the β_i's are the coefficients of nonlinear terms, and $\varepsilon << 1$. The unforced system ($B=0$) exhibits the birth of a stable limit cycle as the damping changes sign from positive to negative (a supercritical Hopf bifurcation) [42]. We investigate the changes that occur in the steady state behavior as the linear damping parameter is varied. A wide variety of bifurcations are observed, including pitchforks, saddle-nodes, Hopfs, limit cycle folds, symmetry-breaking, homoclinic and heteroclinic bifurcations. Approximate analytic expressions for bifurcation curves are obtained using a variety of methods, including normal forms. We accompany the lowest order approximations with numerical comparisons (PPLANE 6 [1] and AUTO [14]). These give good agreement for the homoclinic and symmetry-breaking bifurcations. We show that for large positive damping, the origin is stable, whereas for large negative damping a quasiperiodic behavior occurs. These two

steady states are connected by a complicated series of bifurcations which occur as the damping is varied.

Chapter 5 is an investigation of the effect delay has on the instabilities caused by cubic nonlinearities combined with 2:1 parametric excitation. The system we analyze is a delayed nonlinear Mathieu equation:

$$\ddot{x} + (\delta + \varepsilon\alpha\cos t)x + \varepsilon\gamma x^3 = \varepsilon\beta x(t - T)$$

in the neighborhood of δ=1/4, where δ, α, β, γ and T are parameters: δ is the frequency-squared of the simple harmonic oscillator, a is the amplitude of the parametric resonance, b is the amplitude of delay, c is the amplitude of the cubic nonlinearity, and T is the delay period. The delayed linear Mathieu equation was studied by Insperger and Stépán [24]. The method of averaging (valid for small ε) is used to obtain a slow flow which is analyzed for stability and bifurcations. The bifurcations include pitchforks, saddle-nodes and a degenerate Hopf. We show that the combined effect of 2:1 parametric excitation, cubic nonlinearity and delay stabilizes a region in the T-δ plane for certain combinations of the delay parameters β and T. This system would normally be unstable in the absence of delay. We also show that the delay term behaves like effective damping, adding dissipation to a conservative system. For example, the nonlinear Mathieu equation is known to be a conservative system [42]. When delay is added, the conservative system becomes dissipative, except for certain combinations of the delay parameters β and T.

Chapter 6 offers some ideas for future work which would be an extension of the research conducted in this thesis.

Chapter 2

Parametric Excitation

"We think our theory will provide some guidance to help engineers avoid the problem."

– Steven Strogatz

Parametric excitation is the act of forcing a system by modulating a physical parameter (like stiffness or moment of inertia) [10]. The mathematical result is a time-varying coefficient (usually periodic) in the governing differential equation. In contrast with external excitation, which results in a nonhomogeneous term in the differential equation, small parametric excitation can produce a large response when the frequency of excitation is away from the primary resonance. In this thesis, we consider linear and nonlinear systems where the frequency of parametric excitation is twice that of the natural frequency of the linear system. This chapter examines parametric excitation by considering a mass-spring system and a pendulum with a moving support.

2.1 Mass-Spring Oscillator

The mass-spring systems in Figure 2.1 are analyzed to demonstrate the fundamental difference between external excitation and parametric excitation. That is, a small parametric excitation can produce a large response when the frequency of excitation is away from the primary resonance, whereas external excitation produces a large response at the primary resonance.

The system at the top of Figure 2.1 is a mass attached to two linear springs. The middle diagram is the same mass-spring system forced externally with $F(t) = A \cos \Omega t$. In the bottom diagram, the second of the two springs has a time-varying stiffness.

Let's examine each system separately with the mass taken as one. The equation of motion for the simple harmonic oscillator (SHO) in Figure 2.1a is:

$$\ddot{x}(t) + (k_1 + k_2)x(t) = 0 \tag{2.1}$$

where k_1 and k_2 are positive. The solution to this linear constant coefficient homogeneous ODE is:

$$x(t) = C_1 \cos(\omega_0 t) + C_2 \sin(\omega_0 t) \tag{2.2}$$

where $\omega_0 = \sqrt{k_1 + k_2}$ is the natural frequency. Now, let's consider the externally excited SHO in Figure 2.1b. The equation of motion is:

$$\ddot{x}(t) + (k_1 + k_2)x(t) = A \cos \Omega t \tag{2.3}$$

where Ω is the forcing frequency. Notice the homogeneous part of this ODE is equation (2.1). Hence, the complementary solution is equation (2.2). The particlar solution is of the form:

$$x_p(t) = C_3 \cos \Omega t \tag{2.4}$$
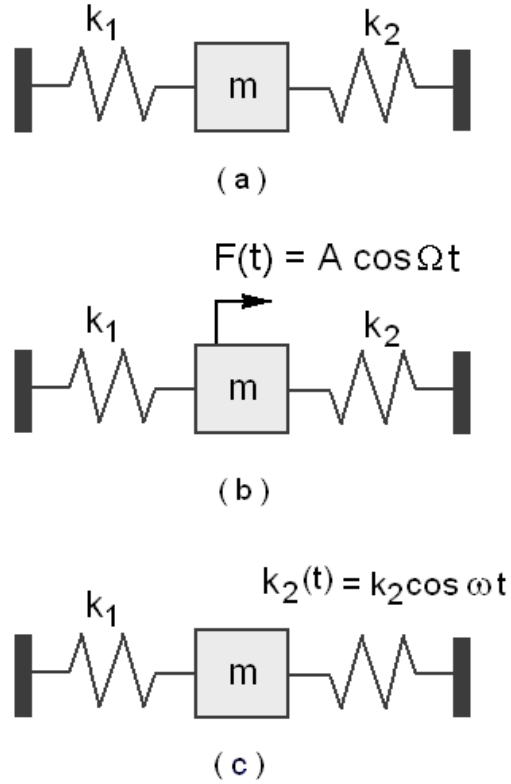
Figure 2.1: Mass-spring oscillators: (a) simple harmonic oscillator with natural frequency of $\sqrt{k_1 + k_2}$, with $m = 1$, (b) simple harmonic oscillator with an external forcing function, $F(t) = A\cos\Omega t$, and (c) simple harmonic oscillator with time-varying stiffness $k_2 = k_2\cos\omega t$.

However, if $\Omega^2 = k_1 + k_2$, then the system is being excited at the primary resonance, generating a secular term in the particular solution, $x_p(t) = C_4 t \cos\Omega t$, which grows linearly in time. However, if the system is forced away from the natural frequency, then the particular solution is:

$$x_p(t) = -\frac{A\cos\Omega t}{\Omega^2 - (k_1 + k_2)} \tag{2.5}$$

Note that as the forcing frequency approaches the linear natural frequency, $\Omega^2 \to (k_1 + k_2)$, the solution, $x_p(t) \to \infty$. This is external resonance.

Finally, let's consider the SHO in Figure 2.1c, where the stiffness of k_2 is modulated at $k_2 \cos \omega t$. The equation of motion is:

$$\ddot{x}(t) + (k_1 + k_2 \cos \omega t)x(t) = 0 \tag{2.6}$$

This is a linear homogeneous ODE with a periodic coefficient, where $k_2 \cos \omega t$ is the parametric excitation. In general, a closed form solution does not exist for this equation. However, we can use a perturbation method to examine the steady state behavior of equation (2.6); this is outlined in the following section. We find that to the lowest order approximation, a large response occurs when

$$\omega^2 = 4k_1 \quad \Rightarrow \quad \omega = 2\sqrt{k_1} \tag{2.7}$$

which yields the condition that a large response occurs if the frequency of the parametric excitation is twice the natural frequency of the unforced system. This is the motivation for examining the dynamics of systems with 2:1 parametric excitation. Let's examine a paradigm of parametric excitation.

2.2   Pendulum with Moving Support

A classical example of parametric excitation is the vertically forced pendulum [4]. Let's consider the motion of a mass m attached to a rod of length L shown in Figure 2.2a. The support of the pendulum is made to vibrate in the α direction by $F(t) = F \cos \omega t$. Applying Newton's Law of Motion in the direction perpendicular to the rod, we obtain the equation of motion:

$$mL^2\ddot{\theta} = -m(g - F_y)L \sin \theta + mF_x L \cos \theta \tag{2.8}$$

For small oscillations about $\theta = 0$, with $m = 1$, equation (2.8) simplifies to

$$\ddot{\theta} + \left(\frac{g}{L} - \frac{F_y}{L}\right)\theta = \frac{F_x}{L} \tag{2.9}$$
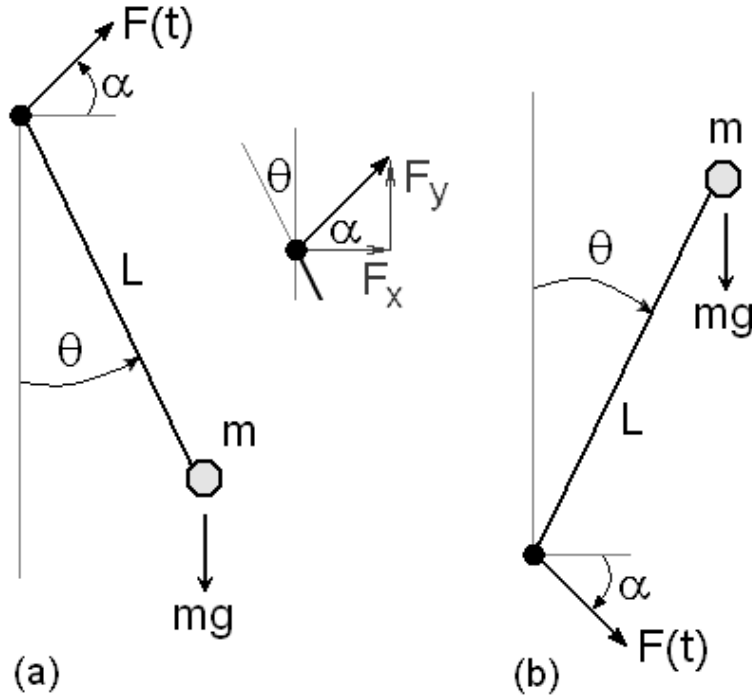
Figure 2.2: The pendulum: (a) simple pendulum with a moving support, $F(t) = F \cos \omega t$ (b) inverted pendulum with moving support.

When we force the support to vibrate at $F(t) = F \cos \omega t$, $F_y = F \cos \alpha \cos \omega t$ and $F_x = F \sin \alpha \cos \omega t$. Hence,

$$\ddot{\theta} + \left(\frac{g}{L} - \frac{F \cos \alpha}{L} \cos \omega t \right) \theta = \frac{F \sin \alpha}{L} \cos \omega t \tag{2.10}$$

Recall that parametric excitation appears as a variable coefficient and external excitation appears as a nonhomogeneous term. Therefore, F_y parametrically excites the pendulum and F_x externally excites the pendulum.

Next, let's consider the inverted pendulum whose support is made to vibrate with $F(t)$ shown in Figure 2.2b. The governing equation of motion is

$$mL^2\ddot{\theta} = m(g - F_y)L \sin \theta + mF_x L \cos \theta \tag{2.11}$$

or for small deflections about $\theta = 0$

$$\ddot{\theta} + \left(-\frac{g}{L} + \frac{F\cos\alpha}{L}\cos\omega t\right)\theta = \frac{F\sin\alpha}{L}\cos\omega t \tag{2.12}$$

The governing equations for the pendulums can be simplified by setting $\delta = \frac{g}{L}$ and $\varepsilon = -\frac{F_y}{L}$ for the simple pendulum and $\delta = -\frac{g}{L}$ and $\varepsilon = \frac{F_y}{L}$ for the inverted pendulum, resulting in,

$$\ddot{x} + (\delta + \varepsilon\cos t)x = F_x \tag{2.13}$$

This equation is known as the forced Mathieu equation. In the following section, we analyze the stability of the Mathieu equation when $F_x = 0$.

2.3 The Mathieu Equation

The Mathieu equation,

$$\ddot{x} + (\delta + \varepsilon\cos t)x = 0 \tag{2.14}$$

is the simplest differential equation that models parametric excitation. The parameter δ is the natural frequency squared of the unforced system ($\varepsilon = 0$), and ε is the amplitude of the parametric excitation. For a given pair of parameter values (δ, ε) the system can exhibit bounded (stable) or unbounded (unstable) solutions. We know the unforced system is stable when $\delta > 0$ and unstable when $\delta < 0$. It has been shown in [42], [35], [7], [41] that when $\varepsilon \neq 0$, transition curves emanate from points on the δ-axis at

$$\delta = \frac{n^2}{4}, \quad n = 0, 1, 2, \dots \tag{2.15}$$

The transition curves shown in Figure 2.3 for $\varepsilon < 1$ separate the stable from unstable regions. Each unstable tongue is a different resonance region. The equations
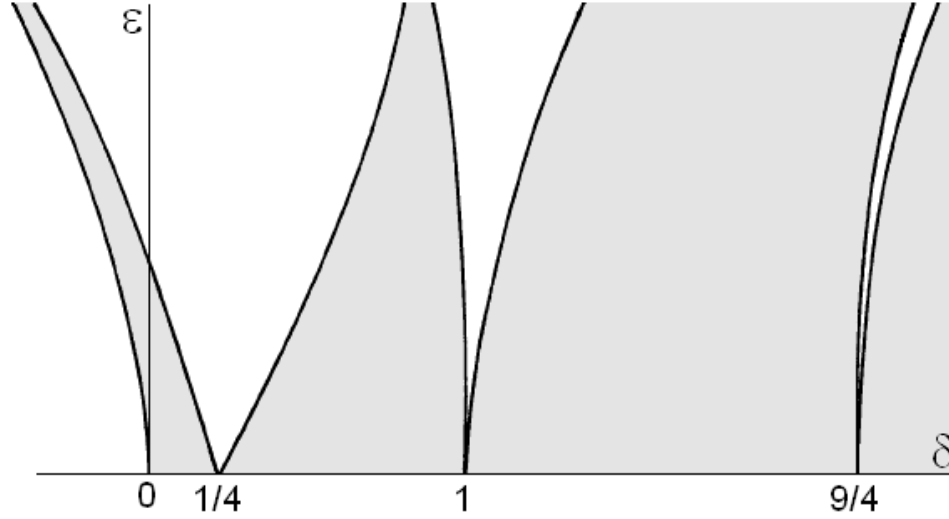
Figure 2.3: Transition curves for the Mathieu equation for $\varepsilon < 1$ which separate regions of stability (gray) from regions of instability (white).

for the transitions curves emanating from $0, \frac{1}{4}, 1, \frac{9}{4}$ and 4 are given out to $O(\varepsilon^{12})$ by Rand (see Chapter 6 in [42]). Note that the instability region emanating from $\delta = 1/4$ is the largest for small ε. This region corresponds to the 2:1 parametric excitation and results in parametric resonance.

Figure 2.3 can be used to evaluate the stability of the inverted pendulum in Figure 2.2b when $F_x = 0$. As defined in the previous section, the parameter δ is less than zero since g and L are both greater than zero. The amplitude of the parametric excitation ε is greater than zero by similar arguments. Let's assume that the pendulum's length $L > F \cos \alpha$. Therefore, $\varepsilon < 1$.

As a first example, consider the parameters (δ, ε) corresponding to the dot labeled a in Figure 2.4. Since the parameters lie in the gray region, the equilibrium solution for $\theta = 0$ (standing vertical) is stable. Therefore, a small perturbation will not cause the inverted pendulum to move to the $\theta = \pi$ position. Hence, vibrating the inverted pendulum at 1 rad/sec with the small amplitude ε causes the unstable
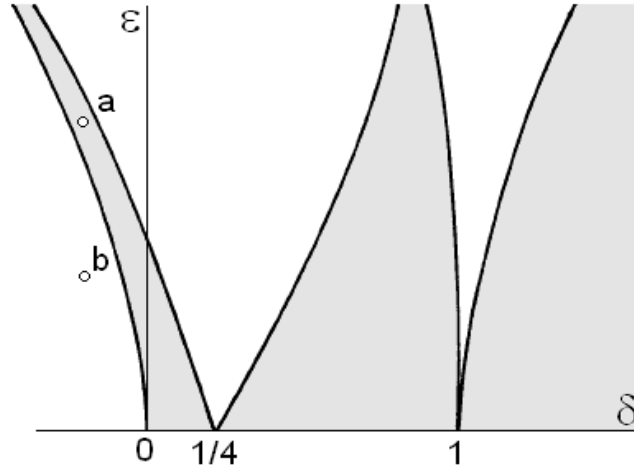
Figure 2.4: Transition curves for the inverted pendulum examples. The dot
a corresponds to a stable $\theta = 0$; the dot b corresponds to an unstable $\theta = 0$.

equilibrium position in the unforced system to become stable.

As a second example, consider the parameters (δ, ε) corresponding to the dot labeled b in Figure 2.4. Since the parameters lie in the white region, the equilibrium solution for $\theta = 0$ (standing vertical) is unstable. Therefore, a small perturbation will cause the inverted pendulum to move to the $\theta = \pi$ position. In this case, vibrating the inverted pendulum at 1 rad/sec with a small amplitude does not change the stability. However, increasing the amplitude to any value in the gray region would cause it to become stable.

As we have shown, parametric excitation can stabilize a system. However, it can also destabilize a system when the parametric excitation is applied at twice the system's primary resonance. In the follow chapters, we examine how a system responds to 2:1 parametric excitation in the presence of a second parametric driver (Chapter 3), in the presence of a Hopf bifurcation (Chapter 4), and in the presence of nonlinearities and delay (Chapter 5).

Chapter 3

2:1:1 Resonance in a Quasiperiodic Mathieu Equation

"The important thing is not to stop questioning."   – *Albert Einstein*

We present a small ε perturbation analysis of the quasiperiodic Mathieu equation

$$\ddot{x} + (\delta + \varepsilon \cos t + \varepsilon \cos \omega t)\, x = 0$$

in the neighborhood of the point $\delta = 0.25$ and $\omega = 0.5$. We use multiple scales including terms of $O(\varepsilon^2)$ with three time scales. We obtain an asymptotic expansion for the associated instability region. Comparison with numerical integration shows good agreement for $\varepsilon = 0.1$. Then, we use the algebraic form of the perturbation solution to approximate scaling factors which are conjectured to determine the size of instability regions as we move from one resonance to another in the δ-ω parameter plane. The chapter title is explained by noting the equation above may be viewed as an oscillator with natural frequency $\sqrt{\delta}$ which is parametrically forced with frequencies 1 and ω. Near the point $\delta = 0.25$ and $\omega = 0.5$, the three frequencies are in the ratio of 2:1:1.

3.1 Motivation

The following quasiperiodic Mathieu equation,

$$\ddot{x} + (\delta + \varepsilon \cos t + \varepsilon \cos \omega t)\, x = 0 \tag{3.1}$$

has been the topic of a number of recent research papers [72],[51]-[9]. In particular, the stability of equation (3.1) has been investigated. Zounes and Rand [72] showed that for given parameters $(\varepsilon, \delta, \omega)$, equation (3.1) is said to be stable if all solutions are bounded, and unstable if an unbounded solution exists.

3.2 Introduction

A system with two parametric drives is modeled as the quasiperiodic Mathieu equation, represented by equation (3.1), where δ is the natural frequency squared of the unforced system. One driver provides 2:1 parametric excitation, while the other provides 1:1 excitation if $\omega = 0.5$. In Chapter 2, we presented the stability chart for the Mathieu equation, $\ddot{x} + (\delta + \varepsilon \cos t)x = 0$. We show the lowest order stability chart in Figure 3.1.

When a second parametric driver is added to the Mathieu equation, we retrieve the quasiperiodic Mathieu equation (3.1). When we examine the equation to the lowest order, we find the second driver adds a second instability tongue in the stability chart, see Figure 3.2.

The stability charts in Figure 3.1 and 3.2 are plotted in the δ-ε plane. We replot the stability chart in the δ-ω plane for the quasiperiodic Mathieu equation in Figure 3.3 for $\varepsilon = 0.1$. Note the overlapping of the instability tongues at $\delta = \frac{1}{4}$.

$$\delta = \frac{1}{4} \pm \frac{\varepsilon}{2} + O(\varepsilon^2)$$
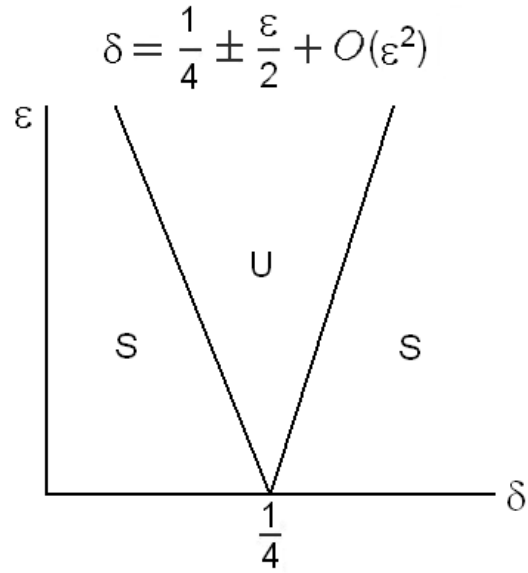
Figure 3.1: Stability chart for the Mathieu equation $\varepsilon < 1$. The lowest order equation is given for the instability tongue. U is unstable, S is stable.

$$\delta_{2:1} = \frac{1}{4} \pm \frac{\varepsilon}{2} + O(\varepsilon^2) \qquad \delta_{\omega:1} = \frac{\omega}{4} \pm \frac{\varepsilon}{2} + O(\varepsilon^2)$$
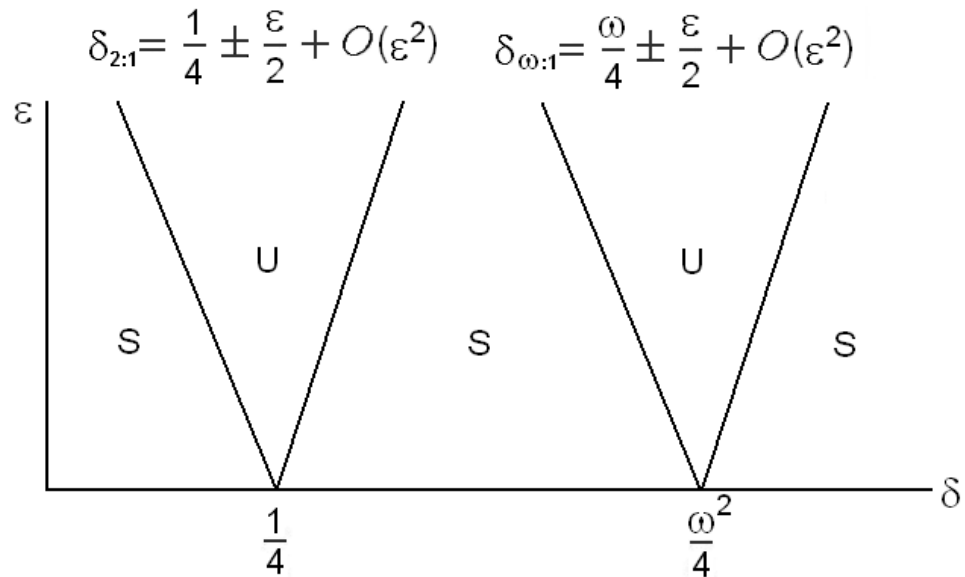
Figure 3.2: Stability chart for the quasiperiodic Mathieu equation $\varepsilon < 1$. The lowest order equations are given for the instability tongues. U is unstable, S is stable.
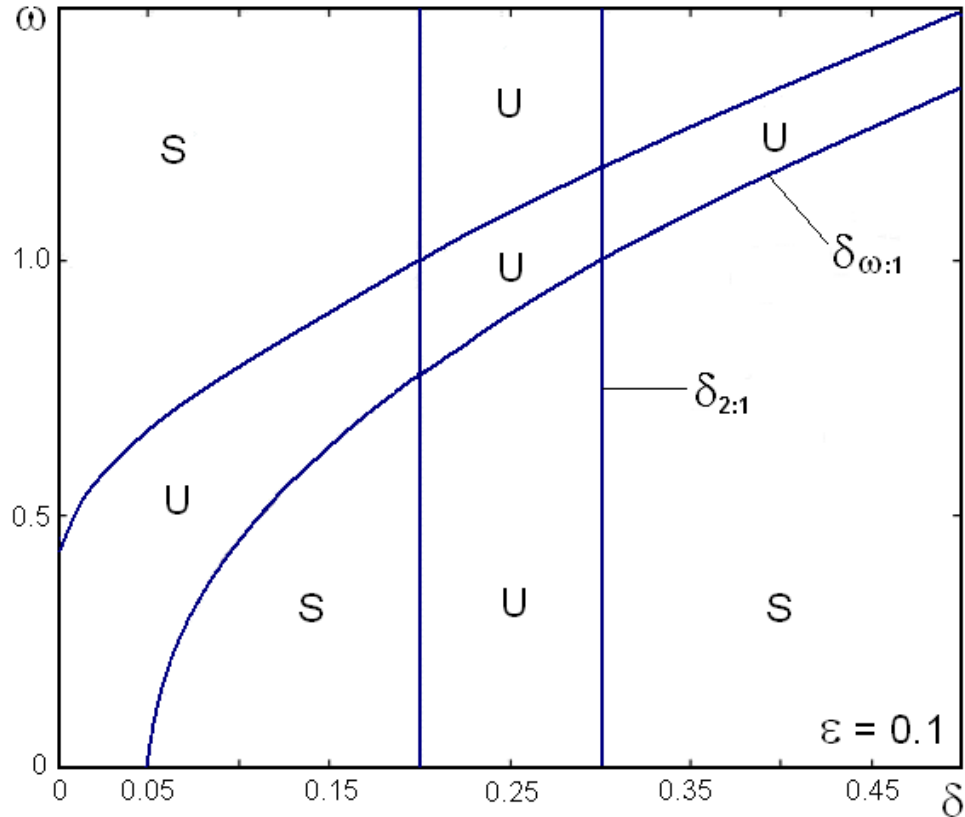
Figure 3.3: Stability chart for the quasiperiodic Mathieu equation in the δ-ω plane for $\varepsilon = 0.1$. $\delta_{2:1}$ and $\delta_{\omega:1}$ are the equations for the instability tongues given in Figure 3.2. This figure is based on the lowest order analytic approximation of Figure 3.2, in contrast with Figure 3.4 which is based on the numerical integration of equation (3.1). U is unstable, S is stable.

The stability of equation (3.1) has been investigated by Zounes [72]. In the previous work, it was shown for given parameters $(\varepsilon, \delta, \omega)$, equation (3.1) is said to be stable if all solutions are bounded, and unstable if an unbounded solution exists. A stability chart in the δ-ω plane was generated for equation (3.1) with $\varepsilon = 0.1$, and is shown in Figure 3.4. The chart was obtained by numerically integrating equation (3.1). A striking feature of this complicated figure is that various details
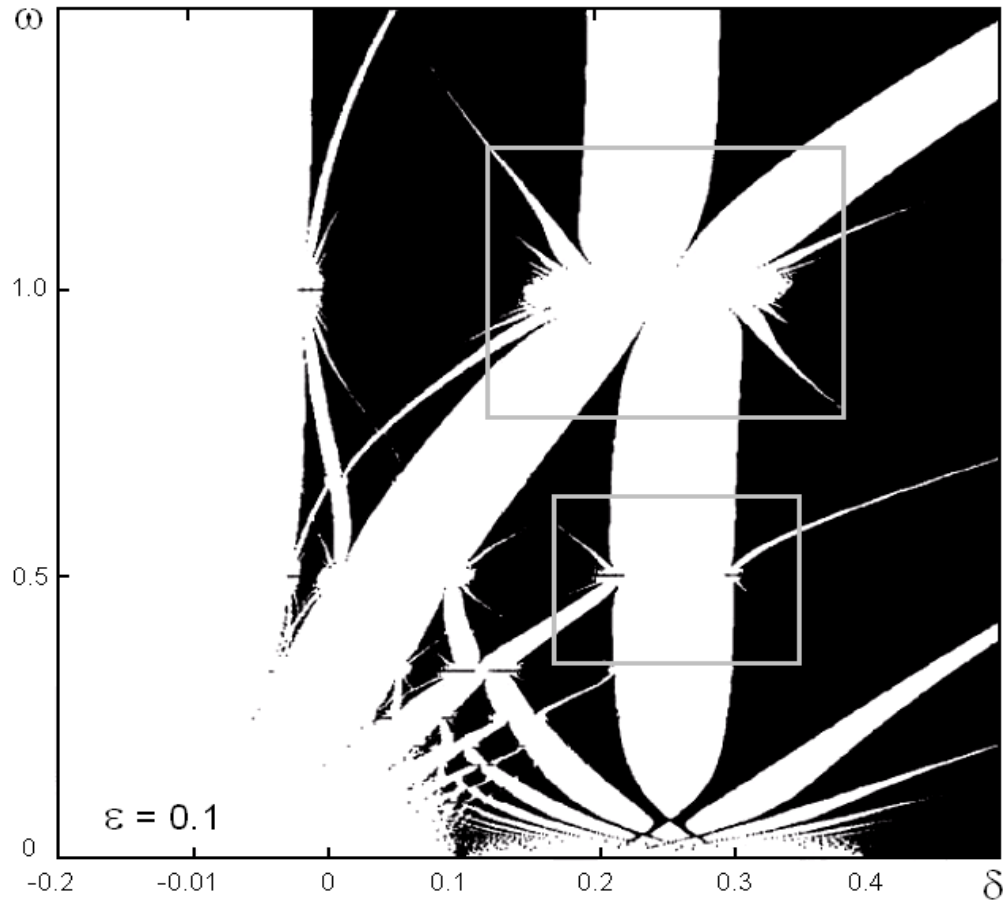
Figure 3.4: Stability diagram of equation (3.1) from Zounes, [72]. This figure is based on the numerical integration of equation (3.1), in contrast with Figure 3.3, which is based on the lowest order analytic approximation of Figure 3.2. White regions are unstable, black regions are stable.

appear to be repeated at different length scales (see the two rectangles). For example, the shape of the instability regions around the point $\delta = 0.25$ and $\omega = 1$ appear to be similar to those near the point $\delta = 0.25$ and $\omega = 0.5$, except that the latter regions are smaller in scale.

The purpose of this work is to investigate this similarity, and to obtain a scaling law which relates the two regions boxed in Figure 3.4 above [49]. Our approach

Figure 3.5: Transition curves near $\delta = 0.25$ and $\omega = 1$ based on equation (3.2) from [19]. Compare with Figure 3.4.

will be based on approximate solutions obtained by perturbation methods. In the case of the instability regions near the point $\delta = 0.25$ and $\omega = 1$, a perturbation analysis has been performed by Rand et al in [48], giving approximate closed form expressions for the transition curves separating regions of stability from regions of instability. For example, the following approximate expression was derived for the largest of the local instability regions near $\delta = 0.25$ and $\omega = 1$, see Figure 3.5:

$$\omega = 1 + \varepsilon \left(S \pm \left(\frac{1}{2} + \frac{\delta_1}{S} \right) \right) + O(\varepsilon^2) \tag{3.2}$$

where

$$\delta = \frac{1}{4} + \delta_1 \varepsilon \quad \text{and} \quad S = \sqrt{4\delta_1^2 - 1} \tag{3.3}$$

In the present work we use a different perturbation method to obtain a comparable approximate expression for the largest of the local instability regions near $\delta = 0.25$ and $\omega = 0.5$. By comparing the two expressions we are able to determine scaling factors which relate their relative sizes.

3.3   Method of Multiple Time Scales

We use the method of multiple time scales on equation (3.1), with the goal of obtaining an approximate expression for transition curves in the neighborhood of $\delta = 0.25$ and $\omega = 0.5$. To accomplish this, we found it necessary to go to $O(\varepsilon^2)$ and to use three time scales:

$$\xi = t, \quad \eta = \varepsilon\, t, \quad \text{and} \quad \zeta = \varepsilon^2\, t \tag{3.4}$$

As usual in this method [42] the dependent variable x becomes a function of ξ, η, and ζ, giving a new expression for the second derivative of x in equation (3.1):

$$\frac{d^2 x}{dt^2} = \frac{\partial^2 x}{\partial \xi^2} + 2\varepsilon\, \frac{\partial^2 x}{\partial \xi \partial \eta} + \varepsilon^2\, \frac{\partial^2 x}{\partial \eta^2} + 2\varepsilon^2\, \frac{\partial^2 x}{\partial \xi \partial \zeta} + O(\varepsilon^3) \tag{3.5}$$

We expand x, ω, and δ as a power series of ε:

$$x = x_0 + \varepsilon\, x_1 + \varepsilon^2\, x_2 + \cdots$$

$$\omega = \tfrac{1}{2} + \varepsilon\, \omega_1 + \varepsilon^2\, \omega_2 + \cdots \tag{3.6}$$

$$\delta = \tfrac{1}{4} + \varepsilon\, \delta_1 + \varepsilon^2\, \delta_2 + \cdots$$

and substitute these series into equations (3.1) and (3.5) and collect terms in ε. Using subscripts to represent partial differentiation, we obtain:

$$\varepsilon^0 : \quad x_{0,\xi\xi} + \frac{1}{4} x_0 = 0 \tag{3.7}$$

$$\varepsilon^1 : \quad x_{1,\xi\xi} + \frac{1}{4}x_1 = -2x_{0,\xi\eta} - \delta_1 x_0 - x_0 \ \cos\xi$$

$$- x_0 \cos\left(\frac{\xi}{2} + \omega_1\eta + \omega_2\zeta\right) \tag{3.8}$$

$$\varepsilon^2 : \quad x_{2,\xi\xi} + \frac{1}{4}x_2 = -2x_{0,\xi\zeta} - x_{0,\eta\eta} - 2x_{1,\xi\eta} - \delta_2 x_0 - \delta_1 x_1$$

$$- x_1 \cos\xi - x_1 \ \cos\left(\frac{\xi}{2} + \omega_1\eta + \omega_2\zeta\right) \tag{3.9}$$

We write the solution to equation (3.7) in the form

$$x_0(\xi, \eta, \zeta) = A(\eta, \zeta) \cos\frac{\xi}{2} + B(\eta, \zeta) \sin\frac{\xi}{2} \tag{3.10}$$

where A and B are as yet undetermined slowly varying coefficients. We substitute equation (3.10) into equation (3.8) and remove resonant terms to retrieve the following equations on A and B:

$$A_\eta = (\delta_1 - \frac{1}{2})B \qquad\qquad B_\eta = -(\delta_1 + \frac{1}{2})A \tag{3.11}$$

Here, $A_\eta = \frac{\partial A}{\partial \eta}$ and $B_\eta = \frac{\partial B}{\partial \eta}$. Equations (3.11) have the solution:

$$A(\eta, \zeta) = A_1(\zeta) \ \cos\frac{S}{2}\eta + A_2(\zeta) \ \sin\frac{S}{2}\eta \tag{3.12}$$

The coefficient $B(\eta, \zeta)$ has a similar expression, where $S = \sqrt{4\delta_1^2 - 1}$. A_1 and A_2 are as yet undetermined slowly varying coefficients.

Having removed resonant terms from equation (3.8), we may solve for x_1, which may be written in the abbreviated form:

$$x_1(\xi, \eta, \zeta) = C(\eta, \zeta) \cos\frac{\xi}{2} + D(\eta, \zeta) \sin\frac{\xi}{2} + \text{periodic terms} \tag{3.13}$$

where the first two terms on the RHS of equation (3.13) are the complementary solution of equation (3.8) involving as yet undetermined slowly varying coefficients

$C(\eta, \zeta)$ and $D(\eta, \zeta)$. The "periodic terms" represent a particular solution of equation (3.8). Although the expressions for these are too long to give here, we note that they consist of sinusoidal terms with arguments

$$\frac{3}{2}\xi \pm \frac{S}{2}\eta, \qquad \omega_1 \eta + \omega_2 \zeta \pm \frac{S}{2}\eta, \quad \text{and} \quad \xi + \omega_1 \eta + \omega_2 \zeta \pm \frac{S}{2}\eta \qquad (3.14)$$

Next we substitute the expressions for x_0 and x_1, equations (3.10) and (3.13), and the expressions for A and B, equation (3.12), into the x_2 equation, equation (3.9), and eliminate resonant terms. This gives equations on C and D which may be written in the following form:

$$C_\eta = (\delta_1 - \tfrac{1}{2})D + \text{periodic terms}$$
$$\tag{3.15}$$
$$D_\eta = -(\delta_1 + \tfrac{1}{2})C + \text{periodic terms}$$

Although the expressions for the "periodic terms" again are too long to give here, we note that they consist of sinusoidal terms with arguments

$$\frac{S}{2}\eta, \qquad (2\omega_1 \pm \frac{S}{2})\eta + 2\omega_2 \zeta, \quad \text{and} \quad (2\omega_1 \pm \frac{S}{2})\eta - 2\omega_2 \zeta \qquad (3.16)$$

Note that equations (3.15) on the arbitrary coefficients C and D of x_1 are similar in form to the equations (3.11) on the arbitrary coefficients A and B of x_0, except that the C-D equations are nonhomogeneous. Thus our next step is to remove resonant terms from equations (3.15). Since $S = \sqrt{4\delta_1^2 - 1}$, we see that the periodic terms in equations (3.15) which have argument $\frac{S}{2}\eta$ are resonant. For general values of ω_1, these are the only resonant terms. However, if $\omega_1 = S/2$, then some of the other periodic terms in equation (3.15) will be resonant as well, because in that case $(2\omega_1 - \frac{S}{2})\eta = \frac{S}{2}\eta$.

First we consider the case in which ω_1 does not equal $S/2$. Eliminating resonant terms in equation (3.15) turns out to give the following equations on the slow flow

coefficients A_1 and A_2 which appeared in the expressions (3.12) for A and B:

$$A_{1\zeta} = -p \ A_2 \qquad\qquad A_{2\zeta} = \ p \ A_1 \qquad\qquad (3.17)$$

where

$$p = \delta_1 \frac{(24\delta_2 - 24\delta_1^2 - 7)}{12 \ S} \qquad\qquad (3.18)$$

Since all solutions to equations (3.17) are periodic and bounded, no instability is possible.

Next we consider the resonant case in which $\omega_1 = S/2$. Elimination of resonant terms in equation (3.15) gives:

$$A_{1\zeta} = -p \ A_2 + q \ (-A_1 \ \sin 2\omega_2\zeta + A_2 \ \cos 2\omega_2\zeta)$$

$$A_{2\zeta} = \ p \ A_1 + q \ (\ A_2 \ \sin 2\omega_2\zeta + A_1 \ \cos 2\omega_2\zeta) \qquad\qquad (3.19)$$

where p is given by equation (3.18), and where q is given by the following equation:

$$q = \frac{1}{2} + \frac{\delta_1}{S} \qquad\qquad (3.20)$$

As we show in the next section, equations (3.19) exhibit unbounded solutions. Parameter values for which unbounded solutions occur in (3.19) correspond to regions of instability in the stability diagram.

3.4 Analysis of the Slow Flow

To investigate stability, we write the slow flow system (3.19) in the form:

$$\dot{u} \ = \ -p \ v + q \ (-u \ \sin \Omega t + v \ \cos \Omega t) \qquad\qquad (3.21)$$

$$\dot{v} \ = \ \ p \ u + q \ (\ v \ \sin \Omega t + u \ \cos \Omega t) \qquad\qquad (3.22)$$

where A_1, A_2, $2\omega_2$ and ζ have been replaced respectively by u, v, Ω and t for convenience. We begin by transforming (3.21) to polar coordinates, $u = r\cos\theta$, $v = r\sin\theta$:

$$\dot{r} = -q\ r\ \sin(\Omega t - 2\theta) \tag{3.23}$$

$$\dot{\theta} = p + q\ \cos(\Omega t - 2\theta) \tag{3.24}$$

Next we replace θ by $\phi = \Omega t - 2\theta$:

$$\dot{r} = -q\ r\ \sin\phi \tag{3.25}$$

$$\dot{\phi} = \Omega - 2p - 2q\ \cos\phi \tag{3.26}$$

Writing equations (3.25) in first order form,

$$\frac{dr}{d\phi} = \frac{-q\ r\ \sin\phi}{\Omega - 2p - 2q\ \cos\phi} \tag{3.27}$$

The general solution to equation (3.27) is:

$$r = \frac{\text{const}}{\sqrt{\Omega - 2p - 2q\ \cos\phi}} \tag{3.28}$$

Equation (3.28) represents a curve in the u-v plane. If the denominator of the RHS vanishes for some value of ϕ, then the curve extends to infinity and the corresponding motion is unstable. This case corresponds to the existence of an equilibrium point in the ϕ equation (the second of equations (3.25)). In the contrary case in which the denominator of the RHS of equation (3.28) does not vanish, the motion remains bounded (stable) and the ϕ equation has no equilibria. Thus the condition for instability is that the following equation has a real solution:

$$\cos\phi = \frac{\Omega - 2p}{2q} \tag{3.29}$$

The transition case between stable and unstable is given by the condition:

$$\frac{\Omega - 2p}{2q} = \pm 1 \qquad \Rightarrow \qquad \Omega = 2p \pm 2q \tag{3.30}$$

Substituting equations (3.18) and (3.20) and using $\Omega = 2\omega_2$, equation (3.30) becomes:

$$\omega_2 = \delta_1 \frac{(24\delta_2 - 24\delta_1^2 - 7)}{12\ S} \pm \left(\frac{1}{2} + \frac{\delta_1}{S} \right) \tag{3.31}$$

where $S = \sqrt{4\delta_1^2 - 1}$. In addition, for resonance we required that

$$\omega_1 = \frac{S}{2} \tag{3.32}$$

Thus we obtain the following expression for transition curves near $\delta = 0.25$ and $\omega = 0.5$:

$$\omega = \frac{1}{2} + \varepsilon \frac{S}{2} + \varepsilon^2 \left(\delta_1 \frac{(24\delta_2 - 24\delta_1^2 - 7)}{12\ S} \pm \left(\frac{1}{2} + \frac{\delta_1}{S} \right) \right) + \cdots \tag{3.33}$$

where

$$\delta = \frac{1}{4} + \varepsilon \delta_1 + \varepsilon^2 \delta_2 + \cdots \tag{3.34}$$

equation (3.33) gives a value of ω for a given value of δ, the latter defined by δ_1, δ_2 and ε. However, for a given value of ε, any value of δ close to 0.25 can be achieved in the form $1/4 + \varepsilon\delta_1$, that is by choosing $\delta_2 = 0$. So in our numerical evaluation of equations (3.33) and (3.34), we take $\delta_2 = 0$. The transition curves in (3.33) are displayed in Figure 3.6 for $\varepsilon = 0.1$ along with the results of previous work, equation (3.2), already displayed in Figure 3.5. (Cf. Figure 3.4).

3.5   Discussion

We now have asymptotic approximations for corresponding instability regions at two points in the δ-ω parameter plane, and we wish to compare them. Based on an expansion about the point $\delta = 0.25$ and $\omega = 1$, we have equation (3.2) from [48]. And from the work presented in this paper, we have equation (3.33), valid in the neighborhood of $\delta = 0.25$ and $\omega = 0.5$. We repeat these expansions here for
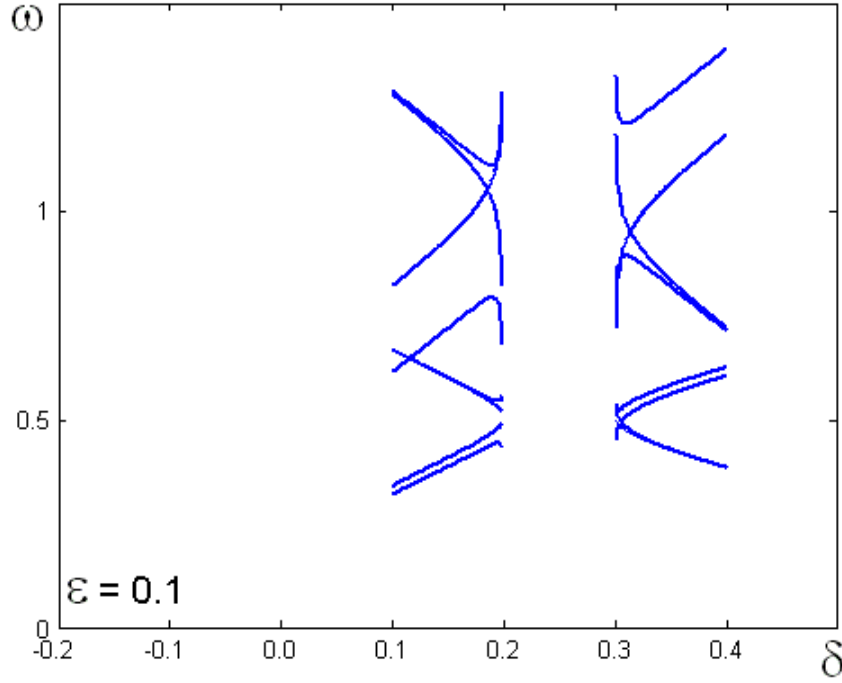
Figure 3.6: Transition curves near $\delta = 0.25$ and $\omega = 0.5$ based on equation (30). Also shown for comparison are th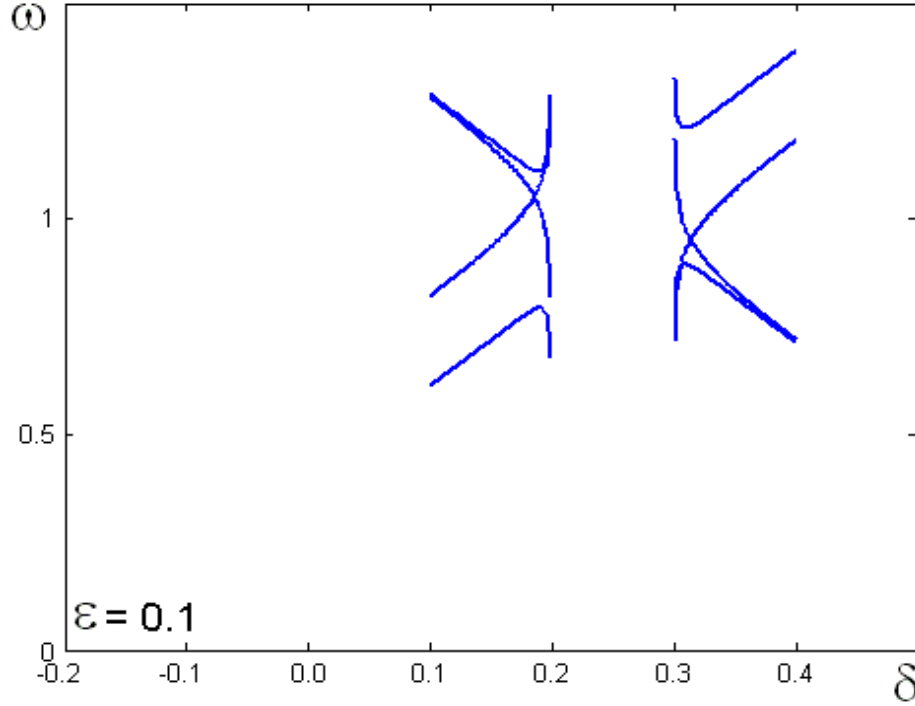e transition curves near $\delta = 0.25$ and $\omega = 1$ based on equation (3.2) from [48]. Compare with Figures 3.4 and 3.5.

the convenience of the reader, using the subscript A for equation (3.2), and the subscript B for equation (3.33):

$$\omega_A = 1 + \varepsilon \left(S \pm \left(\frac{1}{2} + \frac{\delta_1}{S} \right) \right) + O(\varepsilon^2) \tag{3.35}$$

$$\omega_B = \frac{1}{2} + \varepsilon \frac{S}{2} + \varepsilon^2 \left(\delta_1 \frac{(-24\delta_1^2 - 7)}{12\,S} \pm \left(\frac{1}{2} + \frac{\delta_1}{S} \right) \right) + O(\varepsilon^3) \tag{3.36}$$

Note that although these expansions are truncated at different orders of ε, both are the lowest order approximations which respectively yield two transition curves (as represented by the $\pm$ sign), and which therefore allow the thickness of the associated instability region to be computed.

We compare these two expressions in two ways: 1) the centerline of the region, and 2) the thickness of the region.

In the δ-ε plane, the centerline is the location where the tongues intersect the δ-axis, i.e., the tongue has no thickness (cf. Figure 3.2). The respective centerlines in the δ-ω plane are given by the following approximations:

$$\omega_A = 1 + \varepsilon S + O(\varepsilon^2) \tag{3.37}$$

$$\omega_B = \frac{1}{2} + \varepsilon \frac{S}{2} + O(\varepsilon^2) \tag{3.38}$$

From these we may conjecture that the scaling of the centerline in the ω direction goes like ω_0, being the ω value of the point of expansion. That is, in the case of equation (3.37), $\omega_0 = 1$, while for equation (3.38), $\omega_0 = 1/2$, and we observe that the two curves have comparable curvature, but that they are stretched in the ω direction in proportion to their values of ω_0.

Moving on to the question of the thickness of the two instability regions, these are obtained by subtracting the expressions for the upper and lower transition curves, and are given by the following approximations:

$$\text{thickness}_A = 2\varepsilon \left(\frac{1}{2} + \frac{\delta_1}{S} \right) + O(\varepsilon^2) \tag{3.39}$$

$$\text{thickness}_B = 2\varepsilon^2 \left(\frac{1}{2} + \frac{\delta_1}{S} \right) + O(\varepsilon^3) \tag{3.40}$$

We see that once again the two expressions have the same general form, but that the smaller region is a factor of ε thinner than the larger region. This leads us to the conjecture that this is due to the difference in the order of the resonance. For example, this would lead to the guess that the comparable instability region associated with the point $\delta = 0.25$ and $\omega = 1/3$ (which would correspond to a $2 : \frac{2}{3} : 1$ resonance) would have a similar equation for its thickness, but with an ε^3 in the leading term.

3.6 Conclusions

We have presented a small ε perturbation analysis of the quasiperiodic Mathieu equation (3.1) in the neighborhood of the point $\delta = 0.25$ and $\omega = 0.5$. We used multiple scales and found that we needed to go to $O(\varepsilon^2)$ and use three time scales in order to obtain a minimal representation of an instability region. Comparison with numerical integration of equation (3.1) showed good agreement for $\varepsilon = 0.1$.

We used the perturbation approximation to estimate the scaling of instability regions as we go from one resonance to another in the δ-ω parameter plane. This is an interesting use of perturbation approximations. A comparable result could not be easily achieved by purely numerical methods. For example, inspection of Figure 3.4 would lead us to conclude that the instability region near $\delta = 0.25$ and $\omega = 1$ is much thicker than the comparable region near $\delta = 0.25$ and $\omega = 0.5$. However, it would be difficult to conclude using only numerical results that the ratio of thicknesses was approximately ε, as we showed in this investigation.

Chapter 4

2:1 Resonance Near a Hopf Bifurcation

> *"Never, never, never give up."*   *– Winston Churchill*

We investigate the dynamics of a system consisting of a simple harmonic oscillator with small nonlinearity, damping and parametric forcing in the neighborhood of 2:1 resonance:

$$\ddot{z} + \varepsilon A\dot{z} + (1 + \varepsilon k_1 + \varepsilon B \cos 2t)z + \varepsilon(\beta_1 z^3 + \beta_2 z^2 \dot{z} + \beta_3 z \dot{z}^2 + \beta_4 \dot{z}^3) = 0$$

where A is linear damping, k_1 is detuning off the 2:1 resonance, B is the amplitude of parametric forcing, the β_i's are the coefficients of nonlinear terms, and $\varepsilon << 1$. The unforced system ($B=0$) exhibits the birth of a stable limit cycle as damping changes sign from positive to negative. Using perturbation methods and numerical integration, we show that for large positive damping, the origin is stable, whereas for large negative damping a quasi-periodic behavior occurs. These two steady states are connected by a complicated series of bifurcations which occur as the damping is varied.

4.1 Motivation

Our interest in understanding the behavior of equation (4.3) is motivated by two applications. The first is a model of the El Niño Southern Oscillation (ENSO) coupled tropical ocean-atmosphere weather phenomenon [61] and [62] in which the state variables are temperature and depth of a region of the ocean called the thermocline. The annual seasonal cycle is the parametric excitation. The model exhibits a Hopf bifurcation in the absence of parametric excitation.

The second application involves a MEMS device [69] and [39] consisting of a 30 μm diameter silicon disk which can be made to vibrate by heating it with a laser beam resulting in a Hopf bifurcation. The parametric excitation is provided by making the laser beam intensity vary periodically in time.

Parametric excitation of a Hopf bifurcation was previously investigated from a mathematical point of view [3], [16], [40], [33]. In this chapter, we examine the parametrically excited Hopf with relevance to physical applications [46] and [47].

4.2 Introduction

It is well-known that a limit cycle may be born in a process called a Hopf bifurcation. A typical setting is given by the autonomous equation:

$$\ddot{z} + z + \varepsilon A \dot{z} + \varepsilon(\beta_1 z^3 + \beta_2 z^2 \dot{z} + \beta_3 z \dot{z}^2 + \beta_4 \dot{z}^3) = 0 \qquad (4.1)$$

where $\varepsilon << 1$ is a perturbation parameter. Here εA is a linear damping coefficient and the $\varepsilon \beta_i$ are coefficients of nonlinear terms. The bifurcations associated with the system where $A = 0$ was investigate by Ng and Rand [36]-[37]. Perturbation theory [42] shows that equation (4.1) exhibits a limit cycle with amplitude r, where

$$r^2 = -\frac{4A}{3\beta_4 + \beta_2} \qquad (4.2)$$

In the case that $3\beta_4 + \beta_2 > 0$, equation (4.2) gives that the limit cycle occurs for $A < 0$. From (4.1), the origin $z = \dot{z} = 0$ is unstable for $A < 0$ (negative damping), and so the limit cycle, which has the opposite stability from that of the origin, is in this case stable, a situation which is referred to as a supercritical Hopf.

In this chapter we investigate what happens when the system in (4.1) is parametrically excited at close to twice the natural frequency of the linearized undamped system:

$$\ddot{z} + (1 + \varepsilon k_1 + \varepsilon B \cos 2t)z + \varepsilon A\dot{z} + \varepsilon(\beta_1 z^3 + \beta_2 z^2 \dot{z} + \beta_3 z\dot{z}^2 + \beta_4 \dot{z}^3) = 0 \quad (4.3)$$

where k_1 is a detuning coefficient and B is the amplitude of parametric forcing.

The linearized undamped version of equation (4.3) is known as Mathieu's equation:

$$\ddot{z} + (1 + \varepsilon k_1 + \varepsilon B \cos \omega t)z = 0 \quad (4.4)$$

where ω is the frequency of the parametric excitation. It is well-known [35] that for small ε the largest instability occurs for $\omega = 2$, a situation referred to as 2:1 parametric resonance, which motivates our choice of $\omega = 2$ in equation (4.3) (cf Chapter 2).

4.3 Two-Variable Expansion Method

We use the two-variable expansion method to investigate the dynamics of equation (4.3) for small ε [42] and [18]. We define two new time scales, $\xi = t$ and $\eta = \varepsilon t$, where η is referred to as slow time. Equation (4.3) becomes:

$$
\begin{aligned}
z_{\xi\xi} \;+\; 2\varepsilon z_{\xi\eta} \;+\;&(1 + \varepsilon k_1 + \varepsilon B \cos 2\xi)z \;+\; \varepsilon A z_\xi \\
+\;&\varepsilon(\beta_1 z^3 + \beta_2 z^2 z_\xi + \beta_3 z z_\xi^2 + \beta_4 z_\xi^3) \;=\; O(\varepsilon^2) \quad (4.5)
\end{aligned}
$$

Next we expand $z = z_0 + \varepsilon z_1 + O(\varepsilon^2)$ and collect terms, giving:

$$\varepsilon^0 : \quad z_{0\xi\xi} + z_0 = 0 \tag{4.6}$$

$$\varepsilon^1 : \quad z_{1\xi\xi} + z_1 = -2z_{0\xi\eta} - k_1 z_0 - B z_0 \cos 2\xi - A z_{0\xi}$$

$$-(\beta_1 z_0{}^3 + \beta_2 z_0{}^2 z_{0\xi} + \beta_3 z_0 z_{0\xi}{}^2 + \beta_4 z_{0\xi}{}^3) \tag{4.7}$$

We take the solution of (4.6) to be

$$z_0 = u(\eta)\cos\xi + v(\eta)\sin\xi \tag{4.8}$$

where u and v depend only on slow time η. We substitute (4.8) into (4.7) and remove resonant terms to retrieve the following slow flow:

$$u_\eta = -\frac{A}{2}u + \left(\frac{k_1}{2} - \frac{B}{4}\right)v + \frac{1}{8}(\Gamma_1 v - \Gamma_2 u)(u^2 + v^2) \tag{4.9}$$

$$v_\eta = -\frac{A}{2}v - \left(\frac{k_1}{2} + \frac{B}{4}\right)u - \frac{1}{8}(\Gamma_1 u + \Gamma_2 v)(u^2 + v^2) \tag{4.10}$$

Note that the coefficients β_1, β_2, β_3, and β_4 occur in the combinations $3\beta_1 + \beta_3$ and $\beta_2 + 3\beta_4$ directly from the averaging process. We observe that this represents a natural grouping becuase the β_1 and β_3 terms in equation (4.1) are conservative, whereas the β_2 and β_4 are dissipative. Hence, we define:

$$\Gamma_1 = 3\beta_1 + \beta_3, \qquad \Gamma_2 = \beta_2 + 3\beta_4 \tag{4.11}$$

We may obtain an alternate form of the slow flow equations (4.9) and (4.10) by transforming from rectangular coordinates u and v to polar coordinates r and θ via $u = r\cos\theta$ and $v = r\sin\theta$, giving:

$$r_\eta = -\frac{r}{8}(4A + \Gamma_2 r^2 + 2B\sin 2\theta) \tag{4.12}$$

$$\theta_\eta = -\frac{1}{8}(4k_1 + \Gamma_1 r^2 + 2B\cos 2\theta) \tag{4.13}$$

where $r > 0$ and θ depend only on slow time η.

4.4 Analysis of Slow Flow

In the following sections, we analyze the slow flow for equilibria and limit cycles and examine the bifurcations that accompany any changes in stability.

4.4.1 Equilibria

Equation (4.8) tells us the nontrivial equilibria $(r \neq 0)$ of the slow flow (4.12) and (4.13) correspond to limit cycles in the original equation (4.3). These equilibria satisfy $r_\eta = \theta_\eta = 0$:

$$4A + \Lambda\Gamma_1\rho + 2B \sin 2\theta = 0 \tag{4.14}$$

$$4\kappa A + \Gamma_1\rho + 2B \cos 2\theta = 0 \tag{4.15}$$

where we define

$$\rho = r^2, \qquad k_1 = \kappa A, \qquad \Lambda = \frac{\Gamma_2}{\Gamma_1} = \frac{\beta_2 + 3\beta_4}{3\beta_1 + \beta_3} \tag{4.16}$$

Note that although $\rho = r^2$ must be positive for real solutions, there are no sign restrictions on κ and Λ.

Solving (4.14) and (4.15) respectively for $\sin 2\theta$ and $\cos 2\theta$, and using the identity $\sin^2 2\theta + \cos^2 2\theta = 1$, we obtain the following condition on ρ:

$$(\Lambda^2 + 1)\Gamma_1^2\rho^2 + 8A\left(\Lambda + \kappa\right)\Gamma_1\rho + 4\left(4A^2(1 + \kappa^2) - B^2\right) = 0 \tag{4.17}$$

Equation (4.17) is a quadratic on ρ. For real roots, the discriminant must be nonnegative. This gives the condition:

$$\frac{A^2}{B^2} \leq \frac{1}{4}\frac{1 + \Lambda^2}{(1 - \kappa\Lambda)^2} \tag{4.18}$$

In addition, $\rho = r^2$ must be nonnegative. Allowable (nonnegative) values of ρ will be separated from rejected (negative) values of ρ by the condition $\rho = 0$, which

gives:

$$P^2 = \frac{A^2}{B^2} = \frac{1}{4(1 + \kappa^2)} \tag{4.19}$$

From this we are led to define $P = A/B$, the ratio of linear damping coefficient A to parametric forcing amplitude B. P turns out to be an important bifurcation parameter for this system. If we fix the parameters β_i and κ, then we may envision a line parameterized by $P = A/B$ which contains 4 key bifurcation points, $P_1 \leq P_2 < P_3 \leq P_4$:

$$P_1 = -\frac{1}{2}\sqrt{\frac{1 + \Lambda^2}{(1 - \kappa\Lambda)^2}} \qquad P_2 = -\frac{1}{2}\frac{1}{\sqrt{(1 + \kappa^2)}}$$

$$P_3 = \frac{1}{2}\frac{1}{\sqrt{(1 + \kappa^2)}} \qquad P_4 = \frac{1}{2}\sqrt{\frac{1 + \Lambda^2}{(1 - \kappa\Lambda)^2}} \tag{4.20}$$

From equations (4.18) and (4.19) we see that each of these points may represent a change in the number of slow flow equilibria. Equation (4.18) tells us that there are no nontrivial slow flow equilibria to the left of P_1 and to the right of P_4. It also tells us that there are two real roots for $\rho = r^2$ in the interval between P_1 and P_4. However, this does not mean that there are two allowable values of $r > 0$ in this region because some or all of these roots ρ may be negative.

We now appeal to Descartes' Rule of Signs to draw conclusions as to the number of admissible values of r in the interval between P_1 and P_4. To be specific, we assume $(\Lambda + \kappa)\Gamma_1$ and B are positive, although similar conclusions can be drawn in the general case.

First let's consider the case that $A > 0$. If $P > P_3$ then the signs in equation (4.17) are $+ + +$ which tells us that there are no positive roots ρ to the right of P_3, and hence no nontrivial slow flow equilibria to the right of P_3. If $0 < P < P_3$ then the signs in equation (4.17) are $+ + -$ which tells us that there is one positive

and one negative root ρ, which means there is a single admissible value of r in the interval between $P = 0$ and $P = P_3$.

Next, let's consider the case that $A < 0$. If $-P_2 < P < 0$ the signs are $+ \ - \ -$ which again means that there is a single admissible value of r, this time in the interval between $P = P_2$ and $P = 0$. On the other hand, if $P < P_2$ the signs are $+ \ - \ +$ which means that there are no negative roots ρ in the interval between P_1 and P_2. However, we have seen that there are 2 real roots ρ in this interval (from the positiveness of the discriminant), and thus we may conclude that there are 2 positive roots ρ and thus 2 admissible values for r between P_1 and P_2.

Now it turns out that each of the admissible values of r corresponds to a pair of nontrivial slow flow equilibria. This may be seen by considering the value of θ at these equilibrium points. Eliminating ρ from equations (4.14) and (4.15) gives

$$- \sin 2\theta + \Lambda \cos 2\theta = 2\frac{A}{B}(1 - \Lambda\kappa) \tag{4.21}$$

which may be written as

$$\cos(2\theta + \psi) = 2\frac{A}{B}\frac{1 - \Lambda\kappa}{\sqrt{1 + \Lambda^2}} \tag{4.22}$$

where the phase angle ψ satisfies $\cot\psi = \Lambda$. Now if A/B in equation (4.22) corresponds to a value which gives a real positive value for r, then equation (4.22) gives two values for θ which differ by 180 degrees. Thus each admissible value of r found above corresponds to two slow flow equilibria which are located symmetrically with respect to the origin. This may be seen by noting that equations (4.9) and (4.10) are invariant under the transformation $(u, v) \mapsto (-u, -v)$, which means that if (u, v) is a slow flow equilibrium, then so is $(-u, -v)$.

In summary, we have shown that the number of slow flow equilibria (including

the origin $r = 0$) depends on the value of $P = A/B$, as follows:

$$[-\infty, P_1] \quad \text{1 equilibrium}$$

$$[P_1, P_2] \quad \text{5 equilibria}$$

$$[P_2, P_3] \quad \text{3 equilibria}$$

$$[P_3, +\infty] \quad \text{1 equilibrium}$$

This chart is based on the following assumptions:

$$(\Lambda + \kappa)\Gamma_1 > 0, \qquad \Gamma_2 = \Lambda\Gamma_1 > 0, \qquad B > 0, \qquad \varepsilon << 1 \qquad (4.23)$$

Thus we may say that as A/B is decreased, a pitchfork bifurcation occurs as P_3 is crossed, resulting in three slow flow equilibria (the origin and the pair just born). Continuing to decrease A/B, another pitchfork occurs as P_2 is crossed, and now there are 5 slow flow equilibria. Finally a pair of saddle-node bifurcations occur as P_1 is crossed, in which all of the four slow flow equilibria which were created in the two pitchforks now come together in pairs and disappear. The origin is the only remaining equilibria (see Example One).

4.4.2 Limit Cycles

The previous section summarized the occurrence of slow flow equilibria. Let's analyze the slow flow for the existence of limit cycles. One way that limit cycles can occur is through a Hopf bifurcation at the slow flow equilibria. The conditions for a Hopf can be stated in terms of the of the Jacobian matrix, which is the linearized slow flow about an equilibrium point. Generically, for a Hopf bifurcation to occur, the $Tr(J) = 0$ and $Det(J) > 0$ [57] (see Examples 2 and 3). From equations (4.9) and (4.10), we obtain the following expression for J:

$$J = \begin{bmatrix} J_{11} & J_{12} \\ J_{21} & J_{22} \end{bmatrix} \tag{4.24}$$

where

$$
\begin{aligned}
J_{11} &= -\frac{A}{2} - \frac{3}{8}\Gamma_2 u^2 - \frac{1}{8}\Gamma_2 v^2 + \frac{1}{4}\Gamma_1 uv \\[2mm]
J_{12} &= \frac{k_1}{2} - \frac{B}{4} + \frac{1}{8}\Gamma_1 u^2 + \frac{3}{8}\Gamma_1 v^2 - \frac{1}{4}\Gamma_2 uv \\[2mm]
J_{21} &= -\frac{k_1}{2} - \frac{B}{4} - \frac{1}{8}\Gamma_1 v^2 - \frac{3}{8}\Gamma_1 u^2 - \frac{1}{4}\Gamma_2 uv \\[2mm]
J_{22} &= -\frac{A}{2} - \frac{3}{8}\Gamma_2 v^2 - \frac{1}{8}\Gamma_2 u^2 - \frac{1}{4}\Gamma_1 uv
\end{aligned}
$$

where u and v are to be evaluated at the slow flow equilibria. From (4.24) we obtain:

$$Tr(J) = -A - \frac{1}{2}\Gamma_2 \rho \tag{4.25}$$

Setting the $Tr(J) = 0$ for a Hopf bifurcation, we find:

$$Tr(J) = 0 \quad \Rightarrow \quad A = -\frac{1}{2}\Gamma_2 \rho \tag{4.26}$$

and since $\rho \geq 0$, we note that for a Hopf bifurcation to occur, A must have the opposite sign of Γ_2, which is in agreement with equation (4.2).

Next we solve (4.25) for ρ and substitute it into (4.17), obtaining the necessary part of the Hopf condition:

$$P_{Hopf}^2 = \left[1 + \frac{1}{\Lambda^2} + 4\kappa \left(\kappa - \frac{1}{\Lambda} \right) \right]^{-1} \tag{4.27}$$

This condition, however, is not sufficient. We also need to require that $Det(J) > 0$. From equation (4.24), we obtain:

$$
\begin{aligned}
Det(J) = {}& \frac{A^2}{4} - \frac{B^2}{16} + \frac{k_1^2}{4} + \left(\frac{A\Gamma_2}{4} - \frac{B\Gamma_1}{16} + \frac{k_1\Gamma_1}{4} \right)\rho \\[2mm]
& + \frac{3}{64}\left(\Gamma_1^2 + \Gamma_2^2\right)\rho^2 + \frac{B\Gamma_1}{8}v^2 - \frac{B\Gamma_2}{8}uv \tag{4.28}
\end{aligned}
$$

This expression may be simplified by multiplying the RHS of equation (4.9) by u and adding it to the RHS of (4.10) multiplied by v, which gives:

$$uv = -\frac{\rho(4A + \Gamma_2\rho)}{4B} \tag{4.29}$$

Similarly we multiply the RHS of (4.9) by v and subtract from it the RHS of (4.10) multiplied by u, which gives:

$$v^2 = \frac{\rho(4k_1 + 2B + \Gamma_1\rho)}{4B} \tag{4.30}$$

Substituting (4.29) and (4.30) into (5.55), we obtain the following expression for $Det(J)$ as a function of ρ:

$$Det(J) = \frac{A^2}{4} - \frac{B^2}{16} + \frac{k_1^2}{4} + \frac{3}{8}(A\Gamma_2 + k_1\Gamma_1)\rho + \frac{5}{64}\left(\Gamma_1^2 + \Gamma_2^2\right)\rho^2 \tag{4.31}$$

Recall the condition $Det(J) = 0$ corresponds to a saddle-node bifurcation. Therefore, by eliminating ρ between $Det(J) = 0$ in equation (4.31) and the slow flow equilibrium condition (4.17), we retrieve the bifurcation condition:

$$\left(4(\kappa^2 + 1)A^2 - B^2\right)\left(4A^2\kappa^2\Lambda^2 - B^2\Lambda^2 - 8A^2\kappa\Lambda - B^2 + 4A^2\right) = 0 \tag{4.32}$$

Solving (4.32) for $P^2 = A^2/B^2$, we obtain:

$$P^2 = \frac{A^2}{B^2} = \frac{1}{4(1 + \kappa^2)}, \quad \frac{1 + \Lambda^2}{4(1 - \kappa\Lambda)^2} \tag{4.33}$$

which is in agreement with the values computed in equations (4.18) and (4.19).

4.5 One Parameter Bifurcations

The analytical methods thus far show that the slow flow system exhibits pitchfork, saddle-node and hopf bifurcations. These bifurcations have one parameter normal forms associated with them. The normal form for a pitchfork bifurcation is $\dot{x} =$

$x(\mu - x^2)$, for a saddle-node bifurcation, $\dot{x} = \mu - x^2$, and for a Hopf $\dot{r} = r(\mu_1 + r^2)$, where μ is a single bifurcation parameter [57].

The bifurcation curves obtained in section 4.4.1 and 4.4.2 are plotted in the A-κ parameter space in Figure 4.1 for typical parameter values of $B = 1$ and $\Lambda = -1/2$ (where $\beta_1 = -6$, $\beta_2 = 0$, $\beta_2 = 3$ and $\beta_4 = 0$). A is the linear damping and $\kappa = k_1/A$, where k_1 is the detuning off of the 2:1 resonance. In keeping with the assumptions in equation (4.23), the bifurcation set is given for $\kappa \leq -\Lambda$. The curve P_1 is saddle-node bifurcation, P_2 and P_3 are pitchfork bifurcations, and H is the Hopf bifurcation. These curves are given by equations (4.20) and (4.27).

Further numerical analysis reveals the slow flow system also exhibits the following bifurcations: limit cycle folds, symmetry-breaking bifurcations, heteroclinic and homoclinic bifurcations. These are classified as two parameter bifurcations. The numerical bifurcations curves (solid) are plotted in the $\Lambda = -1/2$ parameter space with the analytical bifurcation curves (dotted) in Figure 4.2.

The equilibrium chart presented in section 4.4.1 shows to the right of P_3 there is one stable slow flow equilibrium and to the left of P_1 there one unstable slow flow equilibrium accompanied with a stable limit cycle. Thus, the bifurcation set in Figure 4.2 shows that these two slow flow steady states are connected by a complicated series of bifurcations which occur as the linear damping is varied. Starting with positive damping and decreasing to negative values, we provide three example with different detuning values that demonstrate the complex bifurcations that connect those two steady states. Example One examines the slow flow for $\kappa = -0.8$, Example Two for $\kappa = -0.35$, and Example Three for $\kappa = 0$. Each example has the same starting and ending phase portraits, which translates to the original system having a stable origin for positive damping and quasi-periodic
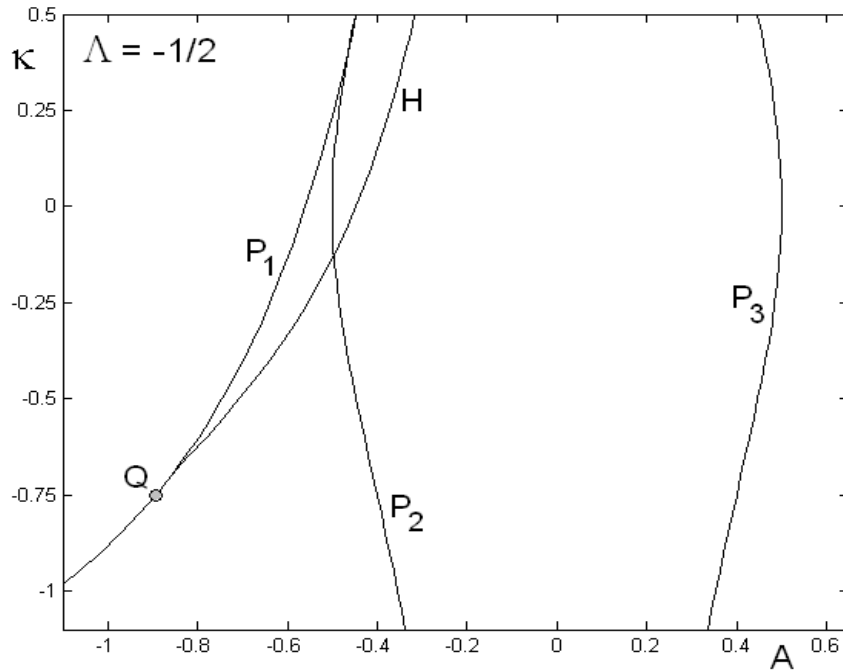
Figure 4.1: Analytical bifurcation set in the A-κ parameter plane for $\Lambda =$ $-1/2$ and $B = 1$. A is linear damping and $\kappa = k_1/A$, where k_1 is detuning. P_1 is a saddle-node, P_2 and P_3 are pitchforks and H is a Hopf. These bifurcation curves are given by (4.20) and (4.27). Point Q is the location where the saddle-node and Hopf bifurcations meet tangentially.

motion for negative damping, whether we are near or away from the 2:1 resonance.

4.6 Examples

In the following section, we examine the phase portraits of three systems that begin with positive damping and, as we decrease to negative values of damping we see a series of complex bifurcations that connect the two stable steady states. The choice of parameters for each example are: $\beta_1 = -2$, $\beta_2 = 0$, $\beta_3 = 0$, $\beta_4 = 1$, $B = 1$, which gives $\Gamma_1 = -6$, $\Gamma_2 = 3$ and $\Lambda = -1/2$. Example One examines
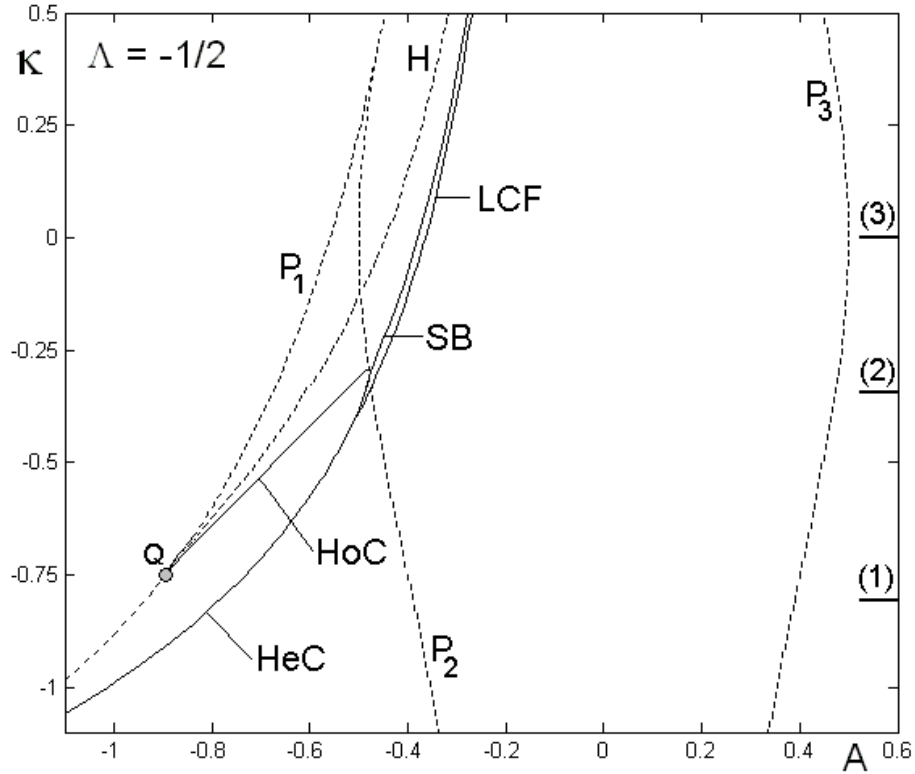
Figure 4.2: Bifurcation set in the A-κ parameter plane for $\Lambda = -1/2$ and $B = 1$. The solid lines are the bifurcation curves found numerically, while the dashed were found analytically. P_1 is a saddle-node, P_2 and P_3 are pitchforks, H is a Hopf, LCF is a limit cycle fold, SB is a symmetry-breaking, HoC is a homoclinic and HeC is a heteroclinic bifurcation. The numbers on the RHS, $(1), (2)$ and (3) reference the location of κ used in Example 1, 2 and 3.

the slow flow for $\kappa = -0.8$, Example Two for $\kappa = -0.35$, and Example Three for $\kappa = 0$. Each example has the same starting and ending phase portraits, which translates to the original system having a stable origin for positive damping and quasiperiodic motion for negative damping. The only parameter to change in each example is the linear damping, A.

4.6.1 Example One

We take as the first example the following system with $\kappa = -0.80$:

$$\ddot{z} + (1 - \varepsilon \, 0.8A + \varepsilon \cos 2t)z + \varepsilon A\dot{z} + \varepsilon(\dot{z}^3 - 2z^3) = 0 \qquad (4.34)$$

From equation (4.20) we obtain:

$$P_1 = -\frac{5\sqrt{5}}{12}, \quad P_2 = -\frac{5}{2\sqrt{41}}, \quad P_3 = \frac{5}{2\sqrt{41}}, \quad P_4 = \frac{5\sqrt{5}}{12} \qquad (4.35)$$

and from equation (4.27) we find:

$$P_{Hopf} = \frac{5}{\sqrt{29}} \qquad (4.36)$$

This system has a single parameter A, and from the foregoing analysis we can say that the number of slow flow equilibria changes with A as follows:

$$[-\infty, -0.9317] \quad \text{1 equilibrium}$$

$$[-0.9317, -0.3904] \quad \text{5 equilibria}$$

$$[-0.3904, 0.3904] \quad \text{3 equilibria}$$

$$[0.3904, +\infty] \quad \text{1 equilibrium}$$

From (4.36), a Hopf bifurcation may occur when $A = -\frac{5}{\sqrt{29}}$, if $Det(J) > 0$. (Here we use the fact that A must have the opposite sign to Γ_2 for a Hopf). In order to compute $Det(J)$ from equation (4.31), we need ρ at the Hopf. From (4.26) we find that $\rho = \frac{10}{3\sqrt{29}}$, and substituting this value for ρ into (4.31), we find $Det(J) = -\frac{5}{116} < 0$. Thus there is no Hopf in this example.

Numerical integration of the slow flow equations (4.9) and (4.10) for the present parameters reveals that a stable limit cycle is born in a saddle connection bifurcation at $A = -0.778$, not a Hopf. See Figure 4.3, bifurcation point C. Bifurcation points A, B, and D in Figure 4.3 correspond to the points P_3, P_2, and P_1, respectively. Nothing special happens at $A = -\frac{5}{\sqrt{29}} = -0.9285$.

Figure 4.3: Phase portraits of the slow flow in the (u, v) plane for Example One with $\kappa = -0.80$. Starting with positive damping, a pitchfork bifurcation occurs at A, followed by a second pitchfork bifurcation at B, a heteroclinic bifurcation at C and ending with a saddle-node bifurcation at D.

4.6.2   Example Two

The following example exhibits qualitatively different behavior from Example One:

$$\ddot{z} + (1 - \varepsilon\, 0.35A + \varepsilon \cos 2t)z + \varepsilon A\dot{z} + \varepsilon(\dot{z}^3 - 2z^3) = 0 \qquad (4.37)$$

This corresponds to the choice of detuning as $\kappa = -0.35$, which lies in the region for linear damping $A < 0$ which has six bifurcation curves in Figure 4.2. From equation (4.20) we obtain:

$$P_1 = -\frac{10\sqrt{5}}{33}, \quad P_2 = -\frac{10}{\sqrt{449}}, \quad P_3 = \frac{10}{\sqrt{449}}, \quad P_4 = \frac{10\sqrt{5}}{33} \qquad (4.38)$$

and from equation (4.27) we find:

$$P_{Hopf} = \frac{10}{\sqrt{269}} \qquad (4.39)$$

As with Example One, this system has the single parameter A, the linear damping and from the foregoing analysis we can say that the number of slow flow equilibria changes with A as follows:

$$[-\infty, -0.6776] \quad \text{1 equilibrium}$$

$$[-0.6776, -0.4719] \quad \text{5 equilibria}$$

$$[-0.4719, 0.4719] \quad \text{3 equilibria}$$

$$[0.4719, +\infty] \quad \text{1 equilibrium}$$

From (4.39), a Hopf bifurcation may occur when $A = -\frac{10}{\sqrt{269}}$, if $Det(J) > 0$. (Here we use the fact that A must have the opposite sign to Γ_2 for a Hopf). In order to compute $Det(J)$ from equation (4.31), we need ρ at the Hopf. From (4.26) we find that $\rho = \frac{20}{3\sqrt{269}}$, and substituting this value for ρ into (4.31), we find $Det(J) = \frac{40}{269} > 0$. Thus, a Hopf bifurcation occurs when $A = -0.6097$ at the equilibria located at $\rho = 0.4065$ where $\theta \approx 22.7°$ and $202.7°$ from equation (4.22). See Figure 4.4, bifurcation point F.
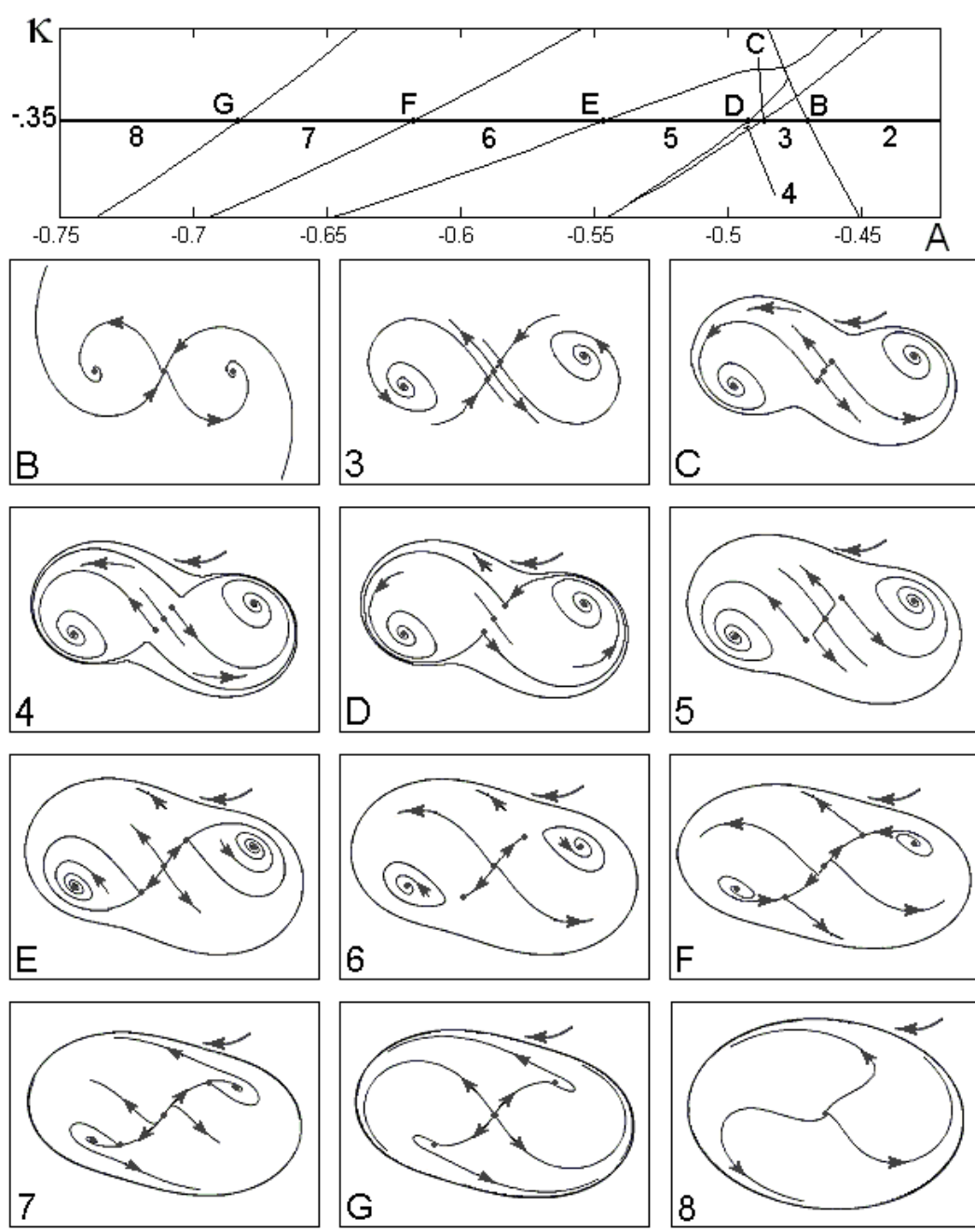
Figure 4.4: Caption for Example Two, $\kappa = -0.35$ begins on the next page.

Figure 4.4: Phase portraits of the slow flow in the (u, v) plane for Example Two with $\kappa = -0.35$. Starting with positive damping, the initial flow is the same as Example One where a pitchfork bifurcation occurs at A, followed by a second pitchfork bifurcation at B, a limit cycle fold at C, a heteroclinic bifurcation at D, a homoclinic bifurcation at E, a subcritical Hopf at F, ending with a saddle-node bifurcation at G.

In order to confirm these results, and to determine any other bifurcations which occur in (4.37) as the linear damping, A is varied, we numerically integrate the slow flow equations (4.9) and (4.10) for the present parameters. The phase plane analysis is displayed in Figure 4.4. We found that the limit cycles born in the Hopf at $A = -0.6097$ are unstable and exist in the range $-0.6097 < A < -0.5359$ (from E to F). Prior to this bifurcation for positive damping, this system behaves like Example 1 up to the bifurcation point B (the second pitchfork) which is followed by the birth of a stable and unstable limit cycle in a limit cycle fold at point C, followed by a homoclinic saddle-connection bifurcation at point D, which destroys the unstable limit cycle. Further decreases in A results in the birth of two unstable limit cycles in a homoclinic saddle-connection bifurcation at point E, which are then destroyed in a subcritical Hopf bifurcation at point F. As we continue to make A more negative, we find the pair of equilibria are destroyed in a saddle-node bifurcation at point G, leaving a stable limit cycle in the slow flow, i.e., quasiperiodic motion in the original system.

4.6.3   Example Three

As a final example, we examine the system at 2:1 resonance ($\kappa = 0$):

$$\ddot{z} + (1 + \varepsilon \cos 2t)z + \varepsilon A \dot{z} + \varepsilon(-2z^3 + \dot{z}^3) = 0 \tag{4.40}$$

From equation (4.20) we obtain:

$$P_1 = -\frac{\sqrt{5}}{4}, \quad P_2 = -\frac{1}{2}, \quad P_3 = \frac{1}{2}, \quad P_4 = \frac{\sqrt{5}}{4} \tag{4.41}$$

and from equation (4.27) we find:

$$P_{Hopf} = \frac{1}{\sqrt{5}} \tag{4.42}$$

As with Example One and Two, this system has the single parameter A, and from the foregoing analysis we can say that the number of slow flow equilibria changes with A as follows:

$$[-\infty, -0.559] \quad \text{1 equilibrium}$$
$$[-0.559, -0.5] \quad \text{5 equilibria}$$
$$[-0.5, 0.5] \quad \text{3 equilibria}$$
$$[0.5, +\infty] \quad \text{1 equilibrium}$$

From (4.42), a Hopf bifurcation may occur when $A = -\frac{1}{\sqrt{5}}$, if $Det(J) > 0$. (Again we used the fact that A must have the opposite sign to Γ_2 for a Hopf.) In order to compute $Det(J)$ from equation (4.31), we need ρ at the Hopf. From (4.26) we find that $\rho = \frac{2}{3\sqrt{5}}$, and substituting this value for ρ into (4.31), we find $Det(J) = \frac{3}{20} > 0$. Thus, a Hopf bifurcation occurs when $A = -0.4472$ at $\rho = 0.2981$. See Figure 4.5, bifurcation point D.

In order to confirm these results, and to determine any other bifurcations which occur in (4.40) as A is varied, we numerically integrate the slow flow equations (4.9)

and (4.10) for the present parameters. The phase plane analysis is displayed in Figure 4.5. We found that the limit cycles born in the Hopf when $A = -0.447$ are unstable and exist in the range $-0.447 < A < -0.377$ (from C to D). As A is increased beyond -0.377, a symmetry-breaking bifurcation occurs in which each of the two limit cycles born in the Hopf unite into one large unstable limit cycle which is point-symmetric about the origin in the u-v plane at point C. Further increases in A increase the size of the unstable limit cycle until $A = -0.364$, at which point it coalesces with a larger stable limit cycle in a limit cycle fold. The behavior beyond this point for $A > -0.364$ is the same as Example 1 and 2. Also note that the behavior following the subcritical Hopf is the same as Example 2.
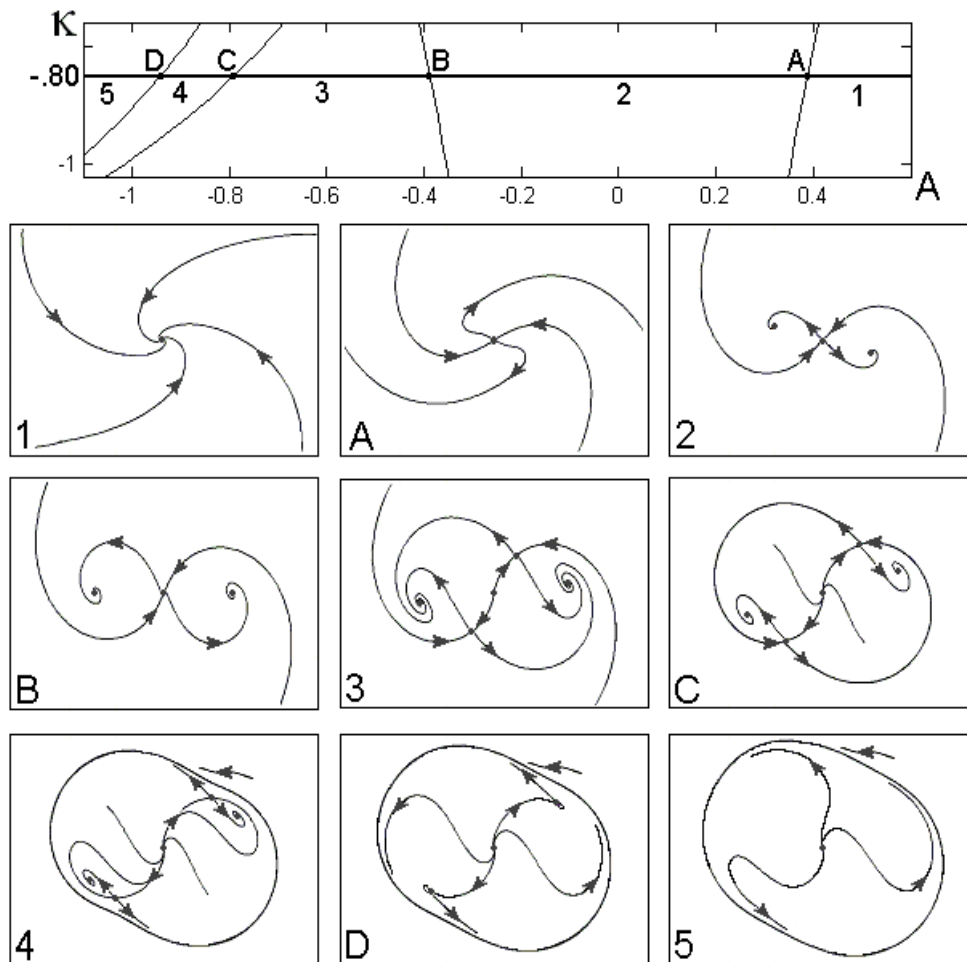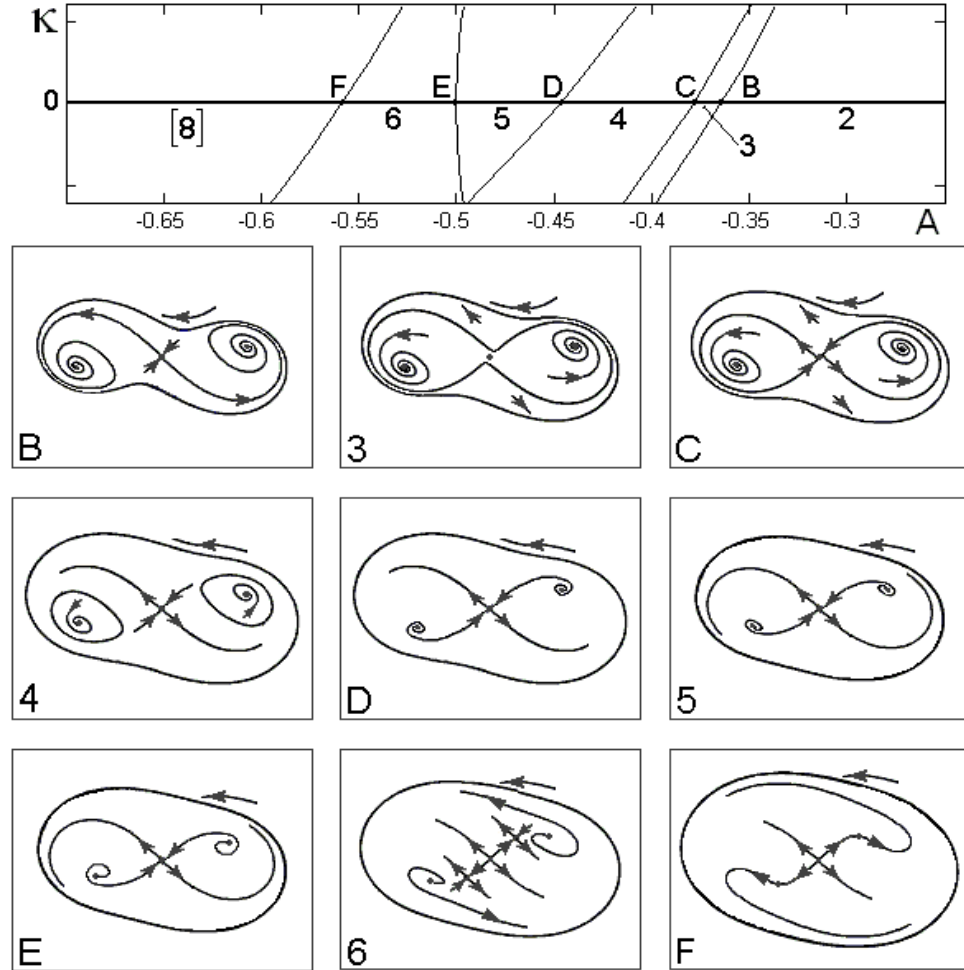
Figure 4.5: Phase portraits of the slow flow in the (u, v) plane for Example Three with $\kappa = 0$. Starting with positive damping, the initial flow is the same as Example One where a pitchfork bifurcation occurs at A, followed by a limit cycle fold at B, a symmetry-breaking bifurcation at C, a subcritical Hopf at D, a second pitchfork at E, and ending with a saddle-node bifurcation at F. The flow at $[8]$ is the same in Figure 4.4.

4.7 Two Parameter Bifurcations

One parameter bifurcations of a system can be found analytically by linearizing about the slow flow equilibria and analyzing the Jacobian matrix, as we did in section 4.4.2. Two parameter bifurcations cannot be found by linearization since they are global bifurcations and usually do not occur in the neighborhood of the equilibrium [12]. In the following sections, we describe analytical techniques to find the symmetry-breaking bifurcation from Example 3 and the homoclinic bifurcations of Example 2 and 3. Their normal forms are respectively [18]:

$$\dot{x} = y, \quad \dot{y} = \mu_1 x + \mu_2 y - x^3 - x^2 y \tag{4.43}$$

$$\dot{x} = y, \quad \dot{y} = \mu_1 x + \mu_2 y + x^2 + x^2 y \tag{4.44}$$

where μ_1 and μ_2 is the parameter space for the bifurcations. Both normal forms can be written as a Hamiltonian (conservative) system with a nonconservative perturbation. This is the ansatz for the two parameter bifurcation analysis [18].

4.7.1 Hamiltonian System

Recall the slow flow equations for the 2:1 resonance near a Hopf bifurcation:

$$u_\eta = \left(\frac{\kappa A}{2} - \frac{B}{4}\right) v + \frac{\Gamma_1}{8}(u^2 + v^2)v - \frac{A}{2}u - \frac{\Gamma_2}{8}(u^2 + v^2)u \tag{4.45}$$

$$v_\eta = -\left(\frac{\kappa A}{2} + \frac{B}{4}\right) u - \frac{\Gamma_1}{8}(u^2 + v^2)u - \frac{A}{2}v - \frac{\Gamma_2}{8}(u^2 + v^2)v \tag{4.46}$$

Note the first two terms are conservative and can form a Hamiltonian system while the last two terms are dissipative. Let's momentarily remove the nonconservative terms and treat them as a perturbation,

$$u_\eta = \frac{\partial H}{\partial v} + f(u, v) \tag{4.47}$$

$$v_\eta = -\frac{\partial H}{\partial u} + g(u, v) \tag{4.48}$$

where the nonconservative perturbation is:

$$f = -\frac{A}{2}u - \frac{\Gamma_2}{8}(u^2 + v^2)u \tag{4.49}$$

$$g = -\frac{A}{2}v - \frac{\Gamma_2}{8}(u^2 + v^2)u \tag{4.50}$$

The Hamiltonian system for 2:1 resonance near a Hopf bifurcation is:

$$\frac{\partial H}{\partial v} = \left(\frac{\kappa A}{2} - \frac{B}{4}\right)v + \frac{\Gamma_1}{8}(u^2 + v^2)v \tag{4.51}$$

$$\frac{\partial H}{\partial u} = \left(\frac{\kappa A}{2} + \frac{B}{4}\right)u + \frac{\Gamma_1}{8}(u^2 + v^2)u \tag{4.52}$$

We investigate the phase plane dynamics by solving the above set of equations for the Hamiltonian, $H(u, v)$. We begin by integrating (4.51):

$$H(u, v) = \left(\frac{\kappa A}{2} - \frac{B}{4}\right)\frac{v^2}{2} + \frac{\Gamma_1}{8}\left(\frac{u^2 v^2}{2} + \frac{v^4}{4}\right) + h(u) \tag{4.53}$$

Next, we differentiate equation (4.53) with respect to u and set it equal to equation (4.52):

$$\frac{\partial H}{\partial u} = \frac{\Gamma_1}{8}(uv^2) + h'(u) = \left(\frac{\kappa A}{2} + \frac{B}{4}\right)u + \frac{\Gamma_1}{8}(uv^2) + \frac{\Gamma_1}{8}(u^3) \tag{4.54}$$

The $\frac{\Gamma_1}{8}(uv^2)$ term cancels out on both sides leaving an expression for $h'(u)$. We integrate this term to find $h(u)$ and the Hamiltonian:

$$h(u) = \left(\frac{\kappa A}{2} + \frac{B}{4}\right)\frac{u^2}{2} + \frac{\Gamma_1}{8}\frac{u^4}{4} \tag{4.55}$$

The Hamiltonian for the conservative slow flow system in equations (4.51) and (4.52) is equation (4.53) with $h(u)$ from (4.55):

$$H(u, v) = \left(\frac{\kappa A}{2} - \frac{B}{4}\right)\frac{v^2}{2} + \left(\frac{\kappa A}{2} + \frac{B}{4}\right)\frac{u^2}{2} + \frac{\Gamma_1}{32}\left(u^2 + v^2\right)^2 \tag{4.56}$$

Equilibria

As we mentioned, the Hamiltonian system is the conservative part of the slow flow equations. Now, let's look for slow flow equilibria in the Hamiltonian system:

$$H_v = 0 \quad : \quad \left[\left(\frac{\kappa A}{2} - \frac{B}{4} \right) + \frac{\Gamma_1}{8} (u^2 + v^2) \right] v \tag{4.57}$$

$$H_u = 0 \quad : \quad \left[\left(\frac{\kappa A}{2} + \frac{B}{4} \right) + \frac{\Gamma_1}{8} (u^2 + v^2) \right] u \tag{4.58}$$

First we find that the origin is always a equilibrium point. Second, from equation (4.58) we find the first term is always nonnegative and gives nontrivial equilibria. However, there may not be a solution to equation (4.57) if $\kappa A < \frac{B}{2}$ (Recall A can be less than zero and κA can be negative or positive), which makes $(u^2 + v^2) = r^2 < 0$. Thus, there are at least two nontrivial equilibria if $\kappa A < \frac{B}{2}$:

$$u^* = \pm \sqrt{\frac{4}{3} \left(\frac{\kappa A}{2} + \frac{B}{4} \right)} \qquad v^* = 0 \tag{4.59}$$

In the case where $\kappa A > \frac{B}{2}$, the term in equation (4.57) that made $r^2 < 0$ changes sign to make $r^2 > 0$. Thus, equation (4.57) yields two additional nontrivial equilibria:

$$u^* = 0 \qquad v^* = \pm \sqrt{\frac{4}{3} \left(\frac{\kappa A}{2} - \frac{B}{4} \right)} \tag{4.60}$$

and equation (4.58) yields the same two from equation (4.59).

In summary, a pitchfork bifurcation occurs when $\kappa A = \frac{B}{2}$, where the Hamiltonian has two nontrivial equilibrium points for $\kappa A < \frac{B}{2}$ and four nontrivial equilibrium points for $\kappa A > \frac{B}{2}$.

Hamiltonian Level Curves

The phase plane for a Hamiltonian system is filled with level curves whereupon the Hamiltonian is constant because it's a conservative system. In the slow flow
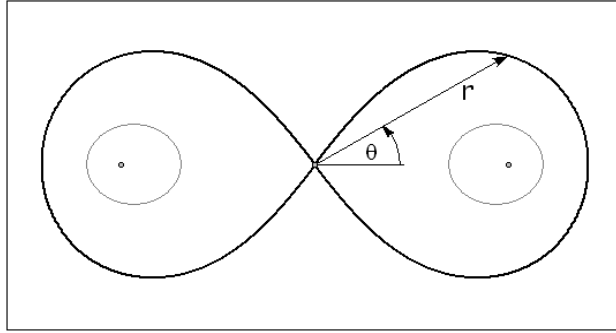
Figure 4.6: Separatrix loop for the Hamiltonian System where $\kappa A < \frac{B}{2}$.

system, the shape of the level curves depend on the number of equilibria in the slow flow, and hence, the value of κA. When $\kappa A < \frac{B}{2}$, there are two centers and one saddle point, located at the origin. For this case, there exists a trajectory in the phase plane that connects the stable and unstable manifolds of the saddle point. This trajectory is called a separatrix; it separates the basin of attraction for the periodic solutions from that of the unbounded solutions. The separatrix is also refereed to as a homoclinic orbit because the stable and unstable manifolds that connect are from the same saddle point. See Figure 4.6.

We previously discovered that the Hamiltonian system above undergoes a pitchfork bifurcation when $\kappa A = \frac{B}{2}$. At the bifurcation point, the separatrix loop persists, but additional equilibria are born. When $\kappa A > \frac{B}{2}$, the origin becomes a center and as a result, two saddle points are born; there is no change to the centers. For this case, these exists a trajectory that connects the stable manifold of one saddle point to the unstable manifold of the other and the unstable manifold on the former to the stable manifold of the latter. This type of separatrix is referred to as a heteroclinic orbit. See Figure 4.7.

When nonconservative terms are added to a Hamiltonian system, the separa-
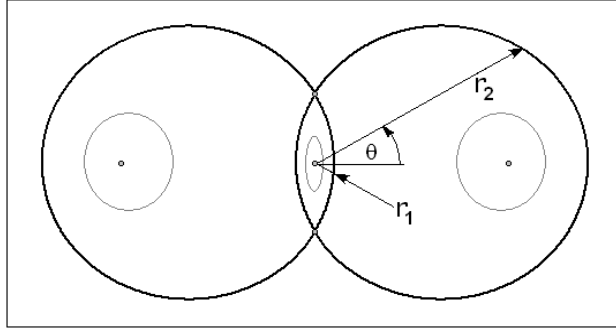
Figure 4.7: Separatrices for the Hamiltonian System where $\kappa A > \frac{B}{2}$.

trices are destroyed. For example, a symmetry-breaking bifurcation is the splitting of two connected homoclinic orbits into separate orbits. See Figure 4.8. The homoclinic separatrix when $\kappa A < \frac{B}{2}$ is the level curve of the Hamiltonian system that passes through the origin. To find the equation of the separatrix, we need the value of the Hamiltonian for that level curve. This is done by locating one point on the separatrix.

Let's change the Hamiltonian to polar coordinates for convenience. We substitute $u = r \cos \theta$ and $v = r \sin \theta$ into equation (4.56):

$$H(r, \theta) = -\frac{p}{2} r^2 \sin^2 \theta + \frac{q}{2} r^2 \cos^2 \theta + \frac{\Gamma_2}{32} r^4 \tag{4.61}$$

where $-p = \frac{\kappa A}{2} - \frac{B}{4}$ and $q = \frac{\kappa A}{2} + \frac{B}{4}$. Note that for $\kappa A < \frac{B}{2}$, $p > 0$ and $q > 0$.

The Hamiltonian for the homoclinic orbit is found by locating one point on the level curve. When $\kappa A < \frac{B}{2}$ the homoclinic orbit passes through the origin. Thus, we know the Hamiltonian is equal to zero on the level curve. We find the equation for the separatrix by setting $H = 0$ and substituting $u^* = v^* = 0$ in equation (4.61):

$$-\frac{p}{2} r^2 \sin^2 \theta + \frac{q}{2} r^2 \cos^2 \theta + \frac{\Gamma_2}{32} r^4 = 0 \tag{4.62}$$
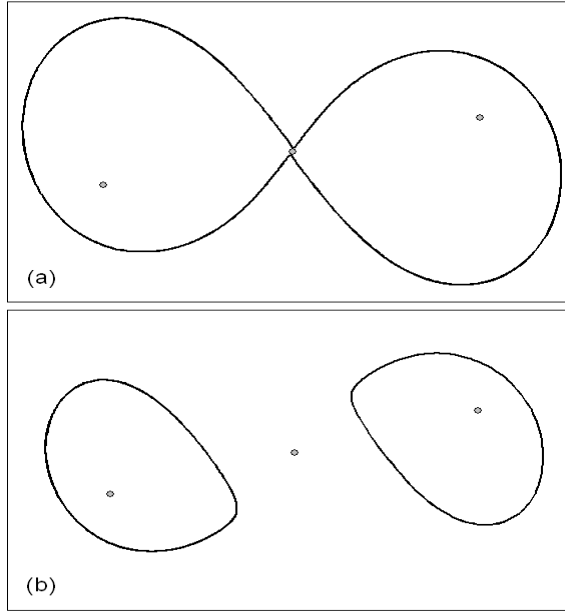
Figure 4.8: Numerical homoclinic orbits for the slow flow system plotted in the u-v plane. (a) the separatrix in the conservative system, (b) the destruction of the separatrix when the nonconservative terms are added.

We cancel the r^2 from both sides and solve for the remaining r^2, which is the radius squared of the homoclinic orbit:

$$r^2 = \frac{16}{\Gamma_2} \left(q \sin^2 \theta - p \cos^2 \theta \right) \tag{4.63}$$

Thus, the separatrix associated with $\kappa A < \frac{B}{2}$ is shown in Figure 4.6.

The separatrices that exists when $\kappa A > \frac{B}{2}$ do not ass through the origin as before because the saddle points are nontrivial. In the previous case, we knew $H = 0$ on the separatrix because it passed through the origin. In this case, we find the value of the Hamiltonian for the separatrix by substituting u^* and v^* from equation (4.60) into equation (4.61):

$$H(u^*, v^*) = \frac{\Gamma_1 + 12}{18} \left(\frac{\kappa A}{2} - \frac{B}{4} \right)^2 \tag{4.64}$$

Again, we find the equation for the separatrix by setting the Hamiltonian equal to the constant in (4.64), and solving for r^2.

$$H = \frac{\Gamma_1 + 12}{18} \left(\frac{\kappa A}{2} - \frac{B}{4} \right)^2 = r^2 \left(-\frac{p}{2} \sin^2 \theta + \frac{q}{2} \cos^2 \theta + \frac{\Gamma_2}{32} r^2 \right) \qquad (4.65)$$

which is rewritten as,

$$r^2 \left(\frac{p}{2} \sin^2 \theta - \frac{q}{2} \cos^2 \theta - \frac{\Gamma_2}{32} r^2 \right) + \frac{\Gamma_1 + 12}{18} \left(\frac{\kappa A}{2} - \frac{B}{4} \right)^2 = 0 \qquad (4.66)$$

This is a fourth order polynomial on r. Thus, the separatrices are composed of four curves. We use MACSYMA (a computer algebra program [44]-[43])) to find the roots,

$$r_2^2 = -r_1^2 \qquad (4.67)$$

$$r_1^2 = -\frac{4}{3\sqrt{2}\Gamma_2} \sqrt{w} - \frac{4\kappa A}{\Gamma_2} - \frac{2B \cos 2\theta}{\Gamma_2} \qquad (4.68)$$

where w is given as:

$$w = \frac{\Gamma_2^2 \kappa A^2}{2} + (6\Gamma_2 + 18)\kappa A^2 + (18B \cos 2\theta - 6B\Gamma_2)\kappa A$$
$$- \frac{B\Gamma_2^2 \kappa A}{2} + \frac{9B^2 \cos 4\theta}{4} + \frac{B^2 \Gamma_2^2}{8} + \frac{3B^2 \Gamma_2}{2} + \frac{9B^2}{4} \qquad (4.69)$$

These two equations create the separatrices shown in Figure 4.7.

The separatrices derived for $\kappa A < \frac{B}{2}$ and $\kappa A > \frac{B}{2}$ in Figures 4.6 and 4.7 exists in the Hamiltonian system only. Recall the original slow flow equations in (4.9) and (4.10) have conservative and nonconservative terms. When the nonconservative terms are added to the Hamiltonian system, they destroy the separatrices since they conservative quanities. However, for particular combinations of κ and A, for a given B and Γ_2, the separatrices may persist. Our strategy is to require the separatrices to persist and find the associated bifurcation curve in the A-κ parameter space for the symmetry-breaking and homoclinic bifurcations presented in Example 2 and 3.

4.7.2 Preserving Closed Orbits

We wish to find the analytical bifurcation curves of the symmetry-breaking and homoclinic bifurcations presented in Example 2 and 3. The strategy is to require the separatrices in the Hamiltonian system to persist when the perturbation (nonconservative terms) are added to the system. Let's for a moment consider preserving *any* closed trajectory in a Hamiltonian system with a small nonconservative perturbation. We call this class of systems nearly Hamiltonian. Before we investigate this class of systems, let's recall Green's Theorem.

Green's Theorem

We use Green's Theorem to investigate the behavior of the separatrix as we vary A and κ. Green's Theorem gives a relationship between a line integral around any simple closed curve C and an area integral over the plane region *int C* bounded by C. We assume that *int C* consists of all points inside C as well as all the points on C. The theorem states:

Let C *be a positively oriented, piecewise-smooth, simple closed curve in the plane and let* int C *be the region bounded by* C. *If* P *and* Q *have continuous partial derivatives on an open region that contains* int C, *then*

$$\oint_C P \, dx + Q \, dy = \int \int_{int\ C} \left(\frac{\partial Q}{\partial x} - \frac{\partial P}{\partial y} \right) \, dxdy \qquad (4.70)$$

Equation (4.70) will be the basis for deriving the Melnikov Integral [17] for systems that are nearly Hamiltonian, like the system in equations (4.45) and (4.46) and looking ahead to equation (4.127).

Nearly Hamiltonian Systems

The autonomous system in equations (4.45) and (4.46) can be separated into a conservative (unperturbed) and nonconservative (perturbation) part. If the conservative system has a separatrix in the phase plane, the perturbation is expected to destroy it. Let's define the Hamiltonian (unperturbed) system as

$$\dot{x} = \frac{\partial H}{\partial y}, \qquad \dot{y} = -\frac{\partial H}{\partial x} \tag{4.71}$$

where $H(x, y)$ is the Hamiltonian function. The phase plane of Hamiltonian systems consists of trajectories with $H(x, y) = $ constant. To see that H is constant on any trajectory, consider the velocity of H, $\frac{dH}{dt}$:

$$\frac{dH}{dt} = \dot{x}\frac{\partial H}{\partial x} + \dot{y}\frac{\partial H}{\partial y} \tag{4.72}$$

Substituting equation (4.71) into the expression above, we find $\frac{dH}{dt}$ equals zero:

$$\frac{dH}{dt} = \left(\frac{\partial H}{\partial y}\right)\frac{\partial H}{\partial x} + \left(-\frac{\partial H}{\partial x}\right)\frac{\partial H}{\partial y} = 0 \tag{4.73}$$

Let's consider a small perturbation of the Hamiltonian system in the phase plane:

$$\dot{x} = \frac{\partial H}{\partial y} + \varepsilon f(x, y) \tag{4.74}$$

$$\dot{y} = -\frac{\partial H}{\partial x} + \varepsilon g(x, y) \tag{4.75}$$

If Γ_ε is a closed orbit in the phase plane of the perturbed system above, then

$$\oint_{\Gamma_\varepsilon} dH = 0 \tag{4.76}$$

Actually, equation (4.76) is true for any piecewise-smooth, simple closed curve in the plane. The Hamiltonian differential dH can also be expressed as $dH = \frac{\partial H}{\partial x}dx + \frac{\partial H}{\partial y}dy$. Therefore equation (4.76) becomes,

$$\oint_{\Gamma_\varepsilon} \underbrace{(-\dot{y} + \varepsilon g(x, y))}_{\partial H/\partial x} \, dx + \underbrace{(\dot{x} - \varepsilon f(x, y))}_{\partial H/\partial y} \, dy = 0 \tag{4.77}$$

Now, let's separate the unperturbed system from the perturbation:

$$\oint_{\Gamma_\varepsilon} (-\dot{y}dx + \dot{x}dy) + \varepsilon(g(x,y)dx - f(x,y)dy) = 0 \qquad (4.78)$$

Since Γ_ε is a closed trajectory we can change the line integral to a time integral:

$$\oint_{\Gamma_\varepsilon} (-\dot{y}\dot{x} + \dot{x}\dot{y}) + \varepsilon(g(x,y)\dot{x} - f(x,y)\dot{y})\ dt = 0 \qquad (4.79)$$

Clearly, the first term in the integrand vanishes. What remains is an expression for the perturbation terms to vanish:

$$\oint_{\Gamma_\varepsilon} (g(x,y)\dot{x} - f(x,y)\dot{y})dt = 0 \qquad (4.80)$$

This expression is an inner product between (f,g) and the normal to the trajectory; it is this inner product whose average value is zero.

At this point, let's change the time integral back to the line integral and apply Green's Theorem in the plane. This yields the Melnikov Integral [42]:

$$\oint_{\Gamma_\varepsilon} g(x,y)\ dx - f(x,y)\ dy = \int\int_{\Gamma_\varepsilon} \left(\frac{\partial f}{\partial x} + \frac{\partial g}{\partial y}\right) dxdy = 0 \qquad (4.81)$$

Note equation (4.81) is an exact expression. If we think of the perturbation as a force *pushing* and *pulling* on the closed trajectory and the integral around the closed trajectory as an *average*, then, the pushing and pulling will average so to cancel each other out.

Let's make a further assumption about the system. If we take $\varepsilon << 1$, then the perturbation is small. We can approximate the integral in (4.81) by assuming $\Gamma_\varepsilon \approx \Gamma$, where Γ is the closed trajectory in the unperturbed system, such that

$$\int\int_{\Gamma} \left(\frac{\partial f}{\partial x} + \frac{\partial g}{\partial y}\right) dxdy = 0 \qquad (4.82)$$

This approximation can also apply to equation (4.80):

$$\oint_{\Gamma} (g(x,y)\dot{x} - f(x,y)\dot{y})\ dt = 0 \qquad (4.83)$$

These approximations to the Melnikov Integral can be used to find a relationship between the parameters in the nonconservative perturbation so as to preserve any closed loop in the phase plane, [17].

4.8 Symmetry Breaking Bifurcation

Let's return to the slow flow equations (4.45) and (4.46) and assume $\kappa A < \frac{B}{2}$. Recall the equilibria in the system are two centers and one saddle point. The condition to preserve the separatrix is simply the area integral of the normal component of the nonconservative perturbation about the unperturbed separatrix, equation (4.82). To compute this integral, we need the derivatives of equations (4.49) and (4.50):

$$\frac{\partial f}{\partial u} = -\frac{A}{2} - \frac{\Gamma_2}{8}(3u^2 + v^2) \tag{4.84}$$

$$\frac{\partial g}{\partial v} = -\frac{A}{2} - \frac{\Gamma_2}{8}(u^2 + 3v^2) \tag{4.85}$$

The integrand of the separatrix condition is the addition of (4.84) and (4.85)

$$\frac{\partial f}{\partial u} + \frac{\partial g}{\partial v} = -A - \frac{\Gamma_2}{2}(u^2 + v^2) \tag{4.86}$$

Since we found the separatrix in polar coordinates, we transform the integral and the integrand to polar coordinates:

$$\int_0^{\theta_0} \int_0^{r_0} \left(A + \frac{\Gamma_2}{2}r^2\right) r \ drd\theta = 0 \tag{4.87}$$

where $r_0 = \frac{16}{\Gamma_2}\left(q\sin^2\theta - p\cos^2\theta\right)$. Recall this equation for r comes from equation (4.63). Let's continue by integrating with respect to r:

$$\int_0^{\theta_0} \left[\frac{Ar^2}{2} + \frac{\Gamma_2 r^4}{8}\right]_0^{r_0} d\theta =$$
$$\int_0^{\theta_0} \left[A\left(q\sin^2\theta - p\cos^2\theta\right) + 16\left(q\sin^2\theta - p\cos^2\theta\right)^2\right] d\theta = 0 \tag{4.88}$$

The integral in equation (4.88) is not difficult to compute, but it is messy. We use MACSYMA to solve this integral. The solution yields a condition on A and κA, for a given B (notice Γ_2 is not part of the condition):

$$\sqrt{B - 2\kappa A}\left(32\kappa A^2 - 8A\kappa A + 4B^2\right)\arctan\left(\frac{\sqrt{B + 2\kappa A}}{\sqrt{B - 2\kappa A}}\right) +$$
$$\sqrt{B + 2\kappa A}\left(-24\kappa A^2 + (12B + 4A)\kappa A - 2AB\right) = 0 \qquad (4.89)$$

The parameter κA cannot be solved for analytically from the expression above. Thus, we employ a root-by-bisection program in MACSYMA to find the values of κA for a given A and B. The result is a curve in the A-κ parameter plane that represents when the separatrix loop persists, which only happens at the bifurcation point.

As in the previous examples, we set $B = 1$, $\Gamma_1 = 6$, and $\Gamma_2 = -3$. The analytical curve for the bifurcation set of $\Lambda = -\frac{1}{2}$ is plotted with the numerical curve in Figure 4.9. Notice that the first order approximation does not completely fit the numerical curve. One explanation stems from the nature of the approximation. When we used equation (4.82), we choose to integrate about the unperturbed separatrix. We did not account for the changes in the shape of the separatrix due to the perturbation. Also, we took the slow flow as nearly Hamiltonian by assuming the nonconservative perturbation was of order epsilon. Actually, the conservative and nonconservative parts of the slow flow areboth of order epsilon as a results of the two-variable expansion.
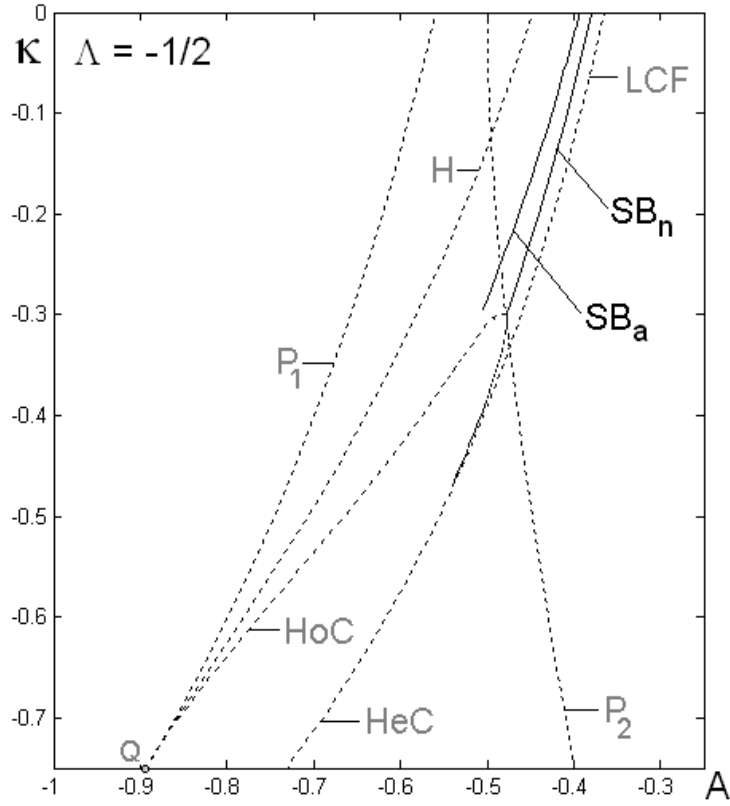
Figure 4.9: Bifurcation set in the A-κ parameter plane for $\Lambda = -1/2$ and $B = 1$. P_1 is a saddle-node, P_2 and P_3 are pitchforks, H is a Hopf, LCF is a limit cycle fold, HoC is a homoclinic and HeC is a heteroclinic bifurcation. SB_n is a symmetry-breaking bifurcation curve found by numerical integration and SB_a is the symmetry-breaking bifurcation curve found analytically.

4.9 Homoclinic Bifurcation

Recall that the slow flow system for 2:1 resonance near a Hopf bifurcation is:

$$u' = \left(\frac{\kappa A}{2} - \frac{B}{4}\right)v + \frac{\Gamma_1}{8}(u^2 + v^2)v - \frac{A}{2}u - \frac{\Gamma_2}{8}(u^2 + v^2)u \qquad (4.90)$$

$$v' = -\left(\frac{\kappa A}{2} + \frac{B}{4}\right)u - \frac{\Gamma_1}{8}(u^2 + v^2)u - \frac{A}{2}v - \frac{\Gamma_2}{8}(u^2 + v^2)v \qquad (4.91)$$

where the prime denotes differentiation with respect to slow time, η. For the examples completed in the previous sections, we chose $\Lambda = \Gamma_2/\Gamma_1 = -3/6$ and $B = 1$. In section 4.4.2 we obtained analytical expressions for the Hopf bifurcation, the pitchfork bifurcation, and the saddle-node bifurcation. In Figure 4.1, we label point Q as the location where the Hopf bifurcation curve meets the saddle-node bifurcation curve. As a result, this point is singular.

Limit cycles can be generically created or destroyed in a Hopf bifurcation. The necessary conditions for a generic Hopf bifurcation in a system of two first order ODE's such as the slow flow (4.90) and (4.91) are $Tr(J) = 0$ and $Det(J) > 0$, where J is the Jacobian matrix evaluated at the equilibria. The condition for a saddle-node bifurcation is the $Det(J) = 0$. Thus, when these two bifurcations occur simultaneously, as at point Q, the $Tr(J) = 0$ and $Det(J) = 0$. When this happens, the Jacobian matrix has a double zero eigenvalue. The Jacobian matrix associated with the slow flow vector field in (4.90) and (4.91) evaluated at the equilibria where these bifurcations occur and with the value of κ and A associated with point Q is:

$$J = \begin{bmatrix} 0 & 1 \\ 0 & 0 \end{bmatrix} \qquad (4.92)$$

The goal of this section is to study the dynamics in the neighborhood of the equilibria having the linear part above. This is accomplished by embedding the

system in a parameterized family of systems where the number of parameters is equal to the codimension of the bifurcation [63]. The parameterized family of systems are called unfoldings. Therefore, we transform the slow flow system into the following two-parameter family of systems, which is the normal form for unfolding the singularity of a matrix with two zero eigenvalues:

$$\dot{x} = y, \qquad \dot{y} = \lambda_1 + \lambda_2 y + x^2 + xy \tag{4.93}$$

where the λ's are the bifurcation parameters [18]. This normal form is widely known as the Takens-Bogdanov normal form [20] and [63]. In our work, we rename the coefficients in equation (4.93),

$$\dot{x} = y, \qquad \dot{y} = \mu_1 + \mu_2 y + \mu_3 x^2 + \mu_4 xy \tag{4.94}$$

where μ_1 and μ_2 are the linear coefficients and μ_3 and μ_4 are the nonlinear coefficients. After we transform the slow flow system into the normal form above, the μ's will be functions of the two bifurcation parameters κ and A. In the following subsection, we outline the necessary steps taken to complete this transformation.

4.9.1 Double Zero Eigenvalue

The investigation of the dynamics of any system begins with finding equilibria and evaluating their stability. In this case, we also are interested in finding the non-saddle slow flow equilibria and the equilibria where the *trace* and *determinant* vanish. Thus, we evaluate the Jacobian matrix of the slow flow in (4.90) and (4.91):

$$J_Q = \begin{bmatrix} \frac{A}{2} - \frac{9}{8}u^2 - \frac{3}{8}v^2 - \frac{3}{2}uv & \frac{\kappa A}{2} - \frac{1}{4} - \frac{3}{4}u^2 - \frac{9}{4}v^2 - \frac{3}{4}uv \\ -\frac{\kappa A}{2} - \frac{1}{4} - \frac{3}{4} + \frac{3}{4}v^2 + \frac{9}{4}u^2 - \frac{3}{4}uv & \frac{A}{2} - \frac{9}{8}v^2 - \frac{3}{8}u^2 + \frac{3}{4}uv \end{bmatrix} \tag{4.95}$$

The *trace* and *determinant* of the Jacobian is:

$$Tr(J_Q) = A - \frac{3}{2}(u^2 + v^2) \tag{4.96}$$

$$Det(J_Q) = \frac{1}{4}A^2(1 + k^2) + \frac{3}{4}A(1 - 2\kappa)(u^2 + v^2)$$

$$+ \frac{135}{64}(u^2 + v^2)^2 - \frac{3}{8}(v^2 + uv - v^2) - \frac{1}{16} \tag{4.97}$$

When we solve the four equations, $u_\eta = 0$, $v_\eta = 0$, $Tr(J_Q) = 0$ and $Det(J_Q) = 0$ simultaneously, we retrieve the (u, v) coordinates of the nontrivial slow flow equilibria and the location of point Q in the A-κ parameter space:

$$u \equiv u_1 = \pm\sqrt{\frac{2}{15}}\sqrt{\sqrt{5} + 1} \qquad v \equiv v_1 = \pm\sqrt{\frac{2}{15}}\sqrt{\sqrt{5} - 1} \tag{4.98}$$

$$A \equiv A_1 = -\frac{2}{\sqrt{5}} \qquad \kappa \equiv \kappa_1 = -\frac{3}{4} \tag{4.99}$$

Point Q is $\left(-\frac{2}{\sqrt{5}}, -\frac{3}{4}\right)$, which we call (A_1, κ_1) in the A-κ parameter space. Let's linearize about the location of the singularity:

$$\kappa = \kappa_1 + \varepsilon\kappa_2 = -\frac{3}{4} + \varepsilon\kappa_2 \tag{4.100}$$

$$A = A_1 + \varepsilon A_2 = -\frac{2}{\sqrt{5}} + \varepsilon A_2 \tag{4.101}$$

and linearize about the location of the slow flow equilibria:

$$u = u_1 + \varepsilon u_2 = \sqrt{\frac{2}{15}}\sqrt{\sqrt{5} + 1} + \varepsilon u_2 \tag{4.102}$$

$$v = v_1 + \varepsilon v_2 = \sqrt{\frac{2}{15}}\sqrt{\sqrt{5} - 1} + \varepsilon v_2 \tag{4.103}$$

The purpose of unfolding the singularity is to capture the dynamics in the neighborhood of the degenerate equilibria. Therefore, by making the transformations in (4.102) and (4.103), we move the coordinate system to the degenerate equilibria, as shown in Figure 4.10.
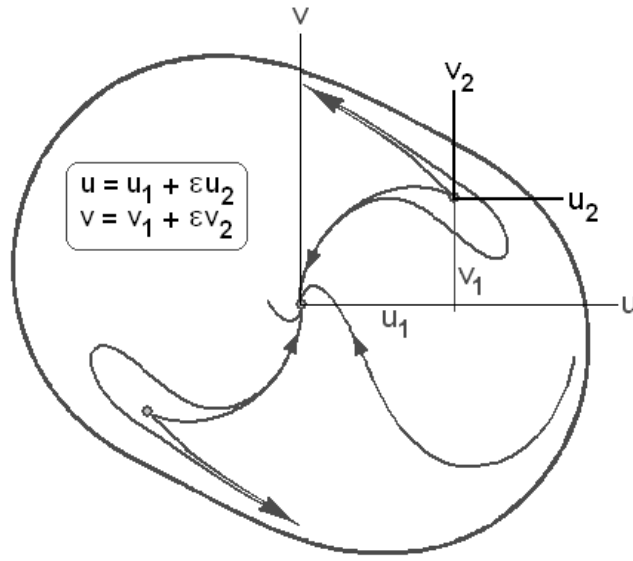
Figure 4.10: Phase portrait of the slow flow at $\kappa = -3/4$ and $A = -2/\sqrt{5}$. The first transformation is moving the system from the origin to the location of the singular slow flow equilibria at (u_1, v_1).

We substitute the transformations (4.100), (4.101), (4.102) and (4.103) into the slow flow equations (4.90) and (4.91), solve for u_2' and v_2' and taylor expand the equations out to $O(\varepsilon)$:

$$u_2' = b_1 A_2 + b_2 \kappa_2 + b_3 u_2 + b_4 v_2 + \varepsilon (\text{ quadratic terms }) \qquad (4.104)$$

$$v_2' = b_5 A_2 + b_6 \kappa_2 + b_7 u_2 + b_8 v_2 + \varepsilon (\text{ quadratic terms }) \qquad (4.105)$$

where the "quadratic terms" are linear combinations of $A_2 u_2$, $A_2 v_2$, $\kappa_2 u_2$, $\kappa_2 v_2$, u_2^2, v_2^2 $u_2 v_2$, and the b_i's are the coefficients of the linear terms:

$$b_1 = -\frac{\sqrt{30}}{40} s_1 - \frac{\sqrt{30}}{30} s_2, \quad b_2 = -\frac{\sqrt{6}}{15} s_1, \quad b_3 = -\frac{1}{2}, \quad b_4 = -\frac{\sqrt{5}+1}{4}$$

$$b_5 = -\frac{\sqrt{30}}{30} s_1 + \frac{\sqrt{30}}{40} s_2, \quad b_6 = \frac{\sqrt{6}}{15} s_2, \quad b_7 = \frac{\sqrt{5}-1}{4}, \quad b_8 = \frac{1}{2} \qquad (4.106)$$

where $s_1 = \sqrt{\sqrt{5}-1}$ and $s_2 = \sqrt{\sqrt{5}+1}$. Therefore, $s_1 s_2 = 2$.

Continuing, we diagonalize the linear part of the (u_2, v_2) equations, which results in a new coordinate system (u_3, v_3) whose axes lie in the eigendirections of the degenerate equilibrium point. Thus, we generate a new transformation:

$$
\begin{aligned}
u_2 &= B_1 u_3 + B_2 v_3 \\
v_2 &= B_3 u_3 + B_4 v_3
\end{aligned}
\quad \text{such that} \quad
\begin{aligned}
u_3' &= v_3 + \text{N.L.} + \text{Unfolding} \\
v_3' &= \ 0 + \text{N.L.} + \text{Unfolding}
\end{aligned}
\tag{4.107}
$$

where the B_i's are to be found, "N.L." refers to the quadratic nonlinear terms and "Unfolding" refers to A_2-κ_2 unfolding terms. When the " N.L." and "Unfolding" are omitted, equations (4.104) and (4.105) become,

$$
\underline{u}' = \mathbf{b}\underline{u} \quad \Rightarrow \quad b = \begin{bmatrix} b_3 & b_4 \\ b_7 & b_8 \end{bmatrix} = \begin{bmatrix} -\frac{1}{2} & -\frac{\sqrt{5}+1}{4} \\ \frac{\sqrt{5}-1}{4} & \frac{1}{2} \end{bmatrix}
\tag{4.108}
$$

In order to solve $u_2' = b_3 u_2 + b_4 v_2$ and $v_2' = b_7 u_2 + b_8 v_2$, we diagonalize the b-matrix in (4.108) by creating the rotation matrix B such that

$$
\begin{pmatrix} u_3' \\ v_3' \end{pmatrix} = [B]^{-1} [\, b \,][B] \begin{pmatrix} u_3 \\ v_3 \end{pmatrix} = \begin{bmatrix} 0 & 1 \\ 0 & 0 \end{bmatrix} \begin{pmatrix} u_3 \\ v_3 \end{pmatrix}
\tag{4.109}
$$

The rotation matrix B yields the following transformation from (4.107):

$$
\begin{aligned}
u_2 &= v_3 \\
v_2 &= (1 - \sqrt{5})/2 \ u_3 + (1 - \sqrt{5}) \ v_3
\end{aligned}
\tag{4.110}
$$

We substitute the transformation (4.110) into the slow flow equations (4.104) and (4.105), solve for u_3' and v_3' and taylor expand the equations out to $O(\varepsilon)$:

$$
u_3' = v_3 + c_1 A_2 + c_2 \kappa_2 + \varepsilon (\text{ quadratic terms })
\tag{4.111}
$$

$$
v_3' = \ 0 \ + c_3 A_2 + c_4 \kappa_2 + \varepsilon (\text{ quadratic terms })
\tag{4.112}
$$

where the quadratic terms are linear combinations of A_2u_3, A_2v_3, κ_2u_3, κ_2v_3, u_3^2, v_3^2, u_3v_3, and the c_i's are the coefficients of the linear terms:

$$
\begin{aligned}
c_1 &= -\frac{\sqrt{30}}{40}s_1 - \frac{\sqrt{30}}{30}s_2, & c_2 &= -\frac{\sqrt{6}}{15}s_1 \\
c_3 &= \frac{2\sqrt{6}+\sqrt{30}}{48}s_1 + \frac{\sqrt{30}-3\sqrt{6}}{96}s_2, & c_4 &= \frac{\sqrt{6}}{30}s_1 - \frac{\sqrt{30}-\sqrt{6}}{60}s_2 \quad (4.113)
\end{aligned}
$$

where $s_1 = \sqrt{\sqrt{5}-1}$ and $s_2 = \sqrt{\sqrt{5}+1}$.

Using a near-identity transformation, we convert the (u_3, v_3) slow flow equations into the normal form equations (4.94). The form of the near-identity transformation is:

$$
u_3 = u_4 + \varepsilon(C_1u_4^2 + C_2u_4v_4 \; + \; C_3v_4^2
$$

$$
+ \; C_4A_2u_4 + C_5A_2v_4 + C_6\kappa_2u_4 \; + \; C_7\kappa_2v_4)
$$

$$
v_3 = v_4 + \varepsilon(C_8u_4^2 + C_9u_4v_4 \; + \; C_{10}v_4^2
$$

$$
+ \; C_{11}A_2u_4 + C_{12}A_2v_4 + C_{13}\kappa_2u_4 + C_{14}\kappa_2v_4) \qquad (4.114)
$$

where the C_i's are to be chosen. We substitute the transformation (4.114) into the slow flow equations (4.111) and (4.112), solve for u_4' and v_4' and taylor expand the equations out to $O(\varepsilon)$:

$$
u_4' = v_4 + d_1 + d_2A_2u_4 + d_3A_2v_4 + d_4\kappa_2u_4
$$

$$
+ \; d_5\kappa_2v_4 + d_6u_4^2 + d_7u_4v_4 + d_8v_4^2 \qquad (4.115)
$$

$$
v_4' = 0 + d_9 + d_{10}A_2u_4 + d_{11}A_2v_4 + d_{12}\kappa_2u_4
$$

$$
+ \; d_{13}\kappa_2v_4 + d_{14}u_4^2 + d_{15}u_4v_4 + d_{16}v_4^2 \qquad (4.116)
$$

where the d_i's are constants that depend on the C_i's in equation (4.114), omitted for brevity. The task here is to simplify equations (4.115) and (4.116) by choosing the constants C_i's judiciously. We choose to eliminate the following coefficients: $d_2, d_3, d_4, d_5, d_6, d_7, d_8$ and d_{16}, giving the simplified system:

$$u'_4 = v_4 + d_1 \qquad (4.117)$$

$$v'_4 = 0 + d_9 + d_{10}A_2u_4 + d_{11}A_2v_4 + d_{12}\kappa_2u_4 + d_{13}\kappa_2v_4 + d_{14}u_4^2 + d_{15}u_4v_4 \quad (4.118)$$

This leads to values for the C_i's, which are not listed here, again for brevity. Now that we have the desired C_i's, and hence d_i's, we convert the two first order slow flow equations in (4.117) and (4.118) to a second order differential equation on u_4:

$$\frac{d^2u_4}{d\eta^2} = D_1 + \varepsilon\left\{D_2 + D_3u_4 + D_4u_4^2 + D_5\frac{du_4}{d\eta} + D_6u_4\frac{du_4}{d\eta}\right\} \qquad (4.119)$$

where the D_i's are:

$$
\begin{aligned}
D_1 &= \frac{5\sqrt{6} + \sqrt{30})}{96}s_1A_2 - \frac{\sqrt{6} + \sqrt{30}}{60}s_1\kappa_2 \\
D_2 &= -\frac{\sqrt{6} + 5\sqrt{6}}{200}s_1A_2\kappa_2 \\
D_3 &= -\frac{\sqrt{5} + 6}{16}A_2 + \frac{1 - 2\sqrt{5}}{10}\kappa_2 \qquad (4.120) \\
D_4 &= -\frac{\sqrt{6}}{4}s_1 \\
D_5 &= \frac{8\sqrt{5} - 16}{25}\kappa_2 \\
D_6 &= -\frac{\sqrt{30}}{5}s_1
\end{aligned}
$$

where $s_1 = \sqrt{\sqrt{5} - 1}$ and $s_2 = \sqrt{\sqrt{5} + 1}$.

As stated at the end of the previous section, our goal is to put equation (4.119) into the normal form:

$$\dot{x} = y, \qquad \dot{y} = \mu_1 + \mu_2 y + \mu_3 x^2 + \mu_4 xy \tag{4.121}$$

which can be written as a second order ODE:

$$\ddot{x} = \mu_1 + \mu_2 \dot{x} + \mu_3 x^2 + \mu_4 x \dot{x} \tag{4.122}$$

Note that this equation has no linear x-term, whereas equation (4.119) contains a linear u_4-term. Thus, we eliminate the u_4-term by generating a final transformation: $u_5 = u_4 + \frac{D_3}{2D_4}$. This yields the final slow flow equation:

$$\frac{d^2 u_5}{d\eta^2} = F_1 + F_2 u_5^2 + F_3 \frac{du_5}{d\eta} + F_4 u_5 \frac{du_5}{d\eta} \tag{4.123}$$

where the F_i's are:

$$
\begin{aligned}
F_1 &= \frac{5A_2}{4\sqrt{30}s_1} - \frac{2\kappa_2}{5\sqrt{6}s_1} - \frac{13\sqrt{30} + 15\sqrt{6}}{4800\sqrt{5} - 14400}\varepsilon A_2 \kappa_2 \\
&\quad - \frac{25\sqrt{30} - 41\sqrt{6}}{1200\sqrt{5} - 3600}\varepsilon s_1 \kappa_2^2 - \frac{29\sqrt{30} + 19\sqrt{6}}{3072\sqrt{5} - 9216}\varepsilon s_1 A_2^2 \\
F_2 &= -\frac{\sqrt{6}}{4}\varepsilon s_1 \\
F_3 &= \frac{6\sqrt{5} + 5}{40}\varepsilon A_2 + \frac{7\sqrt{5} - 6}{25}\varepsilon \kappa_2 \\
F_4 &= \frac{3\sqrt{30} - 5\sqrt{6}}{5\sqrt{5} - 15}\varepsilon s_1
\end{aligned}
\tag{4.124}
$$

where $s_1 = \sqrt{\sqrt{5} - 1}$ and $s_2 = \sqrt{\sqrt{5} + 1}$. The first order form of the (u_5, v_5) slow flow is:

$$\dot{u}_5 = v_5, \qquad \dot{v}_5 = F_1 + F_3 v_5 + F_2 u_5^2 + F_4 u_5 v_5 \tag{4.125}$$

where it is exactly the Takens-Bogdanov normal form when we set $\mu_1 = F_1$, $\mu_2 = F_3$, $\mu_3 = F_2$ and $\mu_4 = F_4$.

Let's recap the transformation with a "road map":

(u, v) original slow flow coordinates for 2:1 resonance near a Hopf

(u_1, v_1) location of the degenerate equilibrium point in the (u, v) coordinates

(u_2, v_2) translation of (u, v) coordinates such that the origin in (u_2, v_2)

            coordinates is at the degenerate equilibrium point

(u_3, v_3) rotation of (u_2, v_2) coordinates such that the axes of (u_3, v_3)

            system lie along the eigendirections of degenerate equilibrium point

(u_4, v_4) near identity transformation to simplify the form of the equations

(u_5, v_5) linear transformation puts equations in Takens-Bogdanov

            normal form

4.9.2   Homoclinic Bifurcation Revisited

The slow flow equations for the 2:1 resonance near a hopf bifurcation were converted to the Takens-Bogdanov normal form by a series of five transformations outlined above. For simplicity, let's use the normal form in equation (4.121). As outlined in section 4.7.1, this system of equations can be written as a sum of a conservative and a nonconservative part [18]:

$$\dot{x} = y$$
$$\dot{y} = \underbrace{\mu_1 + \mu_3 x^2}_{\text{Conservative}} + \underbrace{\mu_2 y + \mu_4 xy}_{\text{Nonconservative}} \qquad (4.126)$$

Thus, we can express the system as function of a Hamiltonian and a nonconservative terms:

$$\dot{x} = \frac{\partial H}{\partial y}$$
$$\dot{y} = -\frac{\partial H}{\partial x} + g(x, y) \qquad (4.127)$$
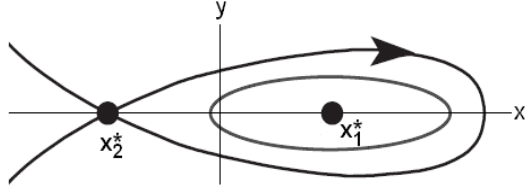
Figure 4.11: Phase portrait of the Takens-Bogdanov normal form.

where $g(x, y) = \mu_2 y + \mu_4 xy$. The Hamiltonian for this system when $g(x, y) = 0$ is:

$$H(x, y) = \frac{y^2}{2} - \mu_1 x - \mu_3 \frac{x^3}{3} = \text{constant} \tag{4.128}$$

Recall that the second transformation, $(u_1, v_1) \mapsto (u_2, v_2)$, moved the coordinate system from the origin to the degenerate equilibrium point. Analyzing the Takens-Bogdanov normal form reveals that in neighborhood of the degenerate point, there are two equilibrium points:

$$(x_1^*, y_1^*) = \left(\sqrt{-\mu_1/\mu_3}, \ 0 \right), \qquad (x_2^*, y_2^*) = \left(-\sqrt{-\mu_1/\mu_3}, \ 0 \right) \tag{4.129}$$

Conversely, when $\mu_1/\mu_3 > 0$, there are no equilibrium points and when $\mu_1 = 0$, there is one equilibrium (the degenerate case). Let's investigate this further.

When we evaluate the Jacobian matrix of the conservative part of the slow flow in (4.126) at each of the equilibrium points in (4.129), we find the $Tr(J_Q) = 0$ at both. However, the $Det(J_Q) > 0$ for one and $Det(J_Q) < 0$ for the other. Therefore, the latter is a saddle point and the former is a center. Since $\mu_1 = F_1$ and $\mu_3 = F_2$ are complicated functions of A_2, κ_2 and ε, we assume the $Det(x_1^*, y_1^*) > 0$ and $Det(x_2^*, y_2^*) < 0$, whereupon the phase portrait for the Hamiltonian system is shown in Figure 4.11.

The trajectory connecting the stable and unstable manifolds of the saddle point is called the separatrix, which separates the basin of attraction for the periodic solutions from that of the unbounded solutions. The periodic solutions lie inside the region of the separatrix on the right.

To proceed as wed did in section 4.8, we would like to know the function that defines the separatrix. The first step is to find the value of H on the separatrix. Thus, we evaluate the Hamiltonian at the equilibrium point: (x_2^*, y_2^*), which yields the $H =$ constant:

$$H\left(-\sqrt{-\mu_1/\mu_3},\ 0\right) = \mu_1\sqrt{-\mu_1/\mu_3} + \frac{\mu_3}{3}(-\mu_1/\mu_3)^{3/2} = \frac{2\mu_1}{3}\sqrt{-\frac{\mu_1}{\mu_3}} = h \quad (4.130)$$

where h is the constant on the separatrix and $\mu_1 = F_1$ and $\mu_3 = F_2$ in (4.124). However, this separatrix does not exist when there is one or zero equilibrium points in the slow flow. Remember, the analysis thus far is for the conservative system. We learned that when the nonconservative perturbation is added to the Hamiltonian system, the separatrix disappears. Therefore, we need to investigate how the separatrix changes when we vary the nonconservative parameters μ_2 and μ_4, which are functions of A and κ. Hence, the unfolding has uncovered the homoclinic bifurcation. To continue, let's return the nearly Hamiltonian system:

$$\dot{x} = \frac{\partial H}{\partial y}$$
$$\dot{y} = -\frac{\partial H}{\partial x} + g(x, y) \quad (4.131)$$

where $g(x, y) = \mu_2 y + \mu_4 xy$ and μ_2 and μ_4 are order of epsilon. Using the approximation to the Melnikov Integral in equation (4.83) with $f = 0$, the condition for the preservation of the separatrix loop (to find the bifurcation curve in the A-κ parameter space) is:

$$\oint_\Gamma (\mu_2 y + \mu_4 xy)\dot{x}\ dt = \oint_\Gamma (\mu_2 + \mu_4 x)\dot{x}^2\ dt = 0 \quad (4.132)$$

where $x(t)$ is the separatrix. In equation (4.130), we found

$$h = \frac{2\mu_1}{3}\sqrt{-\frac{\mu_1}{\mu_3}} = \frac{\dot{x}^2}{2} - \mu_1 x - \mu_3 \frac{x^3}{3} \tag{4.133}$$

Equation (4.128) can be rewritten as a nonlinear first order ODE on x, when we define $\dot{x} = y$:

$$\frac{1}{2}\left(\frac{dx}{dt}\right)^2 = \mu_1 x + \mu_3 \frac{x^3}{3} + h \tag{4.134}$$

We solve for $x(t)$ above by using separation of variables:

$$\int \left(\mu_1 x + \mu_3 \frac{x^3}{3} + h\right)^{-1/2} dx = \int \sqrt{2}dt \tag{4.135}$$

Fortunately, the integrand factors:

$$\mu_1 x + \mu_3 \frac{x^3}{3} + \frac{2\mu_1}{3}\sqrt{-\frac{\mu_1}{\mu_3}} = \left(\frac{\mu_3}{3}\right)\left(x + \sqrt{-\frac{\mu_1}{\mu_3}}\right)^2 \left(x - 2\sqrt{-\frac{\mu_1}{\mu_3}}\right) \tag{4.136}$$

Let's define $\eta_1 = \sqrt{-\mu_1/\mu_3}$ and $\eta_2 = \mu_3/3$ for convenience. Thus, the integral in equation (4.135) simplifies to:

$$\int (x + \eta_1)^{-1}(x - 2\eta_1)^{-1/2} dx = \int \sqrt{2\eta_2}\, dt \tag{4.137}$$

Again we use MACSYMA to solve the integral,

$$\frac{2}{\sqrt{3\eta_1}} \arctan\left(\frac{x - 2\eta_1}{3\eta_1}\right)^{1/2} = \sqrt{2\eta_2}t \tag{4.138}$$

provided $\eta_1 = \sqrt{-\mu_1/\mu_3} > 0$, which is true if $\mu_3 < 0$. Hence,

$$x(t) = 3\eta_1 \tan^2\left(\sqrt{6\eta_1\eta_2}t/2\right) + 2\eta_1 \tag{4.139}$$

provided $\eta_2 > 0$. However, $\eta_2 = \mu_3/3 < 0$ (cf. equation (4.124)). Therefore, $\sqrt{\eta_2}$ is imaginary. This works to our benefit since $\tan(ix) = i\tanh(x)$. Finally,

$$x(t) = -3\eta_1 \tanh^2\left(\sqrt{6\eta_1\eta_2}t/2\right) + 2\eta_1 \tag{4.140}$$

Let's return to equation (4.132), the condition on A and κ to preserve the separatrix,

$$\oint_{\Gamma} (\mu_2 + \mu_4 x)\dot{x}^2 \, dt = 0 \tag{4.141}$$

Substituting equation (4.140) in the integral above, and computing the integral in MACSYMA, we retrieve:

$$A_2 = \frac{8\sqrt{5}}{25}\kappa_2 + \frac{2336\sqrt{5}}{3125}\kappa_2^2 \tag{4.142}$$

We want this bifurcation curve in the original parameter space of A-κ. Therefore, we substitute equation (4.100) and (4.101) into equation (4.142) to yield the homoclinic bifurcation curve:

$$A = \frac{8\sqrt{5}}{25}\left(\kappa + \frac{3}{4}\right) + \frac{2336\sqrt{5}}{3125}\left(\kappa + \frac{3}{4}\right)^2 - \frac{2}{\sqrt{5}} \tag{4.143}$$

Figure 4.12 shows the first order analytical curve in the A-κ parameter space. For parameter values in the neighborhood the singular point $\left(-\frac{2}{\sqrt{5}}, -\frac{3}{4}\right)$, the analytical curve HoC_a is in very good agreement with the numerical curve HoC_n.

4.10   Discussion

The main difference between the three examples is that Examples 2 and 3 involve the occurrence of a Hopf bifurcation, whereas Example 1 does not. Since each examples correspond to the parameter value $\Lambda = -1/2$, we may gain insight into the dependence of the dynamical structure on parameters by varying κ and A as in Figure 4.2. Here Example 1 corresponds to the horizontal line $\kappa = -0.80$, Example 2 corresponds to the horizontal line $\kappa = -0.35$ and Example 3 corresponds to the horizontal line $\kappa = 0$. As can be seen from this figure, the branch of Hopf bifurcations exists for $\kappa > -3/4$. As expected, the horizontal line $\kappa = -3/4$, which
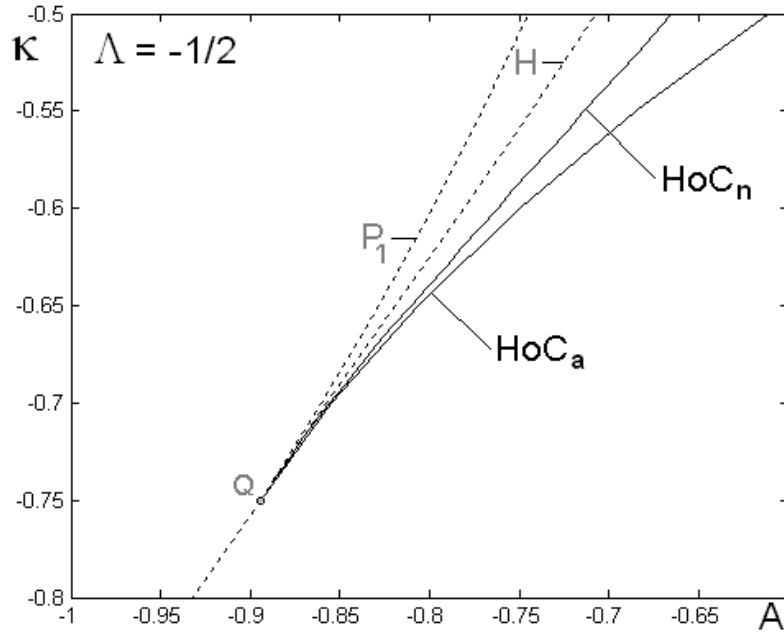
Figure 4.12: Bifurcation set for $\Lambda = -1/2$. Point Q is the location where the double zero eigenvalue occurs. P_1 is the saddle-node bifurcation, H is the Hopf bifurcation, HoC_n is the homoclinic bifurcation curve found by numerical integration and HoC_a is the homoclinic curve found by unfolding point Q.

corresponds to a system for which both the $Tr(J)$ and the $Det(J)$ simultaneously vanish, lies between Examples 1 and 2.

In addition to the saddle-node, pitchfork and Hopfs bifurcations, which are shown in Figure 4.1, and for which we obtained analytical expressions. This system also exhibits limit cycle folds, symmetry-breaking, homoclinic and heteroclinic bifurcations. We have found analytical expressions for the symmetry-breaking and homoclinic bifurcations. We obtained numerical approximations for these bifurcations and they are shown in Figures 4.9 and 4.12.

Although Figures 4.3-4.5 are drawn for the specific value $\Lambda = -1/2$, certain

features of the bifurcation set will occur for a generic value of Λ. These include:

1. Places where the Hopf curve becomes tangent to the P_1 or P_4 saddle-node bifurcation curve and terminates. As just mentioned, both the $Tr(J)$ and the $Det(J)$ vanish at such a point. The corresponding value of κ is $\kappa = \frac{1}{2\Lambda} - \frac{\Lambda}{2}$.

2. Places where the P_1 and P_2 bifurcation curves are tangent. By symmetry, the P_4 and P_3 curves are also tangent there. The associated value of κ is $\kappa = -\Lambda$.

3. Places where the P_1 and P_4 branches go off to infinity. These come from the vanishing of the denominators in equation (4.20) and correspond to $\kappa = \frac{1}{\Lambda}$.

4.11   Conclusions

We have studied the dynamics of a system (4.3) which exhibits the simultaneous phenomena of both parametric excitation and Hopf bifurcation. Imagine that we hold all parameters fixed except for the damping coefficient A, and that we ask what is expected to happen as A decreases through the parametric resonance/Hopf region. We begin with a stable equilibrium point at the origin of the slow flow which corresponds to a stable trivial solution of equation (4.3). Then the first bifurcation is reached while A is still positive, giving rise to a pair of stable equilibria in the slow flow which correspond to a single stable period-2 subharmonic motion in equation (4.3). As A decreases and becomes negative, a variety of bifurcations may occur which culminate for sufficiently negative A in a slow flow which exhibits only a stable limit cycle and an unstable equilibrium at the origin. This limit cycle corresponds in equation (4.3) to a stable quasiperiodic motion which may be thought of as combining the periodic motion which would have been created in the Hopf (in the absence of parametric excitation) with a motion coming from the

periodic parametric forcing.

In many applications, a limit cycle created in a Hopf bifurcation is destroyed in a saddle-connection bifurcation in the unforced system. This scenario occurs, for example, in the Takens-Bogdanov (double-zero eigenvalue) system (see [18], p.371). Such a situation also occurs in the ENSO system [61]-[62] described briefly in the introduction. When such a system is parametrically excited, the analysis in the present work shows that a quasiperiodic motion may be expected to occur in the neighborhood of the Hopf bifurcation. We begin to examine what happens to that motion as the bifurcation parameter proceeds towards the value corresponding to the saddle-connection bifurcation in the unforced system Chapter 6.

Chapter 5

2:1 Resonance of a Delayed Nonlinear Mathieu Equation

> *"The lecturer should give the audience full reason to believe that all his powers have been exerted for their pleasure and instruction."*
>
> *– Michael Faraday*

We investigate the dynamics of a delayed nonlinear Mathieu equation:

$$\ddot{x} + (\delta + \varepsilon\alpha\cos t)x + \varepsilon\gamma x^3 = \varepsilon\beta x(t - T)$$

in the neighborhood of δ=1/4. Three different phenomenons are combined in this system: 2:1 parametric resonance, cubic nonlinearity, and delay. The method of averaging (valid for small ε) is used to obtain a slow flow which is analyzed for stability and bifurcations. We show that the combined effect of 2:1 parametric excitation, cubic nonlinearity and delay stabilizes a region in the T-δ plane for certain combinations of the delay parameters β and T, which would normally be unstable in the absence of delay. We also show that the delay term behaves like effective damping, adding dissipation to a conservative system.

5.1 Motivation

Insperger and Stépán generated the stability chart for the delayed linear Mathieu equation with a delay period of $T = 2\pi$ [24]. Our analysis shows that the behavior of the system for $T = 2\pi$ is a very special case (especially relevant for milling applications, [25]) in that it is qualitatively different from that of systems for T is different from $T = 2\pi$. We present an investigation of the delayed nonlinear Mathieu equation with varying delay period, valid for small ε and small εT.

5.2 Introduction

This chapter concerns the dynamics of the following parametrically excited, nonlinear differential delay equation (DDE):

$$\ddot{x}(t) + (\delta + a \cos t)\, x(t) + cx(t)^3 = bx(t - T) \tag{5.1}$$

where δ, a, b, c and T are parameters: δ is the frequency-squared of the simple harmonic oscillator, a is the amplitude of the parametric resonance, b is the amplitude of delay, c is the amplitude of the cubic nonlinearity, and T is the delay period.

Various special cases of equation (5.1) have been studied previously, depending on which parameters are zero. In the case that b and c are zero, we have the linear Mathieu equation, the stability chart for which is well known (Cf. Chapter 2), see Figure 5.1. In the case that only b is zero, we have a nonlinear Mathieu equation for which the bifurcations associated with stability change are also well known [42]. In the case that a and c are zero, we have the linear autonomous DDE of Hsu and Bhatt [8], who generated stability charts, see Figure 5.2.
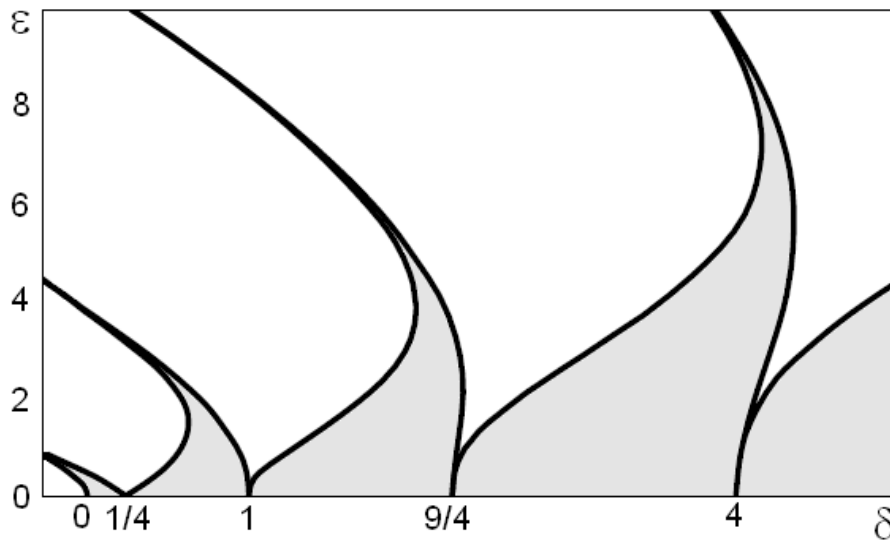
Figure 5.1: Stability chart for the Mathieu equation without delay, equation (5.1) with $b = c = 0$. The solution is stable in the shaded regions.
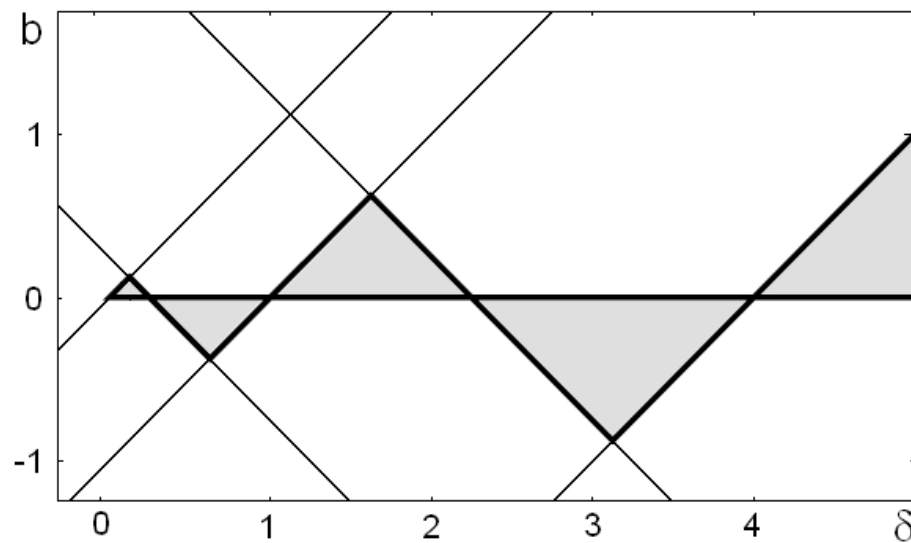
Figure 5.2: Stability chart for the Hsu-Bhatt DDE, equation (5.1) with $a = c = 0$ and $T = 2\pi$. The solution is stable in the shaded regions.
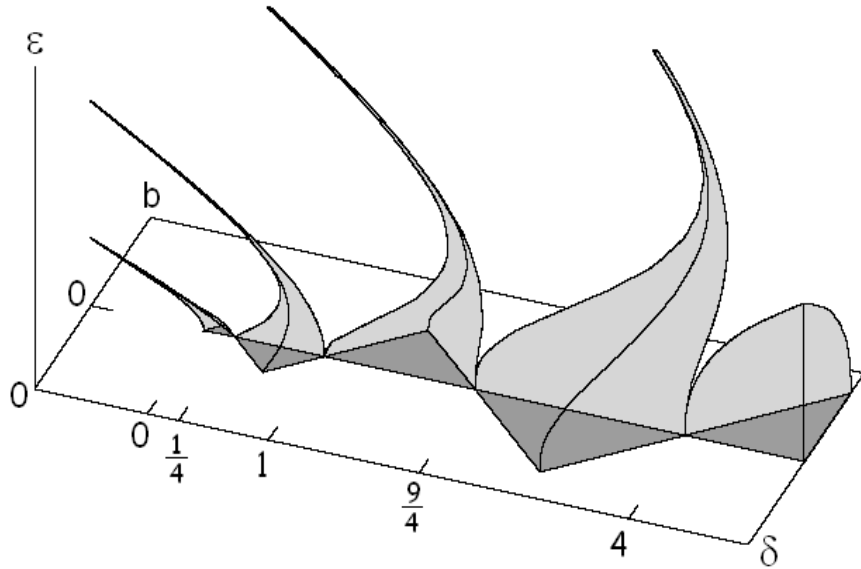
Figure 5.3: Stability chart for the delayed Mathieu equation with $T = 2\pi$, $a = 1$ and $c = 0$, . The solutions in the shaded regions are stable. The darker shaded triangles are those in Figure 5.2.

The linear form of equation (5.1) has been studied previously by Insperger and Stépán [24], who, by utilizing the method of exponential multipliers, generated the stability chart for a fixed delay period $T=2\pi$, where $a=1$ and $c=0$, see Figure 5.3.

In this research effort we use the method of averaging to generate stability charts and associated bifurcations for the delayed nonlinear Mathieu equation (5.1) with a general delay period [32]. We note that although DDE's are infinite dimensional [54], and hence more complicated than ODE's, the averaging method which we use replaces the original DDE by an ODE slow flow, an approximation which is valid for small ε.

5.2.1   The Hsu-Bhatt Equation

The following simple harmonic oscillator with a delay term is the Hsu-Bhatt equation,

$$\ddot{x}(t) + \delta x(t) = bx(t - T) \tag{5.2}$$

where b is the delay amplitude, the T is the delay period, and δ is the frequency-squared of the simple harmonic oscillator. If the delay amplitude was zero ($b=0$), then the simple harmonic oscillator is stable when $\delta > 0$ and unstable when $\delta < 0$. When we turn up (or down) the value of the delay amplitude and fix the system a delay period, the stable system can become unstable and the unstable system can become stable.

Let's consider the solution to equation (5.2). Generally, to solve a second order constant coefficient differential equation, we assume the solution to be of the form:

$$x(t) = e^{\lambda t} \tag{5.3}$$

Substituting this solution into equation (5.2) we obtain the characteristic equation:

$$\lambda^2 + \delta = b \ e^{-\lambda T} \tag{5.4}$$

Note that equation (5.4) is a transcendental equation on λ and therefore has an infinite number of solutions. If we assume that the roots to the transcendental equation are complex, then we can write $\lambda = a + i\omega$. Substituting $\lambda = a + i\omega$ into equation (5.4) and solving for the real and imaginary parts of the equation, we obtain:

$$a^2 - \omega^2 + \delta = be^{-aT} \cos \omega T \tag{5.5}$$

$$2a\omega = be^{-aT} \sin \omega T \tag{5.6}$$

We are interested in knowing for what values of b and T does this system change stability. The roots of the transcendental characteristic equation hold the stability

information. From these roots, we can generate the stability charts (Cf. Figure 5.2).

We know the system is stable when the real part of the root is negative. Thus, the change of stability occurs when the real part equals zero. Therefore, we set $a = 0$ in equations (5.5) and (5.6) to find the values of b and T at the bifurcation point:

$$-\omega^2 + \delta = b \cos \omega T \tag{5.7}$$

$$0 = b \sin \omega T \tag{5.8}$$

Solving these two equations simultaneously, we retrieve expressions for ω and T when the real part of the root is zero:

$$\omega^2 = \delta - b(-1)^n \tag{5.9}$$

$$\omega T = n\pi, \qquad n = 1, 2, 3, \ldots \tag{5.10}$$

where $\cos n\pi = (-1)^n$. Next, solve equation (5.10) for ω and substitute ω into equation (5.9) to obtain:

$$\delta = \left(\frac{n\pi}{T}\right)^2 + b(-1)^n \tag{5.11}$$

which give the stability curves in the δ-b parameter plane for any delay period.

Let's examine this equation for $T = \pi$ and $T = 2\pi$. The stability charts are plotted in the top and bottom of Figure 5.4, respectively. Note that the stability region shrinks as the delay period increases. The first stability region in the top of Figure 5.4 for $T = \pi$ is twice as large as the first stability region in the bottom of Figure 5.4 for $T = 2\pi$. Recall that these stability charts were generated based on the knowledge that an equilibria changes stability when the real part of the imaginary root goes to zero. When this scenario occurs in ordinary differential
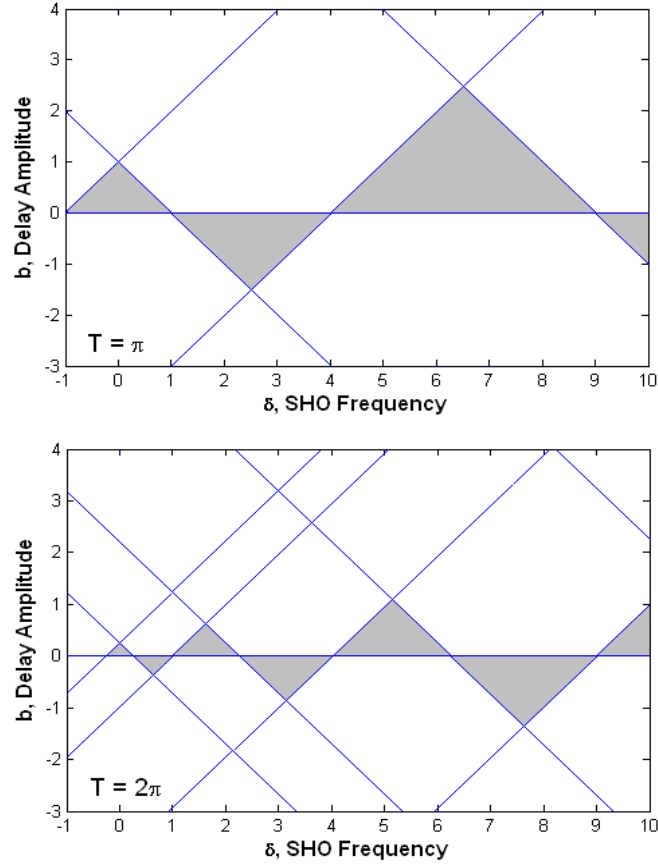
Figure 5.4: Stability charts for Hsu-Bhatt equation (5.2) with T=π (top) and T=2π (bottom). The shaded regions are stable.

equations, a Hopf bifurcation occurs. Since equation (5.2) is linear, only the origin changes stability when we cross the transition curve.

Up to this point we have only recreated the stability charts of Hsu-Bhatt [8]. We have obtained the equation that generates the transition curves, equation (5.11). Let's examine it's limit as $b \to 0$ when $T = 2\pi$:

$$\delta = \frac{n^2}{4}, \qquad n = 1, 2, \ldots \tag{5.12}$$

These values for δ when $b = 0$ are the *same* values of δ when $\varepsilon = 0$ in the Mathieu equation that locate the resonant regions. Thus, the location of the instability

regions are the same. This is one possible reason it would be advantageous to analyze equation (5.1), the linear delayed Mathieu equation, a delay period of $T = 2\pi$ [24]. The location of the instability regions in both cases meet at the same points on the $b = 0$ and $\varepsilon = 0$ axes, as shown in Figure 5.3. As it turns out, $T = 2\pi$ is a special case. In this research effort, we are going to find the stability charts for a fixed b in the T-δ parameter space for small ε. This study will yield insight into the effect various delay periods will have on the system.

5.2.2 The Nonlinear Hsu-Bhatt Equation

The nonlinear Hsu-Bhatt equation is a Duffing oscillator combined with delay:

$$\ddot{x}(t) + \delta x(t) + \varepsilon \alpha x(t)^3 = bx(t - T) \tag{5.13}$$

where α is the amplitude of the cubic nonlinearity. When $\alpha = 0$, we have the Hsu-Bhatt equation analyzed in section 5.2.1. When $b = 0$, we have the equation for a Duffing oscillator, which is a model of a system that includes nonlinear restoring forces (Cf. Chapter 6). The period-amplitude relationship for the periodic motion of the Duffing oscillator is given by [42]:

$$T_{pm} = 2\pi \left(1 - \frac{3}{8} \alpha A^2 \varepsilon + O(\varepsilon^2) \right) \tag{5.14}$$

The nonlinear terms controls the growth of the periodic motion. The period of the periodic motion grows quadratically with amplitude. In the following section, we utilize Lindstedt's perturbation method to investigate what happens to the period-amplitude relationship when delay is added to the system.

Lindstedt's Method

Lindstedt's method is a singular perturbation technique that can be used to derive the period-amplitude relationship in a nonlinear oscillator, even for delay differ-

ential equations [42]. Let's assume that equation (5.13) with $b = 0$ has periodic motion due to the birth of a limit cycle from a Hopf bifurcation. The bifurcation occurs when the roots to the characteristic equation are purely imaginary, $\pm i\omega$, which happens in the $b \neq 0$ system at a critical delay period, T_{crit}. The nonlinear Hsu-Bhatt equation may exhibit a periodic solution, $x(t) = A \cos \Omega t$, for values of delay period T close to the critical value,

$$T = T_{crit} + \varepsilon\mu + \dots \tag{5.15}$$

The main idea behind Lindstedt's Method is to build the period-amplitude relationship by stretching time:

$$\tau = \Omega t, \qquad \text{where} \qquad \Omega = \omega + \varepsilon k_1 + \dots \tag{5.16}$$

where k_1 is to be found. Since the time dimension of the phase space was stretched, the delay period needs to be stretched appropriately. The delay term becomes:

$$x(t - T) = x(\Omega(t - T)) = x(\tau - \Omega T) \tag{5.17}$$

Substituting equations (5.15) and (5.16) into (5.17) we obtain the stretched delay term:

$$x_d = x(\tau - \Omega T) = x(\tau - \omega T_{crit} - \varepsilon(k_1 T_{crit} + \omega\mu)) \tag{5.18}$$

Next we Taylor expand the delay term, x_d, about $\varepsilon = 0$:

$$x_d = x(\tau - \omega T_{crit}) - \varepsilon\frac{dx}{d\tau}(\tau - \omega T_{crit}) \cdot (k_1 T_{crit} + \omega\mu) \tag{5.19}$$

The stretched differential equation comes from substituting equation (5.16) and (5.19) into equation (6.1):

$$(\omega^2 + 2\varepsilon\omega k_1)x(\tau)'' + \delta x(\tau) + \varepsilon\alpha x(\tau)^3 =$$

$$bx(\tau - \omega T_{crit}) - \varepsilon b x_d'(\tau - \omega T_{crit}) \cdot (k_1 T_{crit} + \omega\mu) \tag{5.20}$$

where the prime denotes differentiation with respect to τ. Next we expand $x(\tau)$ in a power series in ε:

$$x(\tau) = x_0(\tau) + \varepsilon x_1(\tau) + \ldots \tag{5.21}$$

We substitute this expression into (5.20) and collect terms of order epsilon:

$$\varepsilon^0 : \quad \omega^2 x_0'' + \delta x_0 = b x_0(\tau - \omega T_{crit}) \tag{5.22}$$

$$\varepsilon^1 : \quad \omega^2 x_1'' + \delta x_1 = b x_1(\tau - \omega T_{crit})$$

$$- 2\omega \delta_1 x_0'' - \alpha x_0^3 - (\delta_1 T_{crit} + \omega \mu) \cdot x_{0d}' \tag{5.23}$$

We take the solution to the ε^0−equation as

$$x_0 = A \cos \tau \tag{5.24}$$

We can check that this is the solution by substituting it back into (5.24):

$$-\omega^2 \cos \tau + \delta \cos \tau = b \cos(\tau - \omega T_{crit}), \quad \text{where} \quad \omega T_{crit} = \pi \tag{5.25}$$

resulting in the following expression for ω and T_{crit}:

$$\omega^2 = \delta + b, \qquad T_{crit} = \frac{\pi}{\sqrt{\delta + b}} \tag{5.26}$$

This checks with equation (5.9). Continuing, we substitute $x_0 = A \cos \tau$ into the ε-equation to obtain the x_1-equation:

$$\omega^2 x_1'' + \delta x_1 - b x_1(\tau - \pi) = -2\omega \delta_1(-A \cos \tau)$$

$$-\alpha A^3 \left(\frac{3}{4} \cos \tau + \frac{1}{4} \cos 3\tau \right) - (\delta_1 T_{crit} + \omega \mu)(-A \sin(\tau - \pi)) \tag{5.27}$$

removal of the resonant terms, $\cos \tau$ and $\sin \tau$, results in two algebraic equations that we solve to obtain the period-amplitude relationship for the periodic motion:

$$2\omega \delta_1 - \frac{3}{4}\alpha A^2 = 0 \qquad \rightarrow \qquad A^2 = \frac{8\omega}{3\alpha}\delta_1 \tag{5.28}$$

$$\delta_1 T_{crit} + \omega\mu = 0 \qquad \rightarrow \qquad \delta_1 = -\frac{(\delta+b)\mu}{\pi} \tag{5.29}$$

Thus, the period-amplitude relationship is:

$$A^2 = -\frac{8(\delta+b)^{\frac{3}{2}}}{3\alpha\pi}\mu \tag{5.30}$$

where μ is the detuning from the critical period, T_{crit} in equation (5.26), where the system changes stability. Thus, for a given δ, delay amplitude b, and $\alpha > 0$, an unstable limit cycle is born when μ changes from positive to negative, i.e., a subcritical Hopf bifurcation.

In summary, we presented the stability charts for the Hsu-Bhatt equation for $T = \pi$ and $T = 2\pi$; we discovered possible motivation as to why Insperger [24] generated the stability for the linear delay Mathieu equation for $T = 2\pi$, and we found the period-amplitude relationship for the periodic motion in the nonlinear Hsu-Bhatt equation. In the following sections, we analyze the behavior of the nonlinear Hsu-Bhatt equation with 2:1 parametric excitation for a general delay period, valid for small ε.

5.3 First Order Averaging Method

In preparation for averaging [45] equation (5.1), we introduce a small parameter ε by scaling $a = \varepsilon\alpha$, $b = \varepsilon\beta$, and $c = \varepsilon\gamma$. In addition, we detune off of 2:1 resonance by setting $\delta = \frac{1}{4} + \varepsilon\delta_1$:

$$\ddot{x}(t) + \left(\frac{1}{4} + \varepsilon\delta_1 + \varepsilon\alpha\cos t\right)x(t) + \varepsilon\gamma x(t)^3 = \varepsilon\beta x(t-T) \tag{5.31}$$

When $\varepsilon = 0$, equation (5.31) reduces to $\ddot{x} + (1/4)x = 0$, with the solution:

$$x(t) = A\cos\left(\frac{t}{2} + \phi\right), \qquad \dot{x}(t) = -\frac{A}{2}\sin\left(\frac{t}{2} + \phi\right) \tag{5.32}$$

For $\varepsilon > 0$, we look for a solution in the form (5.32) but treat A and ϕ as time dependent. Variation of parameters gives the following equations on $A(t)$ and $\phi(t)$:

$$\dot{A}(t) = -2\varepsilon \sin\left(\frac{t}{2}+\phi\right) F\left(A\cos\left(\frac{t}{2}+\phi\right), -\frac{A}{2}\sin\left(\frac{t}{2}+\phi\right), t\right) \qquad (5.33)$$

$$\dot{\phi}(t) = -2\frac{\varepsilon}{A}\cos\left(\frac{t}{2}+\phi\right) F\left(A\cos\left(\frac{t}{2}+\phi\right), -\frac{A}{2}\sin\left(\frac{t}{2}+\phi\right), t\right) \qquad (5.34)$$

where $F(x, \dot{x}, t) = -(\delta_1 + \alpha\cos t)x(t) - \gamma x(t)^3 + \beta x(t-T)$ in which $x(t)$ is given by (5.32). For small ε we use the method of averaging [22], replacing the right-hand sides of (5.33) and (5.34) by their averages over one 2π period of the forcing function $\cos t$:

$$\dot{A} \approx -2\varepsilon\frac{1}{2\pi}\int_0^{2\pi} \sin\left(\frac{t}{2}+\phi\right) F\, dt \qquad (5.35)$$

$$\dot{\phi} \approx -2\frac{\varepsilon}{A}\frac{1}{2\pi}\int_0^{2\pi} \cos\left(\frac{t}{2}+\phi\right) F\, dt \qquad (5.36)$$

in which

$$F = -(\delta_1 + \alpha\cos t)A\cos\left(\frac{t}{2}+\phi\right) - \gamma A^3\cos^3\left(\frac{t}{2}+\phi\right)$$
$$+\beta\tilde{A}\cos\left(\frac{1}{2}(t-T)+\tilde{\phi}\right) \qquad (5.37)$$

where $\tilde{A} = A(t-T)$ and $\tilde{\phi} = \phi(t-T)$. Evaluating the integrals in (5.35) and (5.36) gives the delayed slow flow:

$$\dot{A} = \varepsilon\left(\frac{A\alpha\sin 2\phi}{2} - \tilde{A}\beta\sin\left(\frac{T}{2} - \tilde{\phi} + \phi\right)\right) \qquad (5.38)$$

$$\dot{\phi} = \varepsilon\left(\frac{3\gamma A^2}{4} - \frac{\tilde{A}\beta\cos\left(\frac{T}{2} - \tilde{\phi} + \phi\right)}{A} + \frac{\alpha\cos 2\phi}{2} + \delta_1\right) \qquad (5.39)$$

Equations (5.38) and (5.39) show that $\dot{A}$ and $\dot{\phi}$ are $O(\varepsilon)$. We now Taylor expand $\tilde{A}$ and $\tilde{\phi}$:

$$\tilde{A} = A(t-T) = A(t) - T\dot{A}(t) + \frac{1}{2}T^2\ddot{A}(t) + \dots \qquad (5.40)$$

$$\tilde{\phi} = \phi(t-T) = \phi(t) - T\dot{\phi}(t) + \frac{1}{2}T^2\ddot{\phi}(t) - \dots \qquad (5.41)$$

Thus we can replace $\tilde{A}$ and $\tilde{\phi}$ by $A(t)$ and $\phi(t)$ in equations (5.38) and (5.39) since $\dot{A}$ and $\dot{\phi}$ and $\ddot{A}$ and $\ddot{\phi}$ are of $O(\varepsilon)$ and $O(\varepsilon^2)$, respectively [65]. This approximation reduces the infinite dimensional problem into a finite dimensional problem by assuming εT is small.

After substituting the above approximation into (5.38) and (5.39), we obtain

$$A' = A\left(\frac{\alpha}{2}\sin 2\phi - \beta\sin\frac{T}{2}\right) \tag{5.42}$$

$$\phi' = \frac{3\gamma}{4}A^2 + \frac{\alpha}{2}\cos 2\phi - \beta\cos\frac{T}{2} + \delta_1 \tag{5.43}$$

where primes represent differentiation with respect to *slow time* $\eta = \varepsilon t$. We may obtain an alternate form of the slow flow equations (5.42) and (5.43) by transforming from polar coordinates A and ϕ to rectangular coordinates u and v via $u = A\cos\phi$, $v = -A\sin\phi$, giving:

$$u' = -\left(\beta\sin\frac{T}{2}\right)u + \left(\delta_1 - \frac{\alpha}{2} - \beta\cos\frac{T}{2}\right)v + \frac{3\gamma}{4}v(u^2 + v^2) \tag{5.44}$$

$$v' = \left(-\delta_1 - \frac{\alpha}{2} + \beta\cos\frac{T}{2}\right)u - \left(\beta\sin\frac{T}{2}\right)v - \frac{3\gamma}{4}u(u^2 + v^2) \tag{5.45}$$

Note that from equation (5.32) we have

$$x(t) = A\cos\left(\frac{t}{2} + \phi\right) = A\cos\phi\,\cos\frac{t}{2} - A\sin\phi\,\sin\frac{t}{2} = u\cos\frac{t}{2} + v\sin\frac{t}{2} \tag{5.46}$$

5.4   Analysis of the Slow Flow

From equation (5.46) we see that in general an equilibrium point in the slow flow (5.42) and (5.43) or (5.44) and (5.45) corresponds to a periodic motion in the original system (5.31). The origin $u = v = 0$ is an exception since it is an equilibrium point in both the slow flow equations and in the original system. The goal is to find nontrivial slow flow equilibria and analyze their stability.

5.4.1   Slow Flow Equilibria: Stability and Bifurcation

To find nontrivial slow flow equilibria, we set $A' = \phi' = 0$ in equations (5.42) and (5.43), and utilize the trig identity $\sin^2 2\phi + \cos^2 2\phi = 1$ to obtain the following condition on R, where $R = A^2$,

$$9\gamma^2 R^2 + 24\gamma \left(\delta_1 - \beta \cos \frac{T}{2} \right) R + 4 \left(4\beta^2 - \alpha^2 + 4\delta_1^2 - 8\beta\delta_1 \cos \frac{T}{2} \right) = 0 \quad (5.47)$$

Equation (5.47) is a quadratic on R. The two solutions are:

$$R = \frac{4}{3\gamma} \left[\beta \cos \frac{T}{2} - \delta_1 \pm \frac{1}{2}\sqrt{\alpha^2 - 4\beta^2 \sin^2 \frac{T}{2}} \right] \quad (5.48)$$

Each value of R corresponds to two nontrivial slow flow equilibria located 180° apart. This may be seen by noting that equations (5.44) and (5.45) are invariant under the transformation $(u, v) \mapsto (-u, -v)$, which means that if (u, v) is a slow flow equilibrium, then so is $(-u, -v)$.

R must be nonnegative for nontrivial equilibrium points. This condition yields two inequalities:

$$\delta_1 \leq \beta \cos \frac{T}{2} \pm \frac{1}{2}\sqrt{\alpha^2 - 4\beta^2 \sin^2 \frac{T}{2}} \quad (5.49)$$

And for real roots, the discriminant in the inequality in (5.49) must be positive. This condition yields:

$$\left| \sin \frac{T}{2} \right| \leq \frac{1}{2} \left| \frac{\alpha}{\beta} \right| \quad (5.50)$$

Hence, for a given α and β, the inequality (5.50) gives a condition on the delay period T such that there will exist nontrivial slow flow equilibrium points. In the case that $|\beta/\alpha| \leq 1/2$, there will exist nontrivial fixed points for all T.

When the inequality in (5.50) is satisfied, there are at least **two** nontrivial slow flow equilibrium points if,

$$\delta_1 < \beta \cos \frac{T}{2} + \frac{1}{2}\sqrt{\alpha^2 - 4\beta^2 \sin^2 \frac{T}{2}} \quad (5.51)$$

In addition, there will be **two** more nontrivial slow flow equilibrium points if,

$$\delta_1 < \beta \cos \frac{T}{2} - \frac{1}{2}\sqrt{\alpha^2 - 4\beta^2 \sin^2 \frac{T}{2}} \tag{5.52}$$

Thus it is possible to have up to four nontrivial slow flow equilibria. When we include the origin, this makes a possible total of up to five slow flow equilibria. Next we investigate which parameter combinations of δ_1 and T cause the slow flow equilibrium points to change stability for a given α and β, and which bifurcations, if any, accompany the change in stability.

The *trace* and *determinant* of the Jacobian matrix evaluated at an equilibrium point contain the local stability information. Recall that a saddle-node or pitchfork bifurcation generically occurs when the $Det(J) = 0$, and a Hopf bifurcation generically occurs when the $Tr(J) = 0$ and $Det(J) > 0$ [57]. From the slow flow equations (5.44) and (5.45), the Jacobian matrix is:

$$J = \begin{bmatrix} J_{11} & J_{12} \\ J_{21} & J_{22} \end{bmatrix} \tag{5.53}$$

where

$$J_{11} = -\beta \sin \frac{T}{2} + \frac{3\gamma}{2} uv$$

$$J_{12} = \delta_1 - \frac{\alpha}{2} - \beta \cos \frac{T}{2} + \frac{3\gamma}{4} u^2 + \frac{9\gamma}{4} v^2$$

$$J_{21} = -\delta_1 - \frac{\alpha}{2} + \beta \cos \frac{T}{2} - \frac{3\gamma}{4} v^2 - \frac{9\gamma}{4} u^2$$

$$J_{22} = -\beta \sin \frac{T}{2} - \frac{3\gamma}{2} uv$$

where u and v are to be evaluated at the slow flow equilibria.

The trace of the Jacobian matrix is:

$$Tr(J) = -2\beta \sin \frac{T}{2} \tag{5.54}$$

Note that $Tr(J)$ is a function of the delay parameters only, and in particular does not depend on R. Therefore, $Tr(J) = 0$ at *all* of the slow flow equilibrium points when $\beta = 0$, $T = 0$, or $T = 2\pi$. In particular, a change of stability and a possible Hopf bifurcation (birth of a limit cycle) will occur at $T = 2\pi$ if $Det(J) > 0$.

The determinant of the Jacobian matrix is:

$$Det(J) = \frac{27}{16}\gamma^2 R^2 - 3\gamma \left(\beta \cos \frac{T}{2} - \delta_1 \right) R$$
$$- 2\beta\delta_1 \cos \frac{T}{2} + \delta_1^2 + \beta^2 - \frac{\alpha^2}{4} + \frac{3\alpha\gamma}{4}(v^2 - u^2) \qquad (5.55)$$

where the $(u^2 + v^2)$ terms were replaced with R. The $(v^2 - u^2)$ term is simplified by multiplying the RHS of equation (5.44) by v and subtracting from it the RHS of equation (5.45) multiplied by u. This calculation gives:

$$(v^2 - u^2) = \frac{1}{2\alpha} \left[3\gamma R^2 + 4\left(\delta_1 - \beta \cos \frac{T}{2} \right) R \right] \qquad (5.56)$$

Substituting this expression into equation (5.55) we obtain the following expression for the determinant:

$$Det(J) = \frac{45}{16}\gamma^2 R^2 - \frac{9}{2}\gamma \left(\beta \cos \frac{T}{2} - \delta_1 \right) R - 2\beta\delta_1 \cos \frac{T}{2} + \delta_1^2 + \beta^2 - \frac{\alpha^2}{4} \qquad (5.57)$$

The value of R at the nontrivial slow flow equilibria are given in equation (5.48). Substituting that expression for R into the expression for the determinant yields the value of the determinant at the slow flow equilibria:

$$Det(J) = -4\beta^2 \sin^2 \frac{T}{2} + \alpha^2 \pm 2\left(\beta \cos \frac{T}{2} - \delta_1 \right) \sqrt{\alpha^2 - 4\beta^2 \sin^2 \frac{T}{2}} \qquad (5.58)$$

A change in stability occurs when the determinant vanishes. Thus by setting equation (5.58) equal to zero, we may solve for a critical value of δ_1, the detuning, as a function of T for a given α and β:

$$\delta_1 = \beta \cos \frac{T}{2} \pm \frac{1}{2}\sqrt{\alpha^2 - 4\beta^2 \sin^2 \frac{T}{2}} \qquad (5.59)$$

From equation (5.48), equation (5.59) implies $R = 0$. This means that the stability change associated with equation (5.59) occurs at the origin. Thus, accompanying this change in stability is a bifurcation. If the inequalities (5.50), (5.51) and (5.52) are replaced by equal signs, then (5.50) becomes the condition for a *saddle-node bifurcation* and (5.51) and (5.52) become conditions for *pitchfork bifurcations*. We illustrate these results by considering two examples.

5.4.2 Example 1

We consider the case in which $\beta = \frac{1}{4}$ and $\alpha = \gamma = 1$. Equation (5.59) for this example becomes:

$$\delta_1 = \frac{1}{4}\cos\frac{T}{2} \pm \frac{1}{2}\sqrt{1 - \frac{1}{4}\sin^2\frac{T}{2}} \tag{5.60}$$

As stated in the previous section, the origin changes stability along the curves in the T-δ_1 parameter plane given by equation (5.60), corresponding to $Det(J) = 0$. In addition, there is a stability change along the line $T = 2\pi$, corresponding to $Tr(J) = 0$, when $Det(J) > 0$. See Figure 5.5.

Equation (5.60) also corresponds to the occurrence of pitchfork bifurcations in the slow flow. These curves are shown in the bifurcation set in Figure 5.6. Along with the curves are points labeled a through i. Each letter corresponds to the qualitative phase portrait of the respective slow flow system as shown in Figure 5.7. Pitchfork bifurcations occur as we move from top to bottom in each column of Figure 5.7.

As we move from left to right in each row of Figure 5.7, we cross the line $T = 2\pi$. For those slow flow equilibria for which $Det(J) > 0$ (non-saddles), a stability change is observed, but no limit cycle is seen to be born. The associated Hopf bifurcation turns out to be degenerate, as will be shown later in the paper.

Figure 5.5: Stability of the origin for Example 1, $\beta = \frac{1}{4}$ and $\alpha = \gamma = 1$. Black is stable, white is unstable. The transition curves separating the stability regions are given by equation (5.60) and by $T = 2\pi$.

Figure 5.6: Bifurcations in slow flow equilibria for Example 1, $\beta = \frac{1}{4}$ and $\alpha = \gamma = 1$. The letters a, b, c, d, e, f, g, h, i correspond to the qualitative phase portraits shown in Figure 5.7. Pitchfork bifurcations occur on the $Det(J) = 0$ curves, given by equation (5.60). A change of stability occurs on the $Tr(J) = 0$ curve, $T = 2\pi$, in the case that $Det(J) > 0$ (non-saddle equilibria). No limit cycles are born as we cross the latter curve because the associated Hopf bifurcation is degenerate.

Figure 5.7: Qualitative phase portraits for Example 1, $\beta = \frac{1}{4}$ and $\alpha = \gamma = 1$. The letters a, b, c, d, e, f, g, h, i correspond to various parameter combinations of δ_1 and T as shown in Figure 5.6. The bifurcations from a to g, b to h, and c to i, respectively, are pitchforks. The bifurcations from a to c, d to f, and g to i, respectively, are degenerate Hopfs.

5.4.3   Example 2

We consider the case in which $\beta = \frac{3}{5}$ and $\alpha = \gamma = 1$. This example exhibits qualitatively different behavior from the previous example. Equation (5.59) for this example becomes:

$$\delta_1 = \frac{3}{5} \cos \frac{T}{2} \pm \frac{1}{2} \sqrt{1 - \frac{36}{25} \sin^2 \frac{T}{2}} \qquad (5.61)$$

Figure 5.8 shows the curves (5.61), corresponding to $Det(J) = 0$, which bound stability regions of the origin. In addition, there is a stability change along the line $T = 2\pi$, corresponding to $Tr(J) = 0$, when $Det(J) > 0$. Note that for this example, when $|\sin(T/2)| > 5/6$ the discriminant in (5.61) is less than zero, resulting in a complex conjugate pair. Therefore, it is possible to eliminate the regions of instability by choosing the delay period T appropriately.

Equation (5.61) also corresponds to the occurrence of pitchfork bifurcations in the slow flow. These curves are shown in the bifurcation set in Figure 5.9. The curve $T = 2\pi$ is also shown in Figure 5.9, representing a degenerate Hopf in which no limit cycle is born, as in Example 1. In addition, saddle-node bifurcations occur in Example 2 corresponding to the vanishing of the discriminant in equation (5.61). These occur when $|\sin(T/2)| = 5/6$, and appear as vertical lines marked $Disc = 0$ in Figure 5.9.

Along with these bifurcation curves are points labeled a through o. Each letter corresponds to the qualitative phase portrait of the corresponding slow flow. The points a through i are qualitatively the same as in Figure 5.7. The points j through o are shown in Figure 5.10. Saddle-node bifurcations occur as we move from left to right in each row of Figure 5.10.
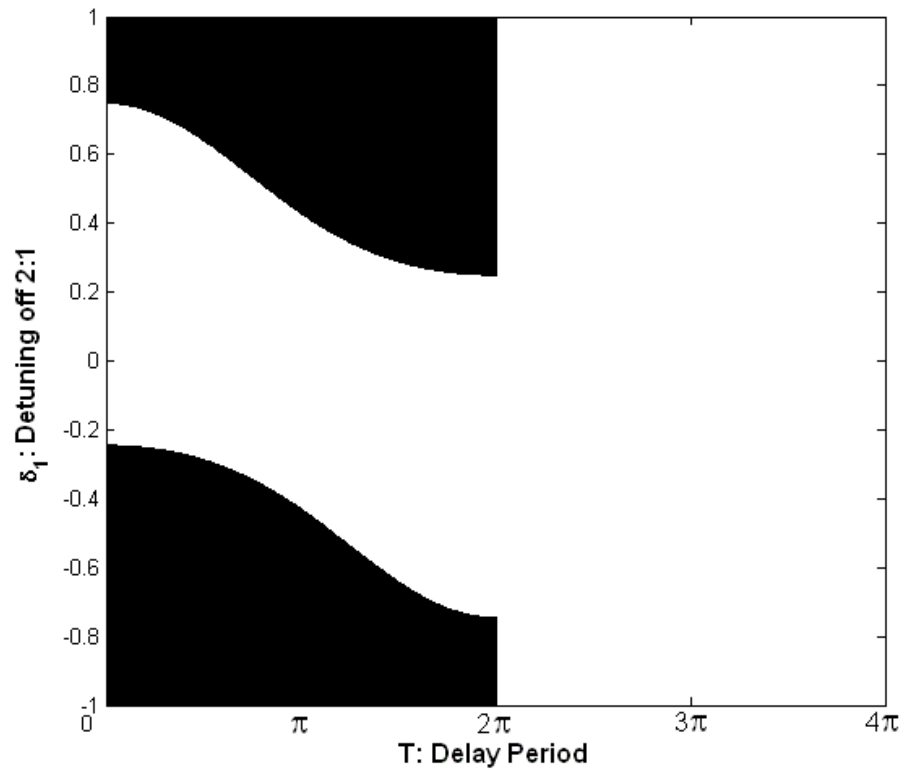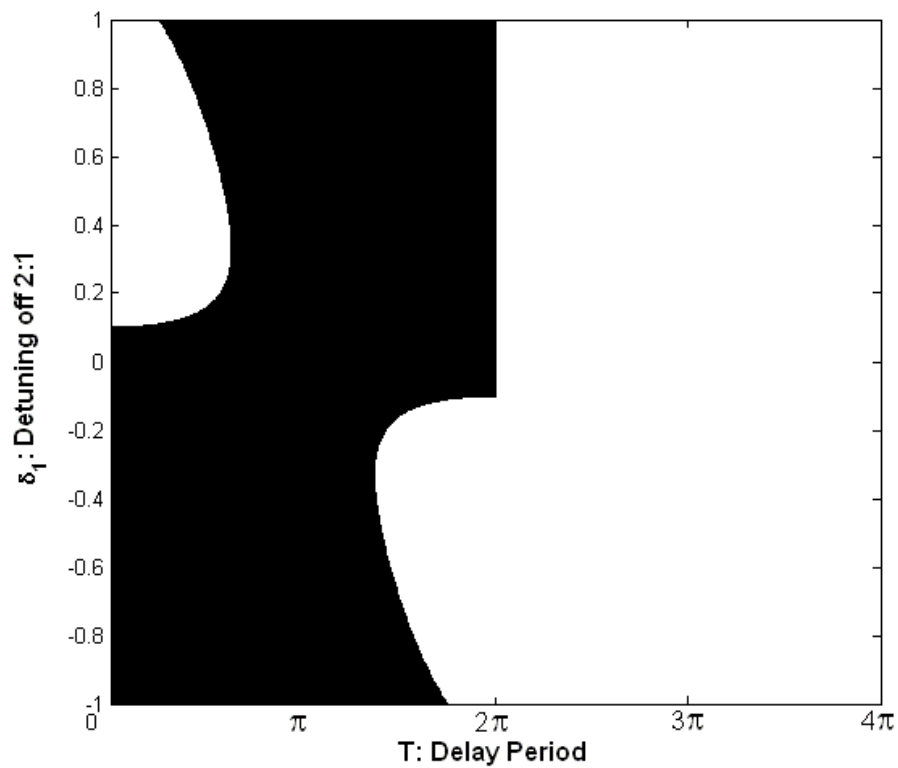
Figure 5.8: Stability of the origin for Example 2, $\beta = \frac{3}{5}$ and $\alpha = \gamma = 1$. Black is stable, white is unstable. The transition curves separating the stability regions are given by equation (5.61) and by $T = 2\pi$.
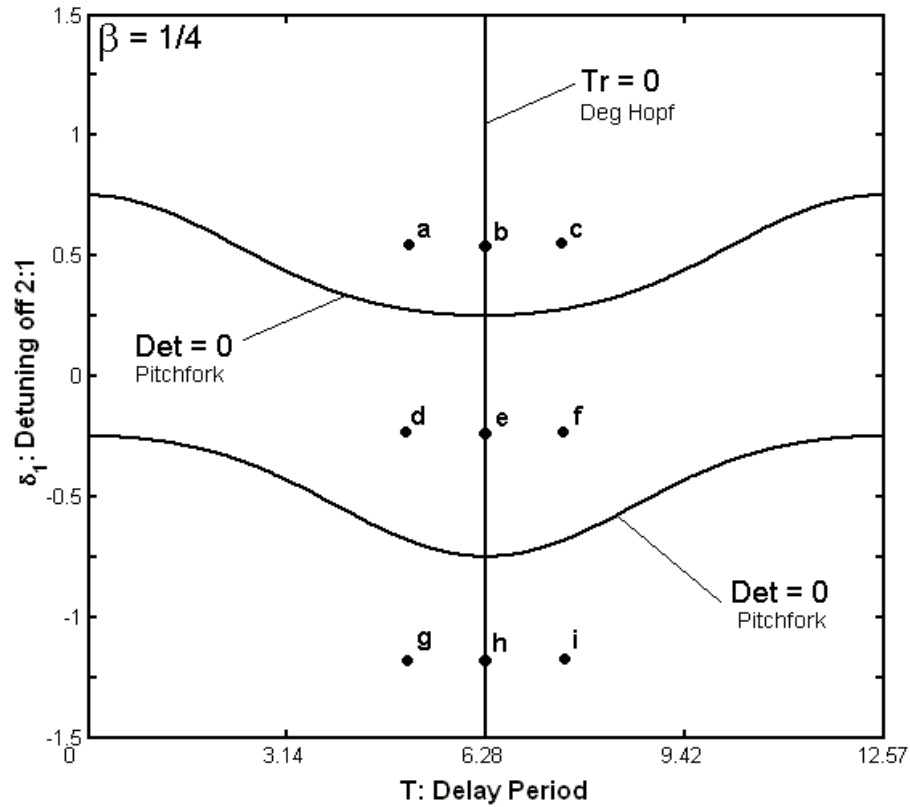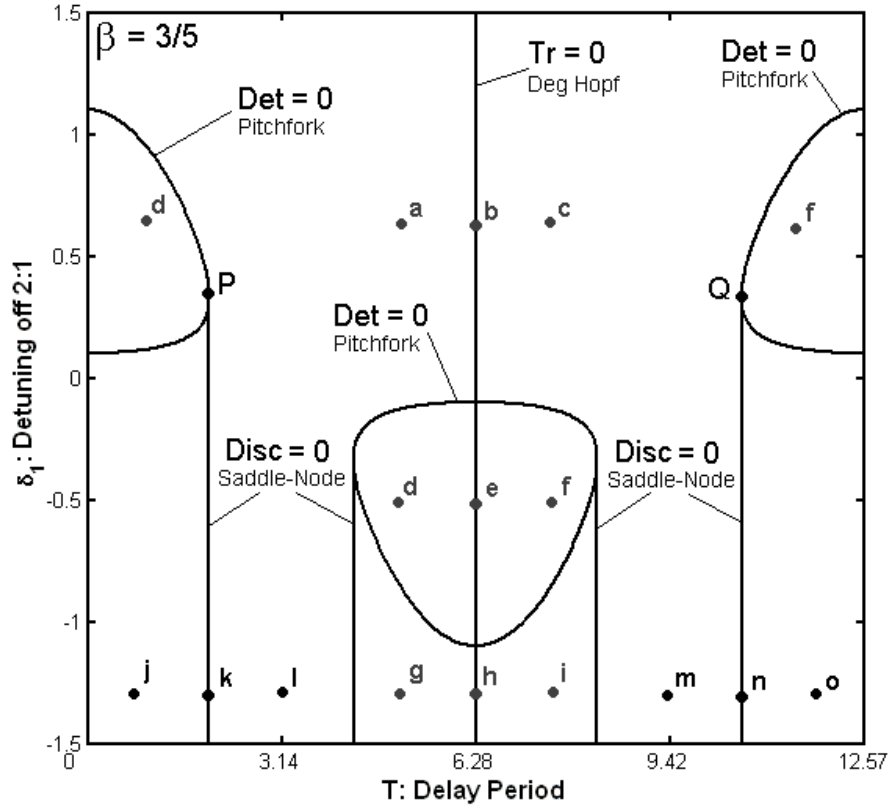
Figure 5.9: Bifurcation set for the slow flow equilibria for Example 2, $\beta = \frac{3}{5}$ and $\alpha = \gamma = 1$. The letters a, b, c, d, e, f, g, h, i correspond to the qualitative phase portraits shown in Figure 5.7. The letters j, k, l, m, n, o correspond to the qualitative phase portraits shown in Figure 5.10. Pitchfork bifurcations occur on the $Det(J) = 0$ curves, given by equation (5.61). Saddle-node bifurcations occur on the $Disc = 0$ curves, given by $|\sin(T/2)| = 5/6$. A change of stability occurs on the $Tr(J) = 0$ curve, $T = 2\pi$, in the case that $Det(J) > 0$ (non-saddle equilibria). No limit cycles are observed to be born as we cross the latter curve because the associated Hopf bifurcation is degenerate.
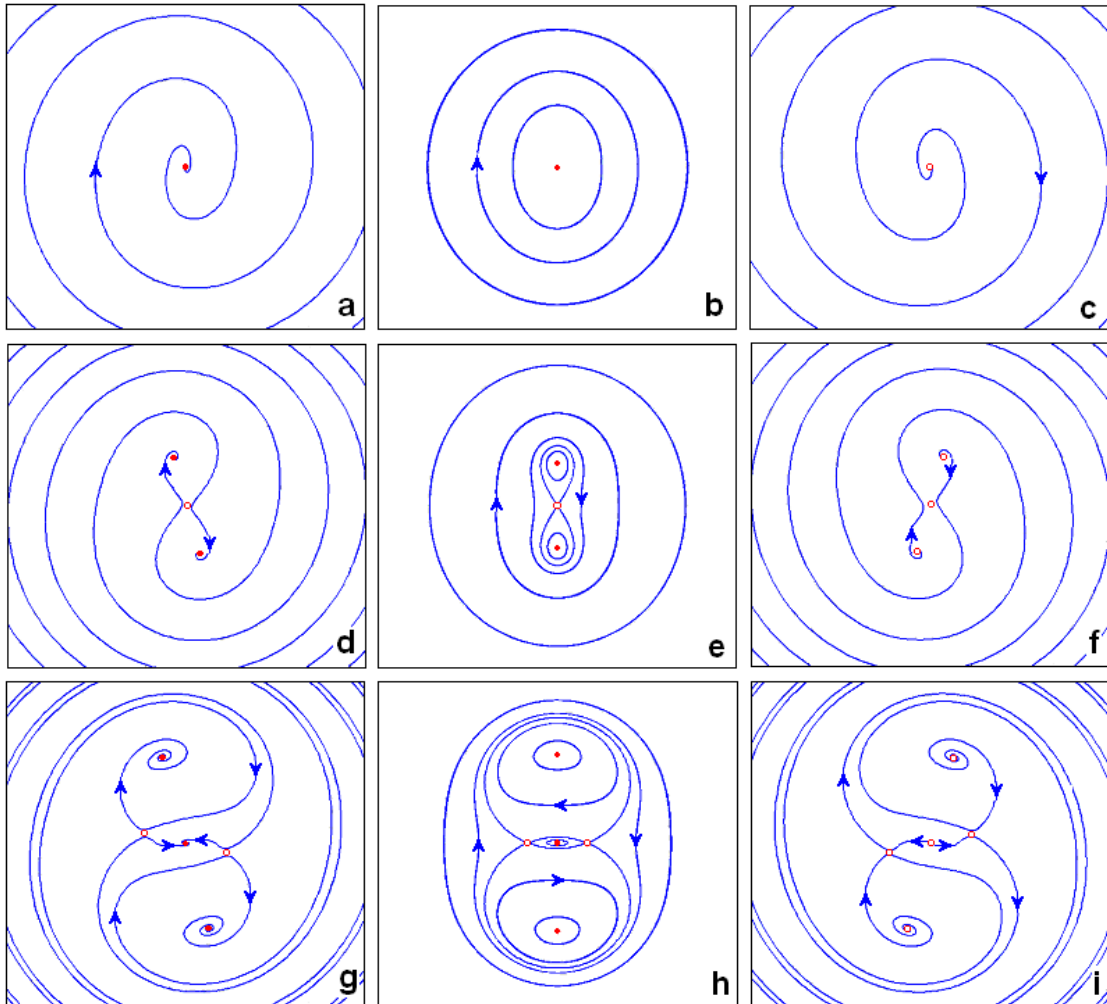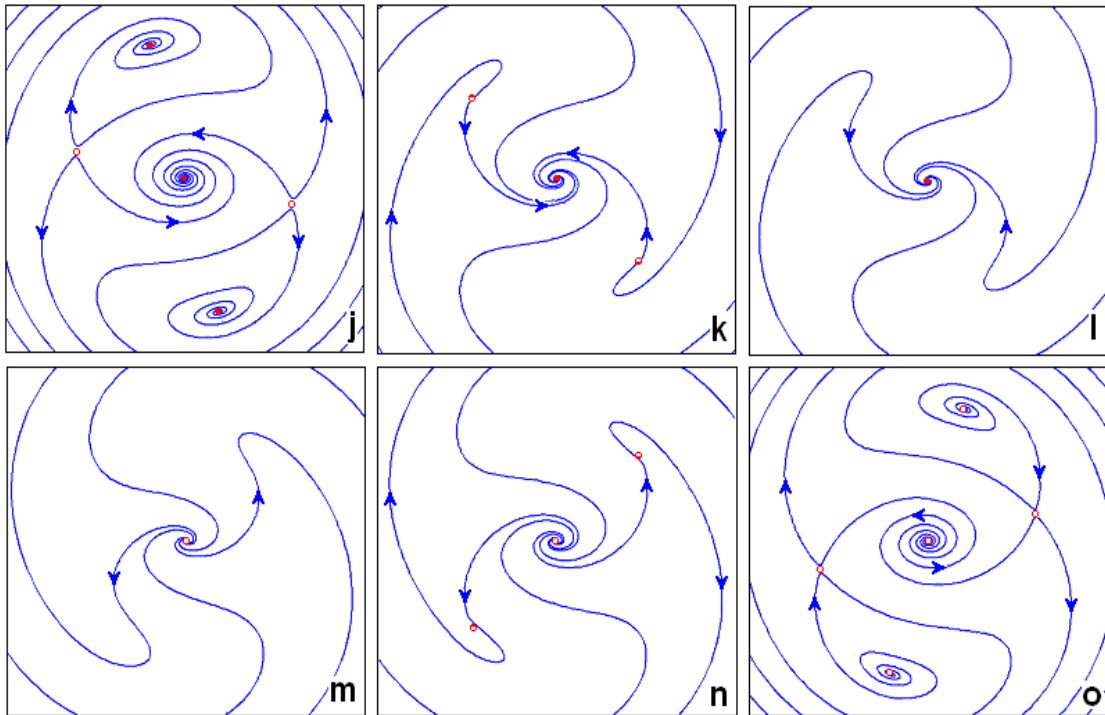
Figure 5.10: Qualitative phase portraits for Example 2, $\beta = \frac{3}{5}$ and $\alpha = \gamma = 1$. The letters j, k, l, m, n, o correspond to various parameter combinations of δ_1 and T as shown in Figure 5.9. The bifurcations from j to l and from m to o are saddle-nodes.

5.5   Degenerate Hopf Bifurcation

Limit cycles can be generically created or destroyed in a Hopf bifurcation. The necessary conditions for a generic Hopf bifurcation in a system of two first order ODE's such as the slow flow (5.44) and (5.45) are $Tr(J) = 0$ and $Det(J) > 0$, where J is the Jacobian matrix evaluated at an equilibrium point. Setting the trace equal to zero in equation (5.54) for the slow flow gives $T = 2\pi$ (we ignore $\beta = T = 0$ because the corresponding systems involve no delay). The condition $Det(J) > 0$ corresponds to a non-saddle equilibrium point. Thus if we were to increase the delay period T through 2π, we would expect to see a limit cycle created or destroyed (depending upon whether the Hopf was sub - or supercritical) in the neighborhood of a spiral equilibrium point. See Figure 5.7 where moving from a to c, from d to f, or from g to i corresponds to increasing the delay period T through 2π. By inspection no limit cycle is observed, contrary to our expectations. In the following two subsections, we analyze this behavior by considering the delay amplitude as is, order ε and we compare it to the case where the delay amplitude is of order 1, therefore perturbing off of the Hsu-Bhatt equation in equation (5.2) rather than the simple harmonic oscillator.

5.5.1   Order ε Delay

In order to understand the behavior associated with the degenerate Hopf, we evaluate the slow flow (5.44) and (5.45) at $T = 2\pi$:

$$u' = \left(\delta_1 - \frac{\alpha}{2} + \beta \right) v + \frac{3\gamma}{4} v (u^2 + v^2) \tag{5.62}$$

$$v' = \left(-\delta_1 - \frac{\alpha}{2} - \beta \right) u - \frac{3\gamma}{4} u (u^2 + v^2) \tag{5.63}$$

Equations (5.62) and (5.63) possess the following first integral:

$$\frac{3\gamma}{4}\left(u^2 + v^2\right)^2 + 2(\delta_1 + \beta)\left(u^2 + v^2\right) + \alpha\left(u^2 - v^2\right) = \text{constant} \qquad (5.64)$$

Note that the existence of this first integral for $T=2\pi$ is in agreement with the phase portraits b, e and h in Figure 5.7, which were obtained by numerical integration.

In a generic Hopf bifurcation, the limit cycle is born with zero amplitude and grows generically like $\sqrt{\mu}$, where μ is the bifurcation parameter. This results in a family of limit cycles, one for each value of μ. What has happened in the slow flow (5.44) and (5.45) is that the entire family of periodic motions has occurred at $\mu = 0$, which corresponds to $T = 2\pi$ here. The Hopf bifurcation in this case is degenerate. This phenomenon is well-known [28], and a condition has been given which guarantees that no such degeneracy will occur, namely that the equilibrium point should be a "vague attractor" (or less generally, asymptotically stable) when $\mu = 0$. Since the slow flow (5.44) and (5.45) has just been shown to be conservative at $T = 2\pi$, this condition does not apply.

Having established that the Hopf bifurcation associated with the slow flow (5.44) and (5.45) is degenerate, we are led to ask if this nongeneric behavior is really part of the dynamics of the original equation (5.1), or if it is due to the nature of the perturbation scheme. In order to investigate this possibility, we apply an alternative perturbation scheme to equation (5.1), based on taking ε small in the following equation (Cf. equation (5.31)):

$$\ddot{x}(t) + \delta_0 x(t) - bx(t - T) = -\varepsilon\left(\delta_1 x(t) + \alpha x(t)\cos t + \gamma x(t)^3\right) \qquad (5.65)$$

We treat this equation in the following section, where we use multiple scales to obtain a slow flow, which we show also exhibits a degenerate Hopf bifurcation.

5.5.2 Order 1 Delay

The occurrence of a degenerate bifurcation in a slow flow system derived from a perturbation method may not be representative of the actual system. The degeneracy may result from the approximation involved in the perturbation method. The slow flow system (5.44) and (5.45) in the previous section was derived by perturbing off of a simple harmonic oscillator with $O(\varepsilon)$ forcing, nonlinearity, detuning, and delay (Cf. equation (5.31)):

$$\ddot{x}(t) + \delta_0 x(t) = -\varepsilon \left(\delta_1 x(t) + \alpha x(t) \cos t + \gamma x(t)^3 - \beta x(t - T) \right) \qquad (5.66)$$

An alternative approach is to perturb off of the Hsu-Bhatt equation [8] $\ddot{x} + \delta_0 x = b(t - T)$. We consider a simple harmonic oscillator with a delay term, which is perturbed by $O(\varepsilon)$ forcing, nonlinearity, and detuning :

$$\ddot{x}(t) + \delta_0 x(t) - b x(t - T) = -\varepsilon \left(\delta_1 x(t) + \alpha x(t) \cos t + \gamma x(t)^3 \right) \qquad (5.67)$$

where the delay amplitude is b, the delay period is T and δ_0 is the frequency squared of the simple harmonic oscillator. If the delay amplitude b and ε were zero, then this system would be stable when $\delta_0 > 0$ and unstable when $\delta_0 < 0$. By changing the delay parameters b and T, the stable system can become unstable and the unstable system can become stable. Thus a change of stability would occur.

From section 5.2.1, we know the solution is of the form:

$$x(t) = e^{\lambda t} \qquad (5.68)$$

where the characteristic equation is:

$$\lambda^2 + \delta_0 = b \, e^{-\lambda T} \qquad (5.69)$$

Note that equation (5.69) is a transcendental equation on λ and therefore has an infinite number of (generally complex) roots. For a Hopf bifurcation, a pair of

roots must be pure imaginary. Substituting $\lambda = i\omega$ into equation (5.69) yields:

$$\omega_{crit}^2 = \delta_0 + b \qquad \omega_{crit}T_{crit} = \pi \qquad (5.70)$$

which gives the solution to the Hsu-Bhatt equation (5.67) for $\varepsilon = 0$ right at a Hopf bifurcation point. This is the starting point for the perturbation method.

We use the multiple time scales method and begin by perturbing off of the critical value of the delay period:

$$T = T_{crit} + \varepsilon\mu + \ldots \qquad (5.71)$$

We then define two time scales $\xi = t$ and $\eta = \varepsilon t$, and expand x in a power series of ε: $x(\xi, \eta) = x_0(\xi, \eta) + \varepsilon x_1(\xi, \eta) + \ldots$ We substitute these expansions into equation (5.67) and collect like terms. The solution to the $\varepsilon = 0$ equation is:

$$x_0(\xi, \eta) = A_1(\eta)\cos\omega_{crit}\xi + A_2(\eta)\sin\omega_{crit}\xi \qquad (5.72)$$

where $A_1(\eta)$ and $A_2(\eta)$ are functions of slow time η. In order for the $\cos t$ term in equation (5.67) to be 2:1 resonant, $\omega_{crit} = \frac{1}{2}$. This implies from equation (5.70):

$$\delta_0 + b = \frac{1}{4} \qquad T_{crit} = 2\pi + \varepsilon\mu \qquad (5.73)$$

The $O(\varepsilon)$ equation is:

$$x_{1\xi\xi} + \delta_0 x_1 - bx_1(\xi - T_{crit}) =$$
$$- \left(2x_{0\xi\eta} + (\delta_1 + \alpha\cos\xi)x_0 + \gamma x_0^3 + \mu x_{0\xi}(\xi - T_{crit})\right) \qquad (5.74)$$

where the subscripts denote partial derivatives and x_0 is given by equation (5.72). In deriving equation (5.74) the product εT_{crit} has been assumed to be small [65]. After substituting equation (5.72) into (5.74), the removal of resonant terms yields

the slow flow:

$$\frac{dA_1}{d\eta} = \frac{b\mu}{2}A_1 + \left(\delta_1 - \frac{\alpha}{2}\right)A_2 + \frac{3\gamma}{4}A_2(A_1^2 + A_2^2) \tag{5.75}$$

$$\frac{dA_2}{d\eta} = \frac{b\mu}{2}A_2 - \left(\delta_1 + \frac{\alpha}{2}\right)A_1 - \frac{3\gamma}{4}A_1(A_1^2 + A_2^2) \tag{5.76}$$

As stated in section 5.5.1, the necessary conditions for a generic Hopf bifurcation in a system of two first order ODE's, such as those above in (5.75) and (5.76), are $Tr(J) = 0$ and $Det(J) > 0$, where J is the Jacobian matrix evaluated at the equilibrium point. The trace and determinant for the slow flow system above about the origin are:

$$Tr(J) = b\mu \qquad Det(J) = \frac{b^2\mu^2}{4} + \delta_1^2 - \frac{\alpha}{4} \tag{5.77}$$

Setting the $Tr(J) = 0$ gives $b = 0$ (which corresponds to a system with no delay) or $\mu = 0$, which is right at the bifurcation point of $T_{crit} = 2\pi$. Using $\mu = 0$, the condition for the $Det(J) > 0$ becomes:

$$\delta_1^2 > \frac{\alpha}{4} \qquad \Rightarrow \qquad |\delta_1| > \frac{\alpha}{2} \tag{5.78}$$

Thus, for a given $\alpha > 0$, and choosing $|\delta_1| > \alpha/2$, we would expect a limit cycle to be born as we change μ from negative to positive or positive to negative. However, a limit cycle is not born in this slow flow system, contrary to what we expect. In fact, the slow flow in (5.75) and (5.76) at the bifurcation point of $\mu = 0$ has the first integral:

$$\left(6\gamma A_2^2 + 8\delta_1 + 4\alpha\right)\frac{A_1^2}{4} + (8\delta_1 - 4\alpha)\frac{A_2^2}{4} + \frac{3\gamma}{4}\left(A_1^4 + A_2^4\right) = C \tag{5.79}$$

The existence of this first integral signifies that the Hopf bifurcation is degenerate, as explained at the end of section 5.5.1.

Thus both perturbation schemes, one in which the delay amplitude is $O(1)$ and the other in which the delay amplitude is $O(\varepsilon)$, give slow flow systems which exhibit degenerate Hopf bifurcations.

5.5.3 Numerical Investigation

Further evidence of the existence of the degenerate Hopf in the original equation (5.1) was obtained by numerically integrating (5.1) in the neighborhood of $T = 2\pi$ for a variety of other parameters. Since a limit cycle in the slow flow corresponds to a quasiperiodic motion in the original equation, we searched for quasiperiodic motions in (5.1). No quasiperiodic motions were observed.

5.6   Comparison with Numerical Integration

In this section we compare the foregoing analytical results based on the slow flow (5.42) and (5.43) or (5.44) and (5.45), with direct numerical integration of the delayed Mathieu equation (5.31). The numerical integration was completed in MATLAB, which has recently extended the differential equation package to numerically integrate systems of delay differential equations [53]. For this task, we used the integrating function dde23. There is an on-line tutorial available at MATLAB Central [26].

The results are for the stability of the origin, $x = \dot{x} = 0$, and are shown in Figures 5.11 and 5.12. The same parameters were used as in Examples 1 and 2, except we took $\gamma = 0$, since the stability of the origin does not involve the nonlinear term in equation (5.31). In particular we used $\beta = 0.25$ in Figure 5.11 and $\beta = 0.60$ in Figure 5.12. A MATLAB script was written to generate these figures numerically, utilizing the dde23 function. The T-δ_1 parameter plane was

divided into a grid of 10,000 points. A point in this space is deemed stable if, after 2000 forcing periods starting with the initial condition $x = 1$, the norm of the amplitude is less than 10^{10}, otherwise it is unstable. For each figure, $\varepsilon = 0.05$.

In Figure 5.11, we note the appearance of a stable region on the right side of the numerical (lower) stability chart which is absent from the analytical (upper) stability chart. This may be explained by recalling that the analytical results are based on a perturbation method which assumed that εT was small.

Figure 5.11: Stability of the origin for $\beta = 0.25$ and $\alpha = 1$. Comparison between analytical result based on slow flow (upper) with numerical integration of equation (5.31) for $\varepsilon = 0.05$ (lower). Black is stable, white is unstable.
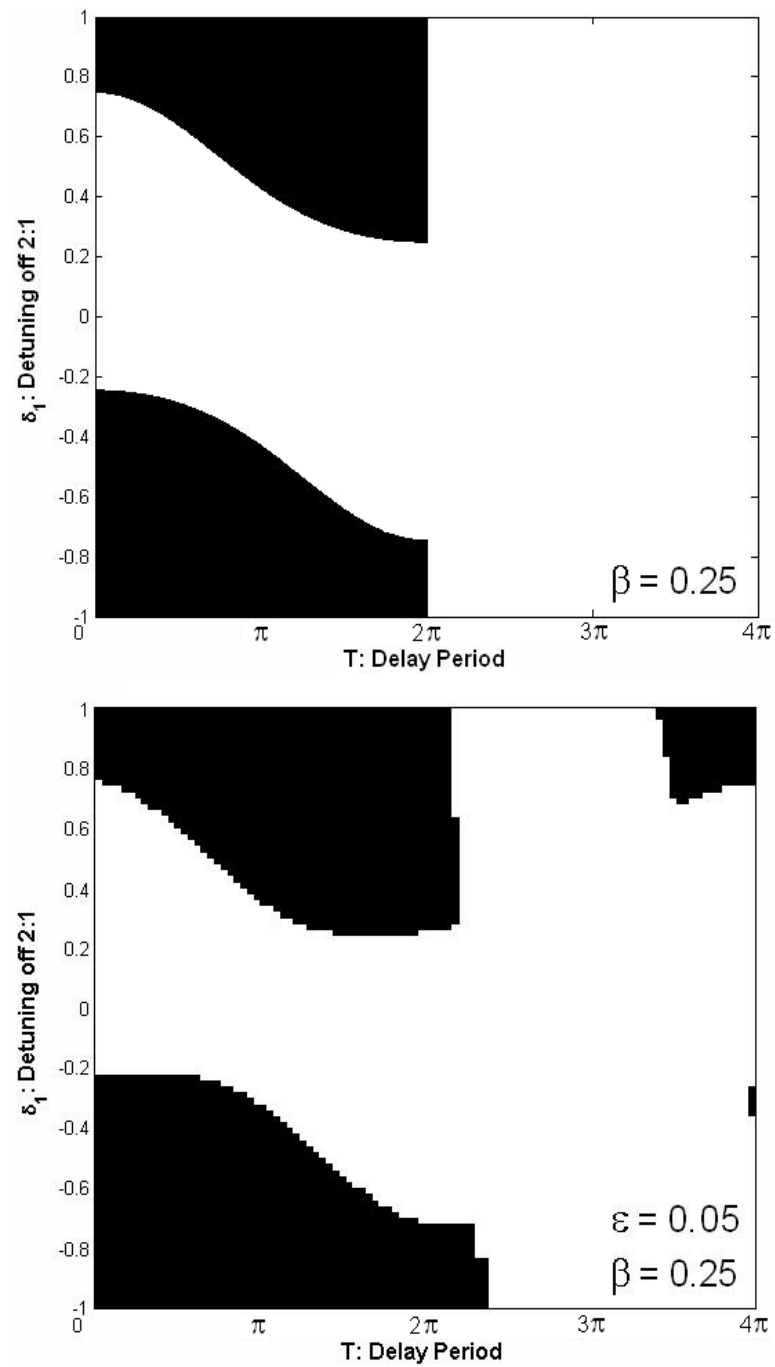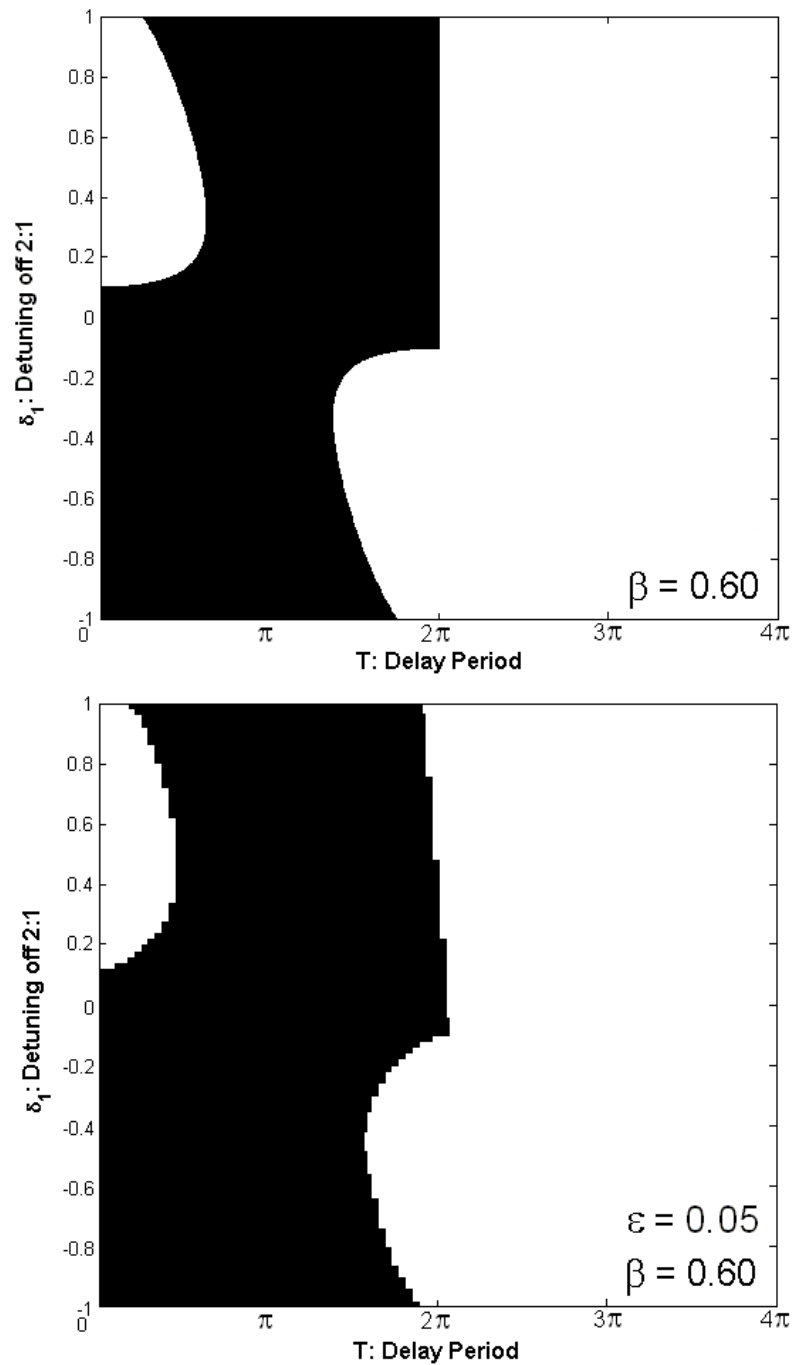
Figure 5.12: Stability of the origin for $\beta = 0.60$ and $\alpha = 1$. Comparison between analytical result based on slow flow (upper) with numerical integration of equation (5.31) for $\varepsilon = 0.05$ (lower). Black is stable, white is unstable.

5.7   Discussion

The main difference between Examples 1 and 2 presented earlier in this chapter is that Example 2 involves a saddle-node bifurcation and Example 1 does not. The saddle-node bifurcation occurs because the condition for nontrivial slow flow equilibria to exist, equation (5.50), is not satisfied for all values of T. Recall that the instability region in the T-δ_1 parameter plane was bounded by curves with equations (5.51) and (5.52). Thus, for each delay period T, and for given values of α and β, there are two critical values of δ_1 if $\beta < \alpha/2$. If $\beta > \alpha/2$, however, there are values of T for which there are no real critical values of δ_1, and therefore there is no instability.

Recalling that $\delta = 1/4 + \delta_1 \varepsilon$, we may write the transition curves separating stable from unstable regions in the form:

$$\delta = \frac{1}{4} + \varepsilon \left(\beta \cos \frac{T}{2} \pm \frac{1}{2} \sqrt{\alpha^2 - 4\beta^2 \sin^2 \frac{T}{2}} \right) \tag{5.80}$$

Figure 5.13 shows the instability region (5.80) in the three dimensional δ-T-ε parameter space for the parameters of Example 2. Figure 5.13 can be compared with Figure 5.12 by intersecting the three dimensional instability tongue with the plane $\varepsilon = 0.05$. Then the white region lying inside the tongue in Figure 5.13 is the same as the white instability region on the left side of Figure 5.12.

In the limiting case of $\beta = 0$ (no delay term), equation (5.1) becomes a nonlinear Mathieu equation, the properties of which are well-known [42] and [74]. See Figure 5.14 which displays a bifurcation diagram for equation (5.1) with $\alpha = \gamma = 1$, $\beta = 0$. The effect of adding a small delay term may be understood by perusing Figures 5.6 and 5.7. These show, first of all, that the presence of delay introduces dissipation

into the slow flow. Moreover we see that if the delay amplitude β is small enough $(0 < \beta < \alpha/2)$, and if the delay period T is small enough $(T < 2\pi)$, then the dynamics of the delayed equation is similar to that of a damped nonlinear Mathieu equation without delay. If, however, the delay amplitude is large enough $(\beta > \alpha/2)$, then we have seen that it is possible to eliminate the tongue of instability by choosing the delay period appropriately. Figure 5.13 shows the tongue closing as $T \to T = 2\sin^{-1}\frac{\alpha}{2\beta}$. See also Figures 5.9 and 5.10.

We have seen that the stability change at the origin is given by equation (5.59). This equation can be rewritten so as to give the following condition for instability at the origin:

$$\delta_1^2 + \beta^2 - 2\beta\delta_1 \cos\frac{T}{2} - \frac{\alpha^2}{4} < 0 \tag{5.81}$$

This shows that the origin is unstable for all delay periods T if the delay amplitude β and the detuning δ_1 are taken to be sufficiently small. For example, in Figure 5.5, where $\beta = \frac{1}{4}$, the origin is always unstable for $|\delta_1| < \frac{1}{4}$.

5.8 Conclusions

In this chapter, we investigated the dynamics of equation (5.1) which involves the interaction of parametric excitation with delay. Our analytical results are based on slow flow equations (5.44) and (5.45) which were obtained by use of first order averaging. We studied the stability of the origin and the bifurcations which accompanied stability changes: pitchforks, saddle-nodes, and degenerate Hopf bifurcations.

We showed that adding delay to an undamped parametrically excited system introduces effective damping. Our most important conclusion is that for sufficiently large delay amplitudes β, and for appropriately chosen delay periods T, the 2:1

instability region associated with parametric excitation can be eliminated. This result has potential utility in applications where instabilities are undesirable.
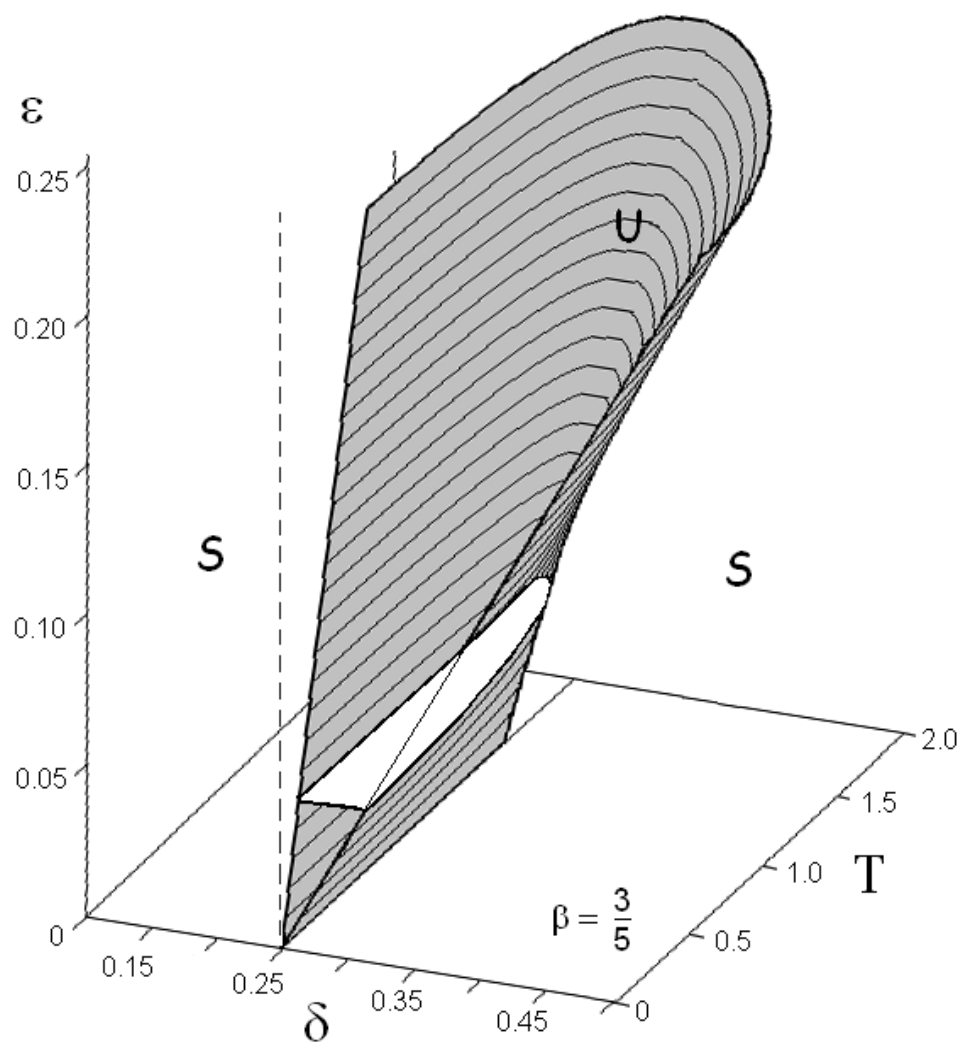
Figure 5.13: The 2:1 instability tongue (5.80), for $\beta = \frac{3}{5}$, $\alpha = \gamma = 1$. U is unstable, S is stable. The white instability region lying in the plane $\varepsilon = 0.05$ corresponds to the white instability region on the LHS of Figure 5.12.
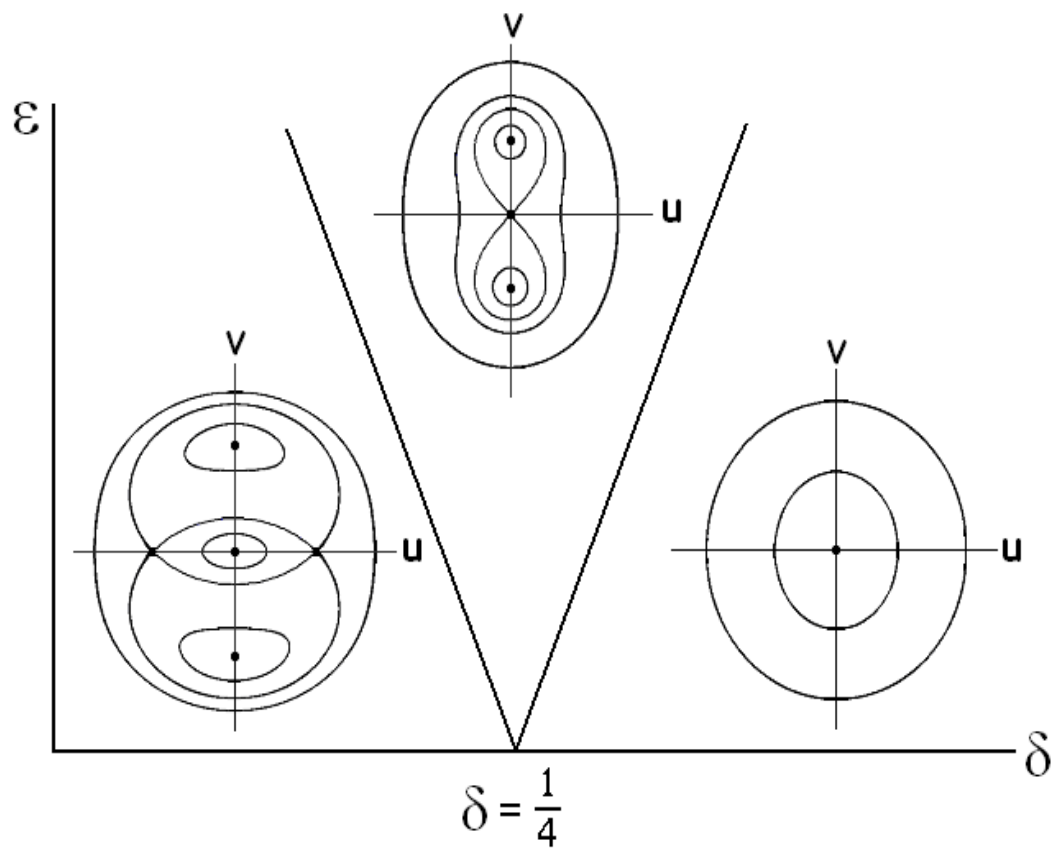
Figure 5.14: Bifurcation diagram for the nonlinear Mathieu equation without delay term, equation (5.1) with $\alpha = \gamma = 1$, $\beta = 0$.

Chapter 6

Conclusions and Future Work

"Science is built up of facts, as a house is with stones. But a collection

of facts is no more a science than a heap of stones is a house."

– Henri Poincaré

Parametric resonance is a phenomenon that can both stabilize and destablize a system. It causes large instabilities when the excitation is applied at twice the system's natural frequency. In this thesis, we examined how a system responded to 2:1 parametric excitation in the presence of a second parametric driver (Chapter 3), in the presence of a Hopf bifurcation (Chapter 4), and in the presence of nonlinearities and delay (Chapter 5). In this final chapter, we offer some ideas for future work which would be an extension of the research conducted in this thesis.

In Chapter 6, we learned that delay adds dissipation to a system for certain delay periods and amplitudes. In Chapter 4, we showed that a system with linear damping and cubic nonlinearities experiences a Hopf bifurcation when the linear damping is tuned from positive to negative. Hence, a possible research effort would

be to investigate the response of a system with 2:1 parametric excitation, cubic nonlinearities, linear damping and delay, focusing on the relationship between the delay and damping parameters.

In Chapter 2, we showed that the Mathieu equation models a system with 2:1 parametric resonance. A second possible research effort would involve analyzing the stability in a Mathieu-like system where the damping coefficient is a periodic function [5], [23], [52]. Then, consider the effect delay has on the transition curves in the δ-ε plane.

In Chapter 5, we showed that a Hopf bifurcation occurs in the unforced non-linear system when $A = 0$, where A is the linear damping coefficient. (Note the a saddle-connection bifurcation occurs in the unforced system when $A = -1$; this was not shown.) We then analyzed the stability of the steady state solution in the presence of 2:1 parametric excitation by detuning off of the resonance with κ. We found that the steady state behavior changed from periodic to quasiperiodic motion for $A < 0$. A third possible research effort would be to examine what happens to that quasiperiodic steady state as the bifurcation parameters A and κ proceed towards the saddle-connection bifurcation at $A = -1$. In the following sections, we provide the foundation for starting that investigation.

6.1 The Duffing Oscillator

The nonlinear constant coefficient second order differential equation

$$\ddot{x} + x + \alpha x^3 = 0 \tag{6.1}$$

is well known as the Duffing oscillator, where αx^3 is a positive restoring force when $\alpha > 0$ or a negative restoring force when $\alpha < 0$ [42]. Let's consider the long term

behavior of this system. The flow in the phase plane for a given initial condition satisfies the following differential equation,

$$\frac{dy}{dx} = \frac{-\alpha x^3 - x}{y} \tag{6.2}$$

where the solution is:

$$\frac{y^2}{2} + \frac{x^2}{2} + \frac{\alpha x^4}{4} = \text{constant} \tag{6.3}$$

The phase plane is filled with these level curves given by equation (6.3). Along each trajectory, the quantity above is conserved.

To further analyze the system, we find the equilibrium points to equation (6.2), which are dependent on the sign of the restoring force, α. When $\alpha > 0$, the origin is the only equilibrium point and the solution is a continuum of level curves that are periodic, shown in Figure 6.1a. However, when $\alpha < 0$, there are two nontrivial equilibria: $x^* = \pm 1/\sqrt{-\alpha}$. Therefore, all initial conditions starting near the origin are periodic and those away from the origin tend to infinity. The curve that separates the periodic from the unbounded solutions is called the separatrix.

After numerically integrating Duffing's equation, we find that the period of the solutions inside the separatrix are amplitude dependent. This behavior is not evident from the phase plane analysis. In the next section, we use elliptic functions to find the period-amplitude relationship for the Duffing Oscillator.
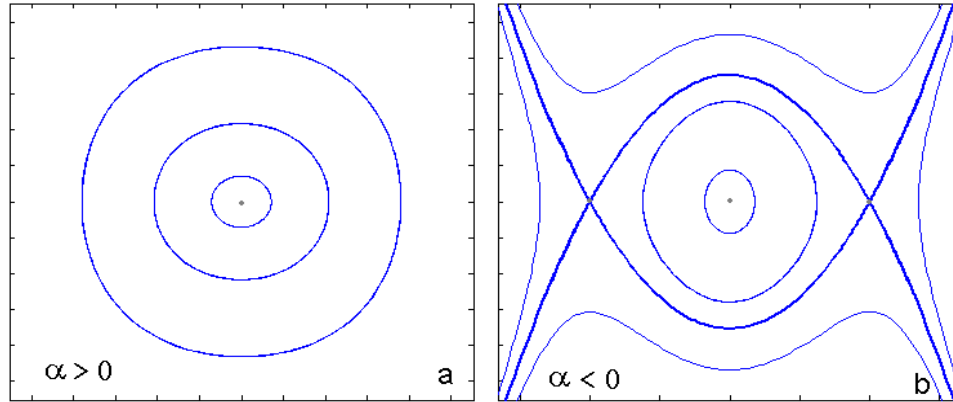
Figure 6.1: The phase plane analysis of the Duffing Oscillator with (a) positive nonlinear restoring forces and (b) negative nonlinear restoring forces.

6.1.1 Elliptic Function Solution

Let's consider the Duffing oscillator with a negative nonlinear restoring force. This form of the equation is also known as the Escape equation [60]:

$$\ddot{x} + x - x^3 = 0 \tag{6.4}$$

Let's assume the solution to equation (6.4) is a combination of elliptic functions [13],

$$x(t) = a_1 \frac{\text{cn}(a_2 t, k)}{\text{dn}(a_2 t, k)} \tag{6.5}$$

where a_1 is the amplitude of oscillation, $a_2 t$ is the amplitude, and k is the modulus. We solve for a_2 and k by substituting $x(t)$ into the equation of motion (6.4) and collecting like terms. In order to make that substitution, we need an expression for $\ddot{x}$:

$$\dot{x}(t) = a_1 a_2 (k^2 - 1) \frac{\text{sn}(a_2 t, k)}{\text{dn}^2(a_2 t, k)} \tag{6.6}$$

$$\ddot{x}(t) = a_1 a_2^2 (k^2 - 1)(1 + k^2 - k^2 \text{cn}(a_2 t, k)) \frac{\text{cn}(a_2 t, k)}{\text{dn}^3(a_2 t, k)}$$

Substituting $\ddot{x}$ into equation (6.4), multiplying by dn^3, and utilizing elliptic function identities, we obtain an algebraic expression on a_1, a_2 and k:

$$\left(a_1 a_2^2 k^2 + a_1 k^2 - a_1 a_2^2 k^4 - a_1^3\right) \mathrm{cn}^3 + \left(a_1 a_2^2 k^4 - a_1 k^2 - a_1 a_2^2 + a_1\right) \mathrm{cn} = 0 \quad (6.7)$$

When we set the coefficients of cn and cn^3 to zero to satisfy equation (6.7), we retrieve two algebraic equations on a_2 and k. Solving those, we obtain

$$k^2 = \left(\frac{a_1^2}{2 - a_1^2}\right) \qquad (6.8)$$

$$a_2^2 = \left(\frac{2 - a_1^2}{2}\right) \qquad (6.9)$$

Thus, the periodic solution to the Duffing equation (6.4) for $\alpha < 0$ is equation (6.5), where a_2 and k are given above. We also obtain from the analysis the period of oscillation, T:

$$T = \frac{4K(k^2)}{a_2} \qquad (6.10)$$

where K is the complete elliptic integral of the first kind.

6.2 The Forced Duffing Oscillator

Next, let's consider the Duffing oscillator with a negative nonlinear restoring force ($\alpha < 0$) and a small perturbing force:

$$\ddot{z} + z - z^3 = -\varepsilon(A\dot{z} + \dot{z}^3) \qquad (6.11)$$

where $\varepsilon << 1$ and A is linear damping. We use regular perturbations to investigate the dynamics of this equation by expanding z as a power series in ε, $z = z_0 + \varepsilon z_1 + O(\varepsilon^2)$ in equation (6.11),

$$\ddot{z}_0 + \varepsilon \ddot{z}_1 + z_0 + \varepsilon z_1 - (z_0^3 + 3\varepsilon z_0^2 z_1) = -\varepsilon(A\dot{z}_0 + \dot{z}_0^3) \qquad (6.12)$$

Collecting orders of ε yields:

$$\varepsilon^0: \qquad \ddot{z}_0 + z_0 - z_0^3 = 0 \tag{6.13}$$

$$\varepsilon^1: \qquad \ddot{z}_1 + z_1 - 3z_0^2 z_1 = -(A\dot{z}_0 + \dot{z}_0{}^3) \tag{6.14}$$

The zeroth order equation (6.13) is the Duffing equation we solved in the previous section. Thus, the zeroth order solution is:

$$z_0(t) = a_1 \frac{\text{cn}(a_2 t, k)}{\text{dn}(a_2 t, k)}, \qquad k = \pm a_1 \left(\frac{1}{\sqrt{2 - a_1^2}}\right), \qquad a_2 = \sqrt{\left(\frac{2 - a_1^2}{2}\right)} \tag{6.15}$$

where a_1 is the amplitude of the periodic motion. Now we are able to solve the z_1 equation (6.14) and find the relationship between the damping coefficient A and the amplitude of the periodic motion, a_1.

The z_1 differential equation is a linear differential equation with coefficients that are elliptic functions. Since it's an ODE, it has a complementary and particular solution. One part of the complementary solution is found by solving the homogeneous equation:

$$\ddot{z}_1 + z_1 - 3z_0^2 z_1 = 0 \tag{6.16}$$

which can also be solved by differentiating the zeroth order equation with respect to time:

$$\frac{d}{dt}\left[\ddot{z}_0 + z_0 - z_0^3\right] = 0 \quad \Rightarrow \quad \frac{d^3 z_0}{dt^3} + \frac{dz_0}{dt} - 3z_0^2 \dot{z}_0 = 0 \tag{6.17}$$

By comparing the above expression with equation (6.16), we see that $z_1 = C_1 \dot{z}_0$ is the periodic solution. Since equation (6.14) is a second order differential equation, we expect the complementary solution to consist of two linearly independent solutions:

$$z_c(t) = C_1 \dot{z}_0 + C_2 f(t) \tag{6.18}$$

where $f(t)$ is not a periodic function. Thus, for the Duffing oscillator, we only consider the periodic term of the complementary solution.

Next, let's consider the periodic solution to the nonhomogeneous equation. Since the terms on the RHS of equation (6.14) are not trigonometric functions (where the removal of resonant terms is straightforward) but elliptic functions, we use the Fredholm Alternative Theorem to find the relationship between the damping coefficient A and the amplitude of the periodic motion a_1.

The Fredholm Alternative Theorem

The Fredholm Alternative Theorem states that in order for a solution to exist, the RHS of the nonhomogeneous equation must be orthogonal to the null space of the adjoint operator of the homogeneous equation.

Recall that given an operator L, the adjoint operator L^* is defined by:

$$(u, Lv) = (v, L^*u) \tag{6.19}$$

where the notation $(\diamond, \diamond)$ refers to the inner product. The linear differential operator for the z_1 equation is,

$$L(\diamond) = \frac{d^2 \diamond}{dt^2} + \diamond - 3z_0^2(\diamond) \tag{6.20}$$

The adjoint operator is found by solving equation (6.19) using the operator given above, and utilizing integration by parts:

$$(u, Lv) = \int u \left[v'' + v - 3z_0^2 v\right] dt = \int v \left[u'' + u - 3z_0^2 u\right] dt = (v, L^*u) \tag{6.21}$$

Thus, $L(v) = L^*(u)$, i.e., the linear differential operator is self-adjoint. Therefore, the null space of the adjoint operator is the solution to the z_1 homogeneous equation. This means, the RHS of the z_1 nonhomogeneous equation must be orthogonal

to the periodic solution of the z_1 homogeneous equation. That is to say, A must satisfy:

$$\int_0^T \dot{z}_0(A\dot{z}_0 + \dot{z}_0^3)dt = 0 \tag{6.22}$$

where T is one period of z_0. Let's simplify this equation by switching the integration variables from t to $u = a_2 t$. Hence, the limits of integration change to 0 and $4K$. Therefore, equation (6.22) becomes,

$$\oint A \frac{\text{sn}^2(u,k)}{\text{dn}^4(u,k)} du + \oint a_1^2 a_2^2 (k^2 - 1)^2 \frac{\text{sn}^4(u,k)}{\text{dn}^8(u,k)} du = 0 \tag{6.23}$$

Solving the above equation for A, we obtain,

$$A = -\frac{a_1^2 a_2^2 (k^2 - 1)^2 \oint \frac{\text{sn}^4(u,k)}{\text{dn}^8(u,k)} du}{\oint \frac{\text{sn}^2(u,k)}{\text{dn}^4(u,k)} du} \tag{6.24}$$

The solution to equation (6.24) yields the relationship between the amplitude of the periodic motion a_1 and the damping coefficient A. In order get an expression for A as a function of a_1, we need to compute integrals of elliptic functions.

Byrd and Friedman's *Handbook of Elliptic Integrals* [11] contains formulas to compute derivatives and integrals of elliptic functions. There are two integrals of elliptic functions that we need to compute. Since these two integrands differ only by an exponent, we can use the same formula to calculate them both: equation 351.51 on page 209 in Byrd and Friedman,

$$\int \text{sn}^{2m} u \; \text{cn}^{2n} u \; \text{nd}^{2p} u \; du \tag{6.25}$$

where nd $= 1/\text{dn}$. For the integral in the numerator of equation (6.24), $m = 2$, $n = 0$, $p = 2$ and for the integral in the denominator $m = 1$, $n = 0$, $p = 2$. The solution to these integrals are found using the following recursive formula:

$$\int \text{sn}^{2m} u \; \text{cn}^{2n} u \; \text{nd}^{2p} u \; du \quad =$$

$$\frac{1}{k^{2(m+n)}} \sum_{j=0}^{m} \sum_{l=0}^{n} \frac{(-1)^{j+l+n} \; k'^{2(n-l)} \; m! \; n!}{(m-j)! \; j! \; (n-l)! \; l!} I_{2(p-j-l)} \quad (6.26)$$

where $k' = \sqrt{1 - k^2}$ is the complementary modulus. The formula for $I_{2(p-j-l)}$ refers to equation 315 on page 195. After these substitutions, the integrals in the numerator and denominator of equation (6.24) simplify to,

$$I_{num} \quad = \quad \frac{1}{k^4} (I_8 - 2 \; I_6 + I_4) \tag{6.27}$$

$$I_{dem} \quad = \quad \frac{1}{k^2} (I_4 - I_2) \tag{6.28}$$

where the I_j are given by:

$$I_2 \quad = \quad \frac{1}{k'^2} E$$

$$I_4 \quad = \quad \frac{1}{3k'^4} \left(4E - 2k^2 E - 4Kk'^2 \right)$$

$$I_6 \quad = \quad \frac{1}{5k'^2} \left(4(2 - k^2) I_4 - 3I_2 \right)$$

$$I_8 \quad = \quad \frac{1}{7k'^2} \left(6(2 - k^2) I_6 - 5I_4 \right) \tag{6.29}$$

and where K and E are the complete elliptic integrals of the first and second kind, respectively. Using MACSYMA to solve the integrals in equation (6.24), we obtain a relationship between amplitude of the periodic motion, a_1 and the damping coefficient, A and a relationship between the amplitude of the periodic motion and it's period, T in equation (6.10). These relationships are plotted in Figure 6.2.

First note that as $A \to A_{crit} \approx -0.34$ [42], the amplitude $a_1 \to 1$, which is the location of the saddle point when $\alpha = -1$ from equation (6.1), see Figure 6.2a. Second, note that as the amplitude of the periodic motion goes to one, the period approaches infinity, see Figure 6.2b. Thus, the elliptic functions formulation is a good approximation to the lightly damped Duffing oscillator with negative restoring force since it predicts that as $a_1 \to 1, k^2 \to \infty$. (Cf. Figure 6.1b.)
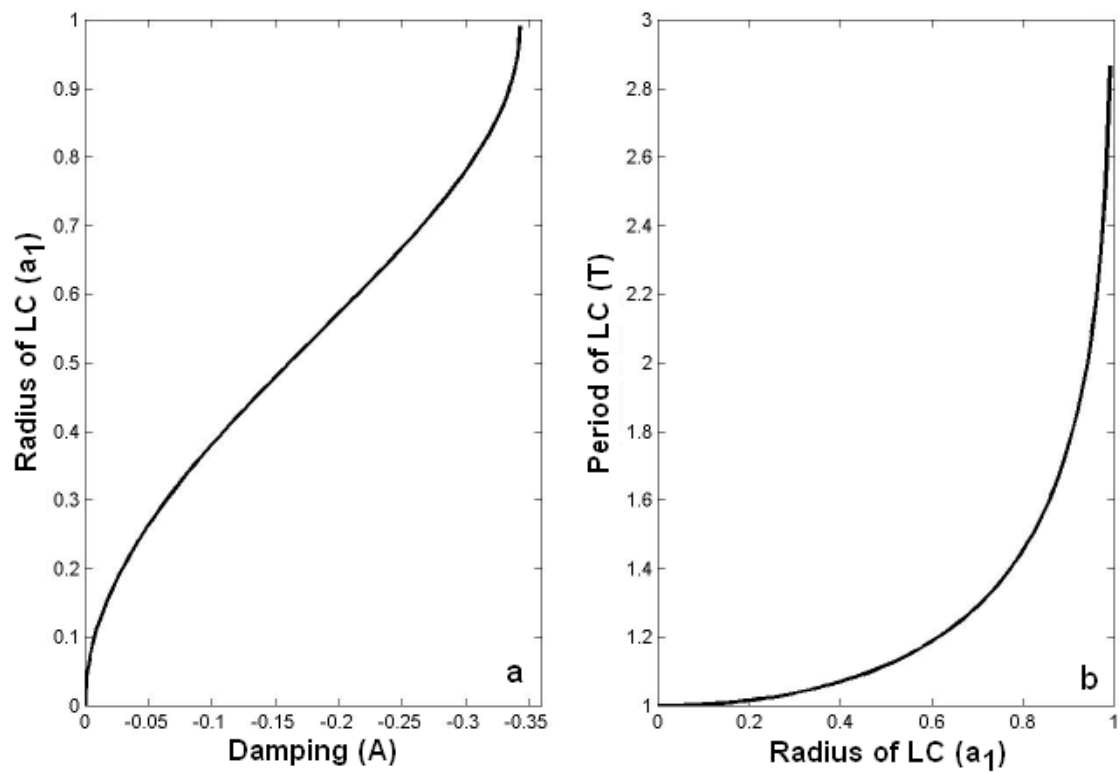
Figure 6.2: (a) The amplitude of the periodic motion as a function of damping. (b) The period as function of the amplitude.

6.3 The Duffing Oscillator with 2:1 Parametric Excitation

To investigate how the quasiperiodic steady state behavior of Chapter 5 is affected by 2:1 parametric excitation, let's consider the Duffing oscillator with 2:1 parametric excitation and small perturbing force:

$$\ddot{x} + x - x^3 + \varepsilon(k_1 + B\cos 2t)x = -\varepsilon(A\dot{x} + \dot{x}^3) \tag{6.30}$$

where A is the linear damping, B is the amplitude of the parametric resonance and k_1 is the detuning off of the 2:1 resonance. Approaching the problem as outlined in the previous section, we obtained an expression for A that included integrals of elliptic functions, trigonometric functions and the parameters B and a_1.

A recent revelation by Rand leads to a possible resolution. He showed in [42] that instead of taking the solution to the Duffing oscillator (6.4) as equation (6.5), it can be rewritten more simply as

$$z(t) \quad = \quad a_1\text{sn}(a_2t + b, k) \tag{6.31}$$

This knowledge would greatly simplify the previous analysis using elliptic functions, and would lead to alternative methods for solving the integrals of elliptic functions. Equation (6.31) should be used in the future investigations of this work.

REFERENCES

[1] Arnold, D. and Polking, J.C., 'Ordinary Differential Equations using MAT-LAB', tutorial available on line at: http://math.rice.edu/~polking/odesoft/

[2] Aubin, K., Zalalutdinov, M., Alan, T., Reichenbach, R. B., Rand, R. H., Zehnder, A., Parpia, J. and Craighead, H. G., 'Limit Cycle Oscillations in CW Laser-Driven NEMS', *Journal of Microelectricalmechanical System* **13** <u>6</u>:1018, 2004.

[3] Bajaj, A. K., 'Resonant Parametric Perturbations of the Hopf Bifurcation', *Journal of Mathematical Analysis and Applications* **115**:214-224, 1986.

[4] Bartuccelli, G., 'KAM Theory, Lindstedt Series and the Stability of the Upside-Down Pendulum', *Discrete and Continuous Dynamical Systems* **9** <u>2</u>:413-426, 2003.

[5] Batchelor, D. B, 'Parametric Resonance of Systems with Time-Varying Dissipation', *Applied Physical Letters* **29**:280-281, 1976.

[6] Belhaq, M., Guennoun, K. and Houssni, M., 'Asymptotic Solutions for a Damped Non-Linear Quasi-periodic Mathieu equation, *International Journal of Non-linear Mechanics* **37**:445-460, 2002.

[7] Bender, C. M. and Orzag, S. A., *Advanced Mathematical Methods for Scientists and Engineers*, McGraw-Hill, NY USA, 1978.

[8] Bhatt, S. J. and Hsu, C. S., 'Stability Criteria for Second-Order Dynamical Systems with Time Lag', *Journal of Applied Mechanics*, **33E**:113-118, 1966.

[9] Broer, H. and Simó, C., 'Hill's equation with Quasi-periodic forcing: Resonance Tongues, Instability Pockets, and Global Phenomena', *Boletim da Sociedade Brasileira De Matemática* **29** <u>2</u>:253-293, 1998.

[10] Butikov, E. I., 'Parametric Excitation of a Linear Oscillator', *European Journal of Physics* **25**:535-554, 2004.

[11] Byrd, P. F. and Friedman, M. D., *Handbook of Elliptic Integrals for Engineers and Physicists*, Spring-Verlag, Berlin, Germany, 1954.

[12] Carr, J., *Applications of Centre Manifold Theory*, Springer-Verlag, NY, USA 1981.

[13] Coppola, V. T., 'Averaging of Strongly Nonlinear Oscillators Using Elliptic Functions', Ph.D. Thesis, Cornell University, Ithaca, NY, 1989.

[14] Doedel, E. J., Paffenroth, R. C., Champneys, A. R., Fairgrieve, T. F., Kuznetsov, Y. A., Oldeman, B. E., Sandstede, B. and Wang, X., *AUTO 2000: Continuation and Bifurcation Software for Ordinary Differential Equations*, 2002, available on line at:
http://sourceforge.net/project/showfiles.php?group_id=21781

[15] Faraday, M., 'On a Peculiar Class of Acoustical Figures and on Certain Forms Assumed by a Group of Particles upon Vibrating Elastic Surfaces', *Philosophical Transactions of the Royal Society* **20** <u>250</u>:299-318, 1831.

[16] Gambaudo, J. M., 'Perturbation of a Hopf Bifurcation by an External Time-Periodic Forcing', *Journal of Differential Equations* **57**:172-199, 1985.

[17] Glendenning, P., *Stability, Instability and Chaos*, Cambridge University Press, NY, USA 1994.

[18] Guckenheimer, J. and Holmes, P., *Nonlinear Oscillations, Dynamical Systems, and Bifurcations of Vector Fields*, Springer-Verlag, NY, USA 1983.

[19] Guennoun, K., Houssni, M. and Belhaq, M., 'Quasi-Periodic Solutions and Stability for a Weakly Damped Nonlinear Quasi-Periodic Mathieu Equation', *Nonlinear Dynamics* **27**:211-236, 2002.

[20] Hale, J. and Koçak, H., *Dynamics and Bifurcations*, Springer-Verlag, NY, USA 1991.

[21] Hale, J. K. and Lunel, S. V., *Introduction to Functional Differential Equations*, Springer-Verlag, NY, USA, 1993.

[22] Hale, J. K., 'Averaging Methods for Differential Equations with Retarded Arguments and a Small Parameter', *Journal of Differential Equations*, **2**:57-73, 1966.

[23] Hartono and van der Burgh, *Periodic Solutions of an Inhomogeneous Second Order Equation with Time-Dependent Damping Coefficient*, Proceedings of the 2001 ASME Design Engineering Technical Conferences, Pittsburg, PA, Sept. 9-12, paper no.DETC2001-21415, 2001.

[24] Insperger, T. and Stepan, G., 'Stability Chart for the Delayed Mathieu Equation', *Proceedings of the Royal Society, Mathematical, Physical and Engineering Sciences*, **458**:1989-1998, 2002.

[25] Kalmár-Nagy, T., 'Subcritical Hopf Bifurcation in the Delay Equation Model for Machine Tool Vibrations', *Nonlinear Dynamics* **26**:121-142, 2001.

[26] Kierzenka, J., 'Solving Delay Differential Equations with dde23', PDF available on-line at *MATLAB Central:*
http://www.radford.edu/ thompson/webddes/tutorial.pdf, 2003.

[27] Lord Rayleigh, *Philosophy Magazine*, April, 1883.

[28] Marsden, J. E. and McCracken, M., *The Hopf Bifurcation and its Applications*, Springer, New York, 1976.

[29] Mason, S. and Rand, R., 'On the Torus Flow Y'=A+B COS Y+C COS X and its Relation to the Quasiperiodic Mathieu Equation', in *Proceedings of the 1999 ASME Design Engineering Technical Conferences*, Las Vegas, NV, Sept. 12-15, paper no.DETC99/VIB-8052, 1999 (CD-ROM)

[30] Mathieu, E., 'Mémoire sur le mouvement vibratoire d'une membrane de forme elliptique', *Journal of Mathematics* **13**:137-203, 1868.

[31] Minorsky N., *Nonlinear Oscillations*, D. Van Nostrand Company, Toronto, Canada 1962.

[32] Morrison, T. M. and Rand, R. H., '2:1 Resonance of a Delayed Nonlinear Mathieu Equation', *Nonlinear Dynamics* submitted for publication in February 2006.

[33] Namachchivaya, N. S. and Ariaratna, S. T., 'Periodically Perturbed Hopf Bifurcation', *SIAM Journal of Applied Mathematics* **47** <u>1</u>:15-39, 1987.

[34] Nayfeh, A.H., *Introduction to Perturbation Techniques*, Wiley Interscience, NY, USA, 1981.

[35] Nayfeh, A.H. and Mook, D.T., *Nonlinear Oscillations*, Wiley Interscience, NY, USA, 1979.

[36] Ng, L. and Rand, R., 'Bifurcations in a Mathieu equation with cubic nonlinearities', *Chaos, Solitons and Fractals* **14**:173-181, 2002.

[37] Ng, L. and Rand, R., 'Bifurcations in a Mathieu equation with cubic nonlinearities: Part II', *Communications in Nonlinear Science and Numerical Simulation* **7**:107-121, 2002.

[38] Pandey, M., 'Entrainment in a Disk-Shaped MEMS Oscillator', M.S. Thesis, Cornell University, Ithaca, NY, 2004.

[39] Pandey, M., Rand, R. and Zehnder, A., 'Perturbation Analysis of Entrainment in a Micromechanical Limit Cycle Oscillator', *Communications in Nonlinear Science and Numerical Simulation*, available online, 2006.

[40] Peckham, B. B., 'The Necessity of the Hopf Bifurcation for Periodically Forced Oscillators', *Nonlinearity* **3**:261-280, 1990.

[41] Rao, S. S., *Mechanical Vibrations*, 3rd Edition, Addison-Wesley, USA 1995.

[42] Rand, R. H., *Lecture Notes on Nonlinear Vibrations (version 52)*, available on-line at http://www.tam.cornell.edu/randdocs/nlvibe52.pdf, 2005.

[43] Rand, R. H., *Computer algebra in applied mathematics: An introduction to MACSYMA* Research Notes in Mathematics, **94** Pitman, Boston, MA 1984.

[44] Rand, R. H., *Topics in Nonlinear Dynamics with Computer Algebra*, Gordon and Breach Science Publishers, USA 1994.

[45] Rand, R. H. and Armbruster, D., *Perturbation methods, bifurcation theory, and computer algebra*, Applied Mathematical Sciences, **65**. Springer-Verlag, NY, USA 1987.

[46] Rand, R. H., Barcilon, A. and Morrison, T. M., 'Parametric Resonance of Hopf Bifurcation', *Nonlinear Dynamics* **39**:411-421, 2005.

[47] Rand, R. H., Barcilon, A. and Morrison, T. M., 'Parametric Resonance of Hopf Bifurcation', Proceedings of the 2005 ASME Design Engineering Technical Conferences, 20th Biennial Conference on Mechanical Vibrations and Noise, Long Beach, CA, Sept. 24-28, paper no. DETC2005-84016, 2005 (CD-ROM).

[48] Rand, R., Guennoun, K. and Belhaq, M., '2:2:1 Resonance in the Quasiperiodic Mathieu Equation', *Nonlinear Dynamics* **31**:367-374, 2003.

[49] Rand, R. H. and Morrison, T. M., '2:1:1 Resonance in the Quasiperiodic Mathieu Equation', *Nonlinear Dynamics* **40**:195-203, 2005.

[50] Rand, R. H., Ramani, D. V, Keith, W. L. and Cipolla, K. M., 'The Quadratically-Damped Mathieu Equation and its Application to Submarine Dynamics', *Control of Vibration and Noise: New Millennium* **61**:39-50, 2000.

[51] Rand, R., Zounes and R., Hastings, R., 'A Quasiperiodic Mathieu Equation', Chapter 9 in *Nonlinear Dynamics: The Richard Rand 50th Anniversary Volume* A.Guran, ed. World Scientific Pub.Co., 203-221, 1997.

[52] Recktenwald, G. D., 'The Stability of Parametrically Excited Systems: Coexistence and Trigonometrification', Ph.D. Thesis, Cornell University, Ithaca, NY, 2006.

[53] Shampine, L. F. and Thompson, S., 'Solving Delay Differential Equations in MATLAB', *Applied Numerical Mathematics.*, **37**:441-458, 2001.

[54] Stépán, G., *Retarded Dynamical Systems: stability and characteristic functions*, Longman Scientific & Technical, Wiley, NY, USA 1989.

[55] Stépán, G., Insperger, T. and Szalai, R., 'Delay, Parametric Excitation, and the Nonlinear Dynamics of Cutting Process', *International Journal of Bifurcation and Chaos* **15** 9:2783, 2005.

[56] Stephenson, A., 'On a New Type of Dynamical Stability', *Mem. Proc. Manchester Literary Philosophical Society* **52**:1907-1908, 1908.

[57] Strogatz, S. H., *Nonlinear Dynamics and Chaos*, Addison-Wesley, Reading, Mass., 1994.

[58] van der Burgh, A. H. P., *Rain-Wind Induced Vibrations of a Simple Oscillator*, Proceedings of the 2001 ASME Design Engineering Technical Conferences, Pittsburg, PA, Sept. 9-12, paper no.DETC2001-21429, 2001.

[59] van der Pol, B. and Strutt, M. J. O., 'On the Stability of the Solutions of Mathieu's Equation', *Philosophy Magazine* **7**:18-38, 1926.

[60] Virgin, L. N., *Introduction to Experimental Nonlinear Dynamics*, Cambridge Press, NY, USA, 200.

[61] Wang, B. and Fang, Z., 'Chaotic Oscillations of Tropical Climate: A Dynamic System Theory for ENSO', *Journal of Atmospheric Sciences* **53**:2786-2802, 1996.

[62] Wang, B., Barcilon, A. and Fang, Z., 'Stochastic Dynamics of El Nino-Southern Oscillation', *Journal of Atmospheric Sciences* **56**:5-23, 1999.

[63] Wiggins, S., *Introduction to Applied Nonlinear Dynamical Systems and Chaos*, Springer-Verlag, NY, USA 1990.

[64] Wirkus, S., Rand, R. H. and Ruina, A., 'How to Pump a Swing', *The College Mathematics Journal* **29** <u>4</u>:266-275, 1998.

[65] Wirkus, S. and Rand, R. H., 'Dynamics of Two Coupled van der Pol Oscillators with Delay Coupling', *Nonlinear Dynamics*, **30**:205-221, 2002.

[66] Yu, M. F., Wagner, G. J., Ruoff, R. S. and Dryer, M. J., 'Realization of Parametric Resonances in a Nanowire Mechanical System with Nanomanipulation Inside a SEM', *Physical Review Letters B* **66**, 2002.

[67] Zalalutdinov,M., Aubin, K.L., Pandey, M., Zehnder, A.T., Rand, R.H., Craighead, H.G. and Parpia, J.M., 'Frequency Entrainment for Micromechanical Oscillator', *Applied Physics Letters* **83**:3281-3283, 2003.

[68] Zalalutdinov, M., Olkhovets, A., Zehnder, A., Ilic, B., Czaplewski, D. and Craighead, H. G., 'Optically Pumped Parametric Amplification for Micromechanical Systems', *Applied Physics Letter* **78** <u>20</u>:3142, 2001.

[69] Zalalutdinov, M., Parpia, J.M., Aubin, K.L., Craighead, H.G., T.Alan, Zehnder, A.T. and Rand, R.H., *Hopf Bifurcation in a Disk-Shaped NEMS*, Proceedings of the 2003 ASME Design Engineering Technical Conferences, 19th Biennial Conference on Mechanical Vibrations and Noise, Chicago, IL, Sept. 2-6, paper no.DETC2003-48516, 2003 (CD-ROM).

[70] Zhang, C. Y., Zhu, Z. Q., Lin, Z. Q. and Wu, T. X., 'Theoretical and Experimental Study on the Parametrically Excited Vibration of Mass-Loaded String', *Nonlinear Dynamics* **37**:1-18, 2004.

[71] Zhang, W., Baskaran R, Turner K. L., 'Nonlinear Dynamics Analysis of a Parametrically Resonant MEMS Sensor', Proceedings of the 2002 SEM Annual Conference & Exposition on Experimental and Applied Mechanics, June 10-12, Milwaukee, WI, 2002.

[72] Zounes, R. S. and Rand, R. H., 'Transition Curves in the Quasiperiodic Mathieu Equation', *SIAM Journal of Applied Mathematics* **58**:1094-1115, 1998.

[73] Zounes, R. S. and Rand, R. H., 'Global Behavior of a Nonlinear Quasiperiodic Mathieu Equation', *Nonlinear Dynamics*, **27**:87-105, 2002.

[74] Zounes, R. and Rand, R., 'Subharmonic Resonance in the Non-linear Mathieu equation', *Int'l Journal of Non-linear Mechanics* **37**:43-73, 2002.

"To raise new questions, new possibilities, to regard old problems from a new angle, requires creative imagination and marks real advance in science."

– Albert Einstein